FORMATION DAMAGE DUE TO IRON PRECIPITATION DURING MATRIX ACIDIZING TREATMENTS OF CARBONATE RESERVOIRS AND WAYS TO MINIMIZE IT USING CHELATING AGENTS

A Thesis

by

AHMED ISSAM ELSAYED SALAMA ASSEM

Submitted to the Office of Graduate Studies of
Texas A&M University
in partial fulfillment of the requirements for the degree of

MASTER OF SCIENCE

Chair of Committee,   Hisham A. Nasr-El-Din
Committee Members,   Jerome J. Schubert
                      Mahmoud El-Halwagi
Head of Department,   A. Daniel Hill

August 2013

Major Subject: Petroleum Engineering

ABSTRACT

Iron precipitation during matrix acidizing treatments is a well-known problem. During matrix acidizing, successful iron control can be critical to the success of the treatment. Extensive literature review highlighted that no systematic study was conducted to determine where this iron precipitates, the factors that affect this precipitation, and the magnitude of the resulting damage.

Iron (III) precipitation occurs when acids are spent and the pH rises above 1, which can cause severe formation damage. Chelating agents are used during these treatments to minimize iron precipitation. Disadvantages of currently used chelating agents include limited solubility in strong acids, low thermal stability, and/or poor biodegradability.

In this study, different factors affecting iron precipitation in Indiana limestone rocks were examined. Two chelating agents, GLDA and HEDTA, were tested at different conditions to assess their iron control ability.

Results show that a significant amount of iron precipitated, producing a minimal or no gain in the final permeability, this indicated severe formation damage. The damage increased with the increase of the amount of iron in solution. When chelating agents were used, the amount of iron recovered depended on both chelate-to-iron mole ratio and the initial permeability of the cores. Calcium is chelated along with iron, which limits the effectiveness of chelating agents to control iron (III) precipitation. Acid solutions should be designed considering this important finding for more successful treatments.

DEDICATION

I dedicate this thesis to my dad, mom, and sister for their continuous support and encouragement.

ACKNOWLEDGEMENTS

TABLE OF CONTENTS

LIST OF FIGURES

LIST OF TABLES

CHAPTER I

INTRODUCTION AND LITERATURE REVIEW

Stimulating wells with acid was firstly reported in 1896 (Walker et al. 1991). The aim was to dissolve large amounts of carbonate rocks near the wellbore region to bypass the damage to the original permeability of the reservoir rock. At high temperatures, HCl does not produce acceptable results because of the fast reaction in the near wellbore area, low acid penetration, and surface dissolution (Huang et al. 2003). Williams et al. (1979) recommended that carbonate acidizing treatments should be carried out at the highest possible injection rate without fracturing the reservoir rock. Several studies investigated the optimum conditions for wormhole formation during carbonate acidizing using HCl. They have shown that the dissolution patterns created can be described as one of the following types (Haung et al. 1997, Fredd 2000a, and Fredd 2000b): face dissolution in which most of the acid is spent near the rock face, conical wormholes, dominant wormholes, ramified wormholes, and uniform dissolution.

At low injection rates, the acid is consumed on the inlet face of the core, resulting in face dissolution or complete dissolution of the core starting from the inlet face. The face dissolution structure consumes large volumes of the acid and provides negligible depths of wormholes propagation. At slightly higher injection rates, the acid or the treating fluid can penetrate into the porous medium and enlarge flow channels. At intermediate injection rates, the acid is transported to the tip of the evolving flow channel, where subsequent consumption propagates the channel and eventually leads to the formation of a dominant wormhole. At high injection rates, the dissolution channels

1

become more highly branched or ramified as the fluid is forced into smaller pores. At very high injection rates, uniform dissolution is observed as the acid is transported to the most pores in the medium. The type of dissolution structure was found to have a significant effect on the volume of acid required to obtain a given penetration depth of wormhole (Fredd 1998, Fredd and Fogler 1999).

Another problem encountered during stimulation using HCl-based fluids is iron precipitation. Iron precipitation is a very serious problem that can be detrimental to the success of any matrix acidizing treatment (Gougler et al. 1985). Iron comes from many sources that may include storage and mixing tanks, mill scale in new pipelines and tubulars, and iron-minerals bearing formations (Dill and Fredette 1983; Crowe 1986; Hall and Dill 1988). Well tubulars are often made of low-carbon steel and may contain rust. HCl will dissolve the rust and produce a significant amount of iron, which in turn will precipitate and cause formation damage. Corrosion becomes more severe at high temperatures, and special additives are needed to compensate for the loss in corrosion inhibition at higher temperatures. The cost of these additives exceeds 5% of the treatment cost (Fredd 1998). Also, the excessive use of corrosion inhibitors may cause other problems, as the corrosion inhibitor may adsorb on the reservoir rock and change its wettability, especially in low permeability reservoirs (Schechter 1992).

Some iron compounds are soluble, others are insoluble in acids, but even the soluble compounds precipitate when the acids are spent (Dill and Fredette 1983). Iron has two forms: Fe^{2+} and Fe^{3+} ions. Fe^{3+} ions start to precipitate at a pH of 1 (Taylor et al. 1999b). Fe^{2+} ions are not a real problem in sweet environments because they remain in

2

solution until a pH of 6.5 (Dill and Fredette 1983), however they can be easily oxidized to Fe^{3+}. For instance, in the case of fracturing fluids, dissolved oxygen is incompatible with formation water carrying ferrous ions. If the treatment does not contain iron control agents, iron will precipitate. Acid readily dissolves iron scale in pipes and also attacks iron-containing minerals in the formation. A small thickness of iron scale can generate large amounts of damaging precipitates (Smith et al. 1969; Gougler et al. 1985; Ford et al. 1992). The precipitation of ferric hydroxide or other iron-containing compounds can seriously damage the flow channels recently opened by the acid reaction with the formation (Smith et al. 1969). The iron problem is even worse with injection wells especially those with new or rusty pipes (Crowe 1986). In sweet wells, sequestering agents are used frequently to address this problem (Crowe 1986; Dill and Fredette 1983).

Chelating agents are aminopolycarboxylic acids which are capable of binding with metal atoms. Chelates have two structural essentials: a metal atom or a stable oxo cation (M) works as electron acceptor, and two or more atoms in the molecule of the chelating agent, or ligand (L) work as electron donor. These two parts are connected by coordinate bonds. Chelating agents are polydentate (two or more coordinate bonds). Principal donor atoms in use are: nitrogen, oxygen, sulfur, phosphorus, arsenic, and selenium also form chelates. Metals are characterized by their coordination number which determines number of donor atoms bound to the central atom. Most common coordination numbers are four and six. A complex (ML_n) is formed if the coordination number of (M) is greater than the number of donor atoms in (L). Chelates are more stable than monodentate metal coordination due to ring formation in chelate complexes

(Chelate Effect), and the increase in entropy resulting from the increase in the number of free molecules. Substituents on a ring produce steric hindrances and more stability, which occur when the large size of groups within a molecule prevents chemical reactions that are observed in related molecules with smaller groups. The structure of different frequently used chelates is shown in **Fig. I.1**. These chemicals have been used extensively in oilfields for different purposes such as iron control, inorganic scale removal, and well stimulation. They can be used to stimulate carbonate and sandstone formations, especially at high temperatures because of the low corrosion and reaction rates compared with live HCl (Fredd and Fogler 1997; Frenier et al. 2001; Frenier et al. 2004).
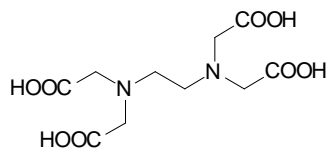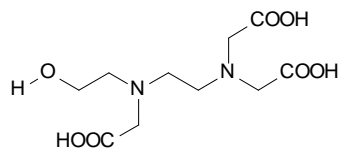
Fig. I.1– Structures of chelating agents commonly used in the oil industry. GLDA is the new chelate tested in the present study.
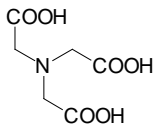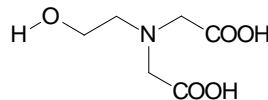
In oilfield chemical treatments, chelates are added to the acid that is used in the stimulation treatment to prevent iron precipitation as acid spends on the formation. EDTA, NTA, and citric acid were frequently used, but these chelating agents had at least some limitations such as: a low solubility in high concentrations of HCl acid, a low stability in high temperatures, and higher chelate-to-iron mole ratio (Dill et al. 1983; Ewing et al. 1983; Hall and Dill 1988). Frenier et al. (2003) reported hydroxyethyliminodiacetate (HEIDA) salts as a biodegradable chelating agent. Also, it has low aquatic toxicity characteristics. Sometimes a blend of two or more chemicals is

used to give better results (Ewing et al. 1983). For instance, using acetic acid (HAC) with citric acid has a synergetic effect of providing a lower pH to maintain iron and Ca-citrate on solution (Dill et al. 1983). Also, another approach is to use sodium erythorbate (SE), which maintains iron ions in the Fe^{2+} state (Dill and Smolarchuk 1988). Different properties of chelates are given in **Table I.1**.

Table I.1– Chelate molecular weights, protonation constants, and metal stability constants (After LePage et al. 2011).

Chelate		Molecular Weight		pK_a Values				Log K	
Abbreviation	Structure	Acid	Sodium Salt	pK_1	pK_2	pK_3	pK_4	Ca^{2+}	Fe^{3+}
EDTA		292	380	10.2	6.2	2.7	2	10.7	25.1
HEDTA		278	344	9.9	5.4	2.6	–	8.1	19.7
GLDA		263	351	9.36	5.0	3.5	2.6	5.9	11.7*
NTA		191	257	9.7	2.5	1.8	–	6.4	15.9
EDG		177	221	8.7	2.2	–	–	4.7	11.6

* Value is not listed in the National Institute of Sciences and Technology Standard Reference Database 46 version 7.0 for Critically Selected Stability Constants of Metal Complexes. Experimental results indicate that the Fe^{3+} stability constant of GLDA is comparable to NTA.

Fe^{2+} is more stable under anaerobic conditions and Fe^{3+} has a tendency to be reduced to Fe^{2+}. Fe^{3+} is responsible for formation damage, so the Fe^{3+}/ Fe^{2+} ratio should be determined. Fe^{3+} can convert to Fe^{2+} by the effect of pipe iron. The best approach is to determine Fe^{3+}/ Fe^{2+} ratio and add iron control agents accordingly. Also, non-damaging

iron control agents should produce soluble by-products (Smith et al. 1969). Amount and type of dissolved iron are important factors when designing acid treatments to optimize the amount of iron control agents. Knowing the exact iron (II) to iron (III) ratio saves significant and unnecessary expenses (Taylor et al. 1999a). A good practice is to clean the tubing prior to acid treatment, and iron control agents should be used if there is any chance of its entering the formation (Walker et al. 1991; Ford et al. 1992; Al-Mutairi and Nasr-El-Din 2005; Nasr-El-Din et al. 2007).

In sour environments, however, the problem is more complicated. Reducing agents are useless, as iron (II) reacts with H_2S to produce iron sulfide. Also, when iron (III) is in contact with H_2S, it is reduced to free sulfur (Hall and Dill 1988). Iron sulfide precipitates at a pH of 1.9. Erythorbic acid reduces Fe^{3+} to Fe^{2+}, but it does not work in sour environments because of iron sulfide deposition (Hall and Dill 1988; Taylor et al. 2001). Iron sulfides of 1:1 stoichiometry are readily soluble while those with high sulfur content are less soluble (Walker et al. 1990; 1991). The iron to sulfide ratio, pH, and hydrogen sulfide concentration are important in finding the most effective way to remove scale. Acid will dissolve the scale and maintain it in solution as long as the acid content is high. When acid is spent in the formation, the concentrations of HS^- and S^{2-} will increase and precipitation will occur. Iron control agents should be used with sulfide control agents, as precipitation is a function of both Fe (II) and S^{2-} (Walker et al. 1990; 1991). The physical texture of scale depends on the well type. In gas wells, scale is porous, loose and is not protecting the base metal. In water wells, iron sulfide scale is dense, adherent and protective to the metal. While using acid for treatments, hydrogen

sulfide scavengers should be used to prevent elemental sulfur deposition (Nasr-El-Din and Al-Humaidan 2001; Nasr-El-Din et al. 2002).

LePage et al. (2011) introduced a new environmentally friendly chelating agent, GLDA, which falls below strong chelates, HEDTA and EDTA. GLDA is a chelating agent that contains a single nitrogen atom. GLDA has a singular structure because a major portion of it is derived from monosodium glutamate (MSG). Monosodium glutamate is achieved from corn sugar fermentation and is considered a renewable raw material. Furthermore, the carbon source in EDTA is fossil-based, but in GLDA it is bio-based, which makes it the only chelating agent with green carbon atoms (Kolodynska 2010; LePage et al. 2011). At high pH chelate solubility is high, but at low pH all chelates except GLDA exhibit low solubility. There are two means for calcium dissolution: chelation and acidizing.

In the first part of this work, the damage due to iron precipitation was studied. Different HCl acid solutions (5 - 15 wt%) containing 5,000 - 10,000 ppm of Fe^{3+} were used in the experiments to simulate the typical amount of iron that can be present during acid treatments. No iron control agents were used.

In the second part of this work, HCl acid solutions containing 5,000 - 10,000 ppm of Fe^{3+} were used in the experiments to simulate the typical amount of iron that can be present during acid treatments. Chelating agents were tested at different acid concentrations (5 - 20 wt%) and chelate-to-iron mole ratios (1:1 - 2:1).

The objectives were to understand the damage resulting from iron precipitation during a matrix acidizing treatment of carbonates formations, and to explore the use of chelating agents to minimize the precipitation and damage.

CHAPTER II

EXPERIMENTAL METHODOLOGY

Materials

The acid solutions are prepared using 36.5 wt% hydrochloric acid (HCl) obtained from Mallinckrodt. Hydrated ferric trichloride ($FeCl_3.6H_2O$) 99.95% pure, to simulate the iron concentration in the acid, was obtained from Sigma Aldrich. Corrosion inhibitor, quaternary ammonium compound based, was obtained from a local service company. Chelating agents: NaH_3-GLDA (35.6 wt%) of pH = 3 and NaH_2-HEDTA (40.8 wt%) of pH = 4 were obtained from AkzoNobel. The cores used were Indiana limestone of different permeabilities, of 1.5 in. diameter and 6 and 20 in. length. The brine used was 5 wt% NaCl, which was obtained from Sigma Aldrich. The de-ionized water, used throughout the experiments, was obtained from a purification water system that has a resistivity of 18.2 MΩ.cm at room temperature.

Equipment

Coreflood

The coreflood setup, described in **Fig. II.1**, was constructed to simulate a matrix stimulation treatment. A back pressure of 1100 psi is applied to keep the most CO_2 in solution. Overburden pressure was maintained at 1800 psi. Pressure transducers are connected to a computer to monitor and record the pressure drop across the core during the experiments. A Teledyne ISCO D500 precision syringe pump, that has a maximum allowable working pressure of 2000 psi, is used to inject the treatment into the core.

10
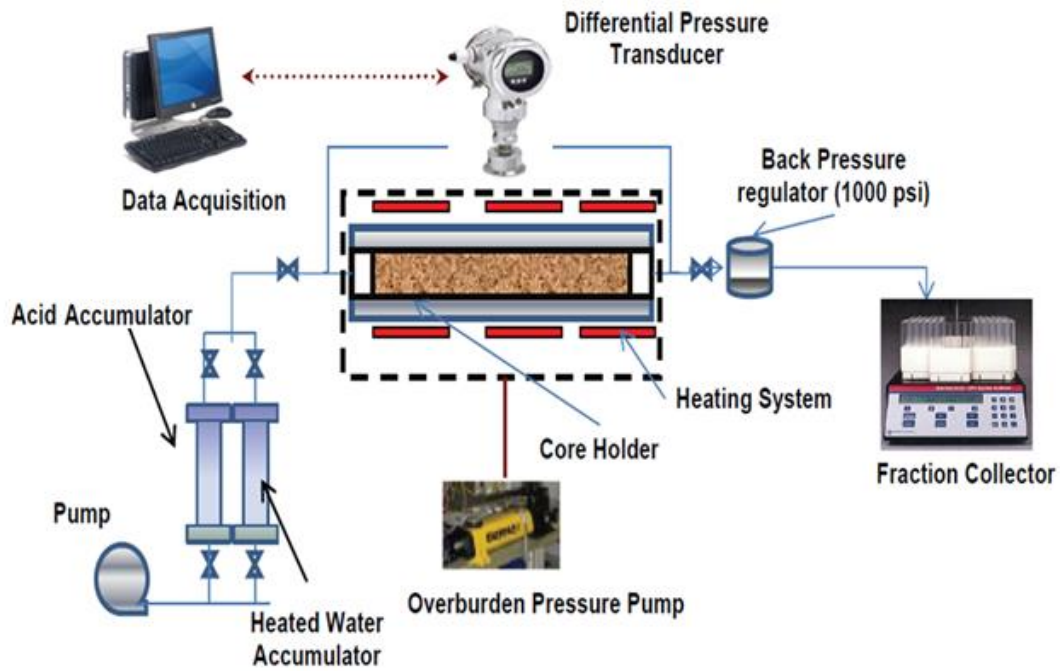
Fig. II.1– Coreflood setup.

Core preparation

Cores were dried in the oven at 250°F for 6 hrs, weighed, saturated with 5 wt% NaCl brine under vaccum, and weighed again. The difference between wet and dry weight was used to calculate porosity.

$$V_p = \frac{W_{wet} - W_{dry}}{\rho}$$
(II.1)

where:

V_p: pore volume, cm³; ρ: brine density, g/cm³

Initial permeability was measured at room temperature by injecting 5 wt% NaCl brine. Darcy's equation for laminar flow was used:

$$k = 122.8 \frac{qL\mu}{\Delta p \, d^2} \qquad\qquad (II.2)$$

where:

k: permeability, md; L: core length, inch, d: core diameter, inch; q : flow rate, cm^3/min;

μ: dynamic viscosity, cp; Δp: psia

Solution preparation

1. An example of solution preparation is 5 wt% HCl solution containing 10,000 ppm Fe(III):

To prepare 100 g of the solution:

HCl acid weight $= \frac{5}{36.5} \times 100 = 13.7$ g

36.5 wt% HCl is the bottle concentration.

One mole of Fe is 56 g however one mole of $FeCl_3.6H_2O$ is 270 g. So, to have 10,000 ppm Fe^{3+} the following amount should be added.

$FeCl_3.6H_2O$ weight $= \frac{270 \times 1}{56 \times 100} \times 100 = 4.82$ g

1 g of corrosion inhibitor is added.

Finally, deionized water is added.

DI H_2O weight $= 100 - (13.7 + 4.82 + 1) = 80.48$ g

2. An example of solution preparation is 15 wt% HCl solution containing 10,000 ppm Fe(III), GLDA:Fe = 1:1

To prepare 100 g of the solution:

HCl acid weight $= \frac{15}{36.5} \times 100 = 41.1$ g

$FeCl_3.6H_2O$ weight $= \frac{270 \times 1}{56 \times 100} \times 100 = 4.82$ g

1 g of corrosion inhibitor is added.

One mole of GLDA is 285 g and bottle concentration is 35.6 wt%

GLDA weight $= \frac{285 \times 1}{56 \times 100} \times \frac{1}{0.356} \times 100 = 14.3$ g

Finally, deionized water is added.

DI H_2O weight $= 100 - (41.1 + 4.82 + 14.3 + 1) = 38.79$ g

Inductively Coupled Plasma Optical Emission Spectrometry (ICP-OES)

Optical emission spectroscopy (OES) uses quantitative measurement of the optical emission from excited atoms to determine analyte concentration. Analyte atoms in solution are aspirated into the excitation region where they are desolvated, vaporized, and atomised by a plasma. Electrons can be in their ground state (unexcited) or enter one of the upper level orbitals when energy is applied to them. This is the excited state. A photon of light is emitted when an electron falls from its excited state to its ground state. Each element has a unique set of wavelengths that it can emit. An illustration is given in **Fig. II.2**.
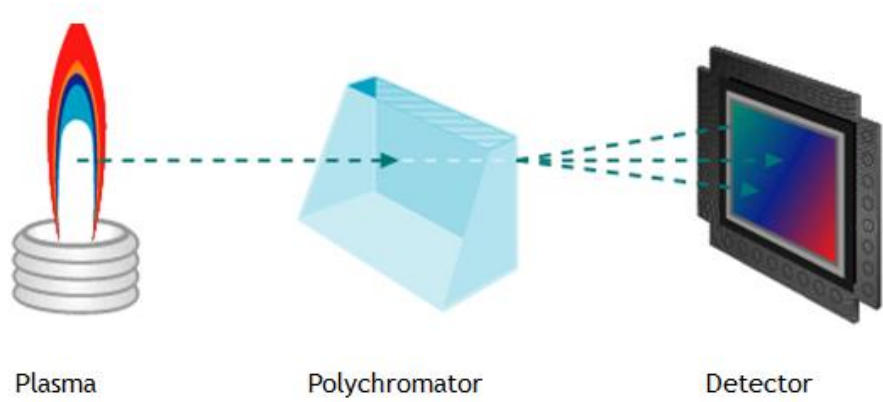
Fig. II.2– An illustration of ICP theory.

We use an Optima 7000 ICP-OES Spectrometer, **Fig. II.3**, to analyze core effluent samples for the total iron and calcium concentrations.

Fig. II.3– Optima 7000 ICP-OES Spectrometer

Steps for using ICP-OES

1. Make sure that the ventilation is working.

2. Open the air and argon tanks and adjust their pressures.

3. Switch the machine on.

4. Go to computer and select the method.

5. Light the lamp and leave it 30 min, to warm up.

6. Aspirate deionized water and select auto zero.

7. Aspirate the calibration blank (2% HNO3) and select auto zero.

8. Calibrate using standards (5, 15, and 30) ppm and check the linearity of the standard and the correlation coefficient value.

9. If everything is right, analyze samples.

10. Save the method and close the Winlab program window after closing air and argon and bleeding them from the pipes. The results will be in ppm.

11. If any samples are deviated from the range of the standard curve (0-30 ppm), make the appropriate dilution and reanalyze them again.

Knowing the initial amount of iron injected, the volume, and the iron concentration recovered from each sample; the percent of iron recovered can be calculated from the following equation:

$$\% \text{ iron recovered} = \frac{\sum_{i=1}^{n} Sample\ volume \times iron\ concentration}{Amount\ of\ iron\ injected} \times 100\ \% \qquad \text{(II.3)}$$

Ca Ion-Selective Electrode

The calcium ion concentration, which we get from ICP, is the total calcium concentration. We use a Cole-Parmer® ISE (EW-27502-09) calcium ion-selective electrode, **Fig. II.4**, to get the free calcium concentration. From both values, we can get the amount of calcium chelated.

1. Calibrate Ca-ion selective electrode between two known concentrations like 10 and 100 ppm.

2. Measure free calcium concentration in the samples.

Fig. II.4– Ca Ion-Selective Electrode.

CT Scan

The CT scanner shown in **Fig. II.5** is used to get 2D scan images for the cores used in the coreflood experiments. It can be used to detect wormhole propagation. This can be detected through the inspection of the dark spots indicating a low CT number and so, low density.

Fig. II.5– CT Scanner.

Titrator

The acid titration is based on the volumetric method for determining the acid concentration. The Thermo Scientific Orion 950 Titrator used is shown in **Fig. II.6**. An auxiliary reagent (NaOH) of a known concentration (1M) is added to the pre-dose volume of titrant (acid solution). The auxiliary reagent is added using a dispenser, until a pH electrode measures a preset pH value of 7. Then the volume of the reagent of a known molarity will be used to calculate the molarity and then the acid concentration of the effluent fluid samples using the flowing equation:

$$M_{acid} \times V_{acid} = M_{base} \times V_{base} \tag{II.4}$$

Where M_{acid} is the acid molarity, V_{acid} is the acid volume, M_{base} is the base molarity, and V_{base} is the base volume.

Acid titration is needed if there is unreacted HCl acid after treatment. Also, titration is used to measure the contribution of hydrated ferric trichloride ($FeCl_3.6H_2O$) to the total acidity of the solution.

Fig. II.6– Thermo Scientific Orion 950 Titrator.

Scanning Electron Microscope (SEM)

Scanning electron microscopy (SEM) is a type of electron microscopy that images the sample surface by scanning it with a high-energy beam of electrons in a raster scan pattern. The electrons interact with the atoms that make up the sample producing signals that contain information about the sample's surface topography, composition and other properties such as electrical conductivity. The Evex Mini-SEM is shown in **Fig. II.7**. If the sample is not conductive, an Ion Sputter Coater MCM-100, **Fig. II.8**, is used.

Fig. II.7– Evex Mini-SEM.

Fig. II.8– Ion Sputter Coater MCM-1000.

Steps for using Evex Mini-SEM

1. Sample is crushed into small fragments.

2. Sample is stuck to the sample holder.

3. Ion Sputter Coater is used to coat samples with gold.

4. Sample is inserted into the SEM chamber and is fixed into its place.

5. High vacuum is applied to the SEM chamber.

6. The electron beam is applied and magnification can be adjusted.

7. SEM image, elemental and spectral analysis can be acquired.

Analysis of Indiana limestone rock was done. **Fig. II.9** shows an image of Indiana limestone using SEM, and the calcium carbonate crystals are obvious. A spectral analysis is shown in **Fig II.10**.
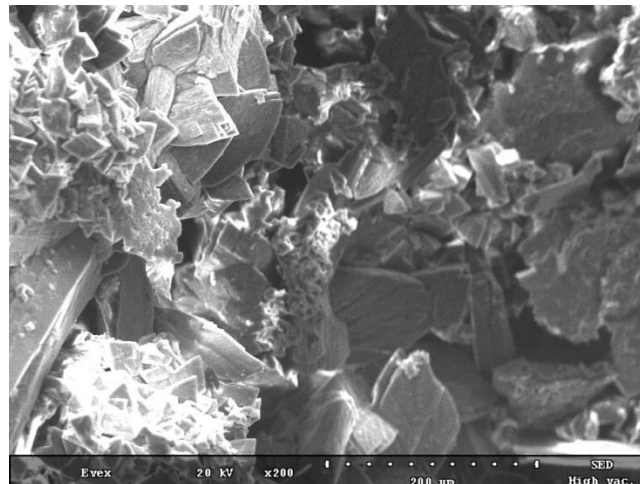
Fig. II.9– SEM image for Indiana limestone core.
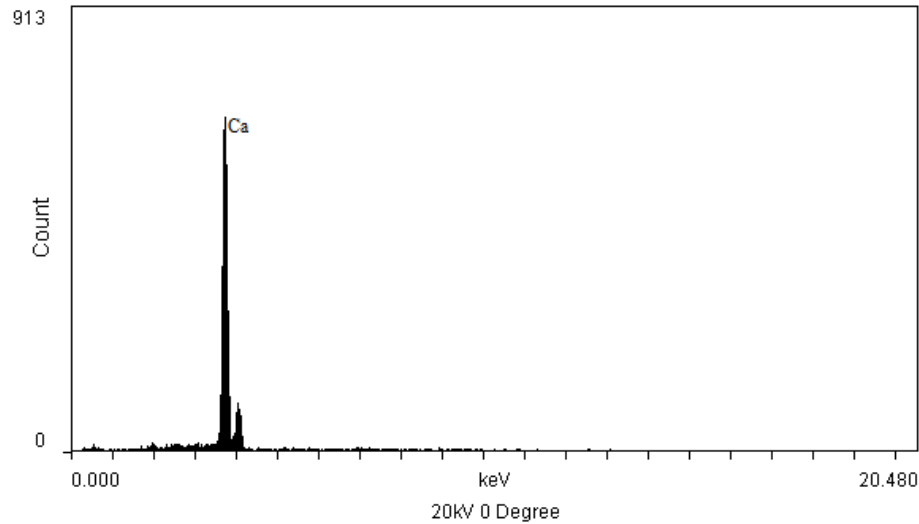
Fig. II.10– Spectral Analysis for Indiana limestone.

X-Ray Fluorescence (XRF)

In X-Ray Fluorescence, the sample is bombarded with X-rays. This excites the sample to generate X-ray fluorescence. The X-rays "shoot" individual electrons out of the atoms of the elements, primarily out of the inner atomic shells K and L. The resulting vacancies are filled up again by electrons from higher energy shells. The excess energy of these electrons is then emitted in the form of X-ray fluorescence radiation. This radiation is characteristic for each element like a fingerprint and virtually independent of the atom's chemical bond. The intensity of the radiation is proportional to the concentration of the element in the sample. A schematic for the process is shown in **Fig. II.11**.
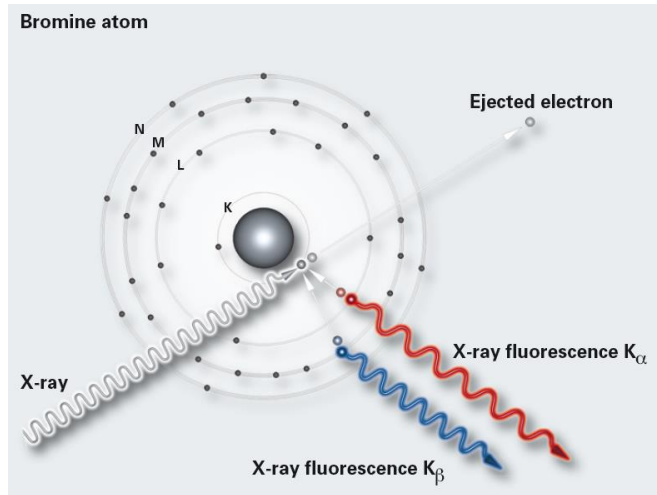
Fig. II.11– X-Ray Fluorescence (XRF).

The S2 RANGER, shown in **Fig. II.12**, uses a 50 W X-ray tube to directly excite the X-ray fluorescence in a sample. By specifying the high voltage and choosing a filter, an elemental or energy range is selected. In order to analyze lighter elements, the sample chamber is either evacuated by means of an integrated vacuum pump, or it is flooded with helium. The XFlash detects the X-ray fluorescence radiation of the sample. The multi-channel analyzer divides up the different energies and accumulates counts to form intensity vs. energy spectrum. An illustration is given in **Fig. II.13**.

Fig. II.12– S2 RANGER.
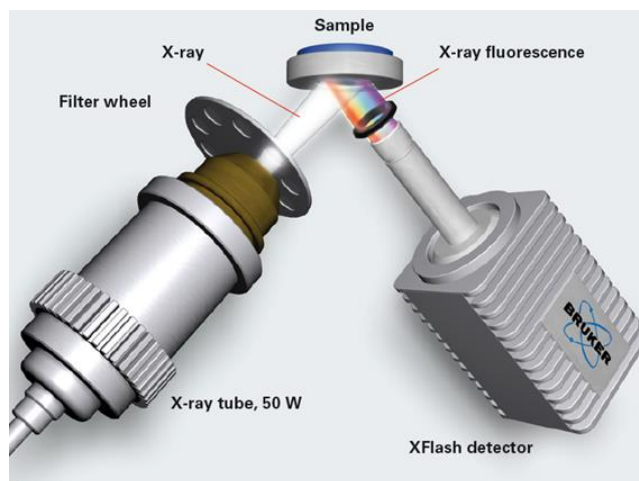
Fig. II.13– S2 RANGER Illustration.

Steps for using S2 RANGER

1. Wait for the machine to warm up.

Usually it takes around 20 minutes for the machine to warm up.

2. Run the Copper Disk Calibration.

The copper disk is loaded inside the sample recess of the chamber. Then the measurement is started. After it is finished, two green lights should be seen or the measurement should be repeated.

3. Run the QC (Quality check) sample.

A BAXS-S2 glass standard is loaded inside the sample recess of the chamber. 'QualityCheck' is selected for measurement. After it is finished, six green lights should be seen or drift-correction is needed.

Analysis of Indiana limestone rock was done. The data is given in **Tables II.1 and II.2**. It is clear that limestone cores are mainly calcium carbonates with traces from other compounds.

Table II.1– XRF analysis for Indiana limestone, compound wt%

Compound	Concentration, wt%
Al_2O_3	0.232
$CaCO_3$	98.3
Cl	0.0457
Fe_2O_3	0.107
K_2O	0.109
MgO	0.574
SiO_2	0.368
SnO_2	0.0144
SO_3	0.213
SrO	0.0227

Table II.2– XRF analysis for Indiana limestone, element wt%.

Element	Concentration, wt%
Al	0.123
C	11.8
Ca	39.4
Cl	0.0457
Fe	0.0751
K	0.0906
Mg	0.346
O	47.9
S	0.0853
Si	0.172
Sn	0.0113
Sr	0.0192

CHAPTER III

FORMATION DAMAGE DUE TO IRON PRECIPITATION IN

CARBONATE ROCKS

Introduction

Iron precipitation during matrix acidizing treatments is a well-known problem. However, extensive literature review highlighted that no systematic study was conducted to determine where this iron precipitates, the factors that affect this precipitation, and the magnitude of the resulting damage.

In this chapter, the effect of iron precipitation in the acidizing operations is studied. HCl solutions (5 - 15 wt%) containing 5,000 to 10,000 ppm of Fe^{3+} were used for these experiments. The effect of varying acid concentration, initial core permeability, core length, temperature, and flow rate was studied. Coreflood experiments were conducted on 6 and 20 in. long Indiana limestone cores over a wide range of permeabilities and up to 300°F. In these experiments, 0.5 PV of acid solution was injected. The cores were scanned after treatments using a CT scanner. The core effluent samples were analyzed for iron and calcium concentrations using ICP-OES.

Results showed a significant amount of iron precipitated on the injection face of the cores and the sides of the wormholes, i.e. where the contact occurs between the acid and the rock, producing a minimal or no gain in the final permeability, which indicated severe formation damage. The damage increased with the increase of the amount of iron

in the solution. At higher temperatures and flow rates, the damage was significant. Core length did not affect the degree of damage.

Experimental Studies

Equipment

The coreflood setup, described in **Fig. II.1**, was constructed to simulate the matrix stimulation treatment. pH values for collected effluent samples were measured using an Orion PrepHecT Ross Electrode. The total iron and calcium concentrations of the core effluent samples were measured using the Optima 7000 ICP-OES Spectrometer. Thermo Scientific Orion 950 Titrator was used for acid titration using the volumetric method.

Acid titration

The acid titration was based on the volumetric method for determining the acid concentration. An auxiliary reagent (NaOH) of a known concentration (1M) was added to a pre-dose volume of titrant (acid solution). The auxiliary reagent was added using a dispenser, until a pH electrode measures a preset pH value of 7. Then, the volume of the reagent of a known molarity will be used to calculate the molarity and then the acid concentration of the effluent fluid samples using the flowing equation:

$$M_{acid} \; X \; V_{acid} = M_{base} \; X \; V_{base} \qquad \text{(III.1)}$$

Where M_{acid} is the acid molarity, V_{acid} is the acid volume, M_{base} is the base molarity, and V_{base} is the base volume. **Table III.1** gives the details of the solutions.

28

Table III.1– Data for the final acid concentration using volumetric titration method.

Run #	Initial Acid Conc., wt%	Iron Amount, ppm	Final Acid Conc., wt%
1	5	5,000	6.25
2	5	10,000	7.50
3	10	5,000	11.25
4	10	10,000	12.50

Results and Discussion

Coreflood Studies

Coreflood experiments were run using the coreflood setup shown in **Fig. II.1**. Two sets of coreflood experiments were performed using Indiana limestone of a wide range of permeabilities. The first set of experiments was performed with HCl acid solutions containing no iron, to study the effect of live HCl acid (5 - 10 wt%) in the absence of iron precipitation. In the second set of experiments HCl solutions (5 - 10 wt%) containing 5,000 to 10,000 ppm of Fe^{3+} were used. The experiments were performed at temperatures up to 300°F.

Before the acid treatment, the core was saturated using 5 wt% NaCl brine, the initial permeability was measured when pressure stabilized. During coreflood runs, 5 wt% NaCl brine was injected while the core was heated to the desired temperature. After that, 0.5 PV of the acid solution was injected. Then the cores were flushed again with 5 wt% NaCl brine. Finally, the cores were left to cool down and 5 wt% NaCl brine was injected at a constant rate until the pressure drop restabilized and the final permeability was measured.

These runs were performed to test the effects of amount of iron, acid concentration, initial core permeability, core length, flow rate, and temperature on the damage due to iron precipitation. For each coreflood experiment, the pressure drop across the core was plotted using Lab-View software. Samples of the core effluent were analyzed for both iron and calcium concentrations. The pH values of the effluent samples were measured.

Live acid without iron

Different solutions of HCl (7.5 – 12.5 wt%) were injected through 6 in. Indiana Limestone cores (1 – 5 md) to determine the permeability enhancement in the absence of iron precipitation. To eliminate the effect of hydrated ferric trichloride on the solution acidity. The acid concentration of (5 - 10 wt%) HCl solutions containing 5,000 to 10,000 ppm of Fe^{3+} were measured using a titrator. **Table III.2** gives the details of the tested cores.

Table III.2– Data for coreflood experiments with live acid.

Run #	Acid Conc., wt%	Core Porosity, Fraction	Initial K, md	Injection Rate, cm³/min	Final K, md	K Enhancement
1	5	0.13	6.04	1	8.34	1.30
2	10	0.14	7.81	1	7.30	0.93
3	5	0.14	2.10	1	3.99	1.9
4	10	0.14	2.80	1	Breakthrough*	-

* At breakthrough, the pressure drop decreased to values around 10 psi. The permeability enhancement was greater than 500 fold in all cases.

Four experiments were performed using (7.5 – 12.5 wt%) HCl acid solutions. **Figs. III.1 through III.4** show the pressure drop profile across the cores during HCl acid injection. When the initial permeability of the cores was relatively high, there was no overall stimulation. The pressure drop across the core remained constant throughout the experiments. At low initial permeability the stimulation depended on acid concentration. At the instant when the 7.5 wt% HCl acid injection started, the pressure drop increased due to the higher viscosity of the acid, CO_2 released during the acid reaction with the rock, and/or iron precipitation. Then, the pressure drop decreased due to the HCl acid reaction with the rock and wormholes creation. Finally, pressure drop stabilized again. The final pressure drop was almost half the initial pressure drop before acid injection, indicating stimulation. Likewise, in the case of the 12.5 wt% HCl acid injection, breakthrough occurred. It's obvious that the degree of stimulation depends on both factors: the acid concentration and injection rate.
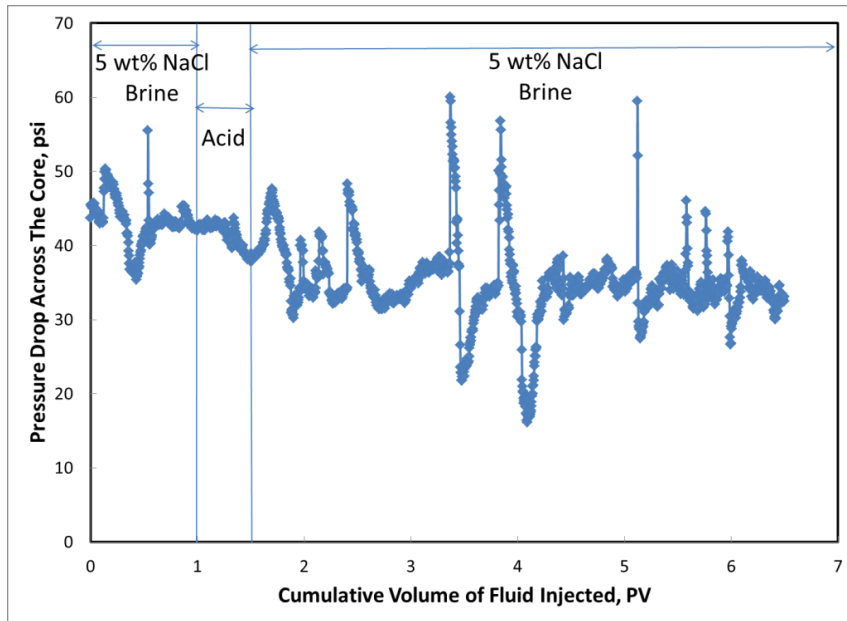
Fig. III.1– Pressure drop across the core for 7.5 wt% HCl solution with no Fe^{3+} at 200°F and a relatively high permeability.
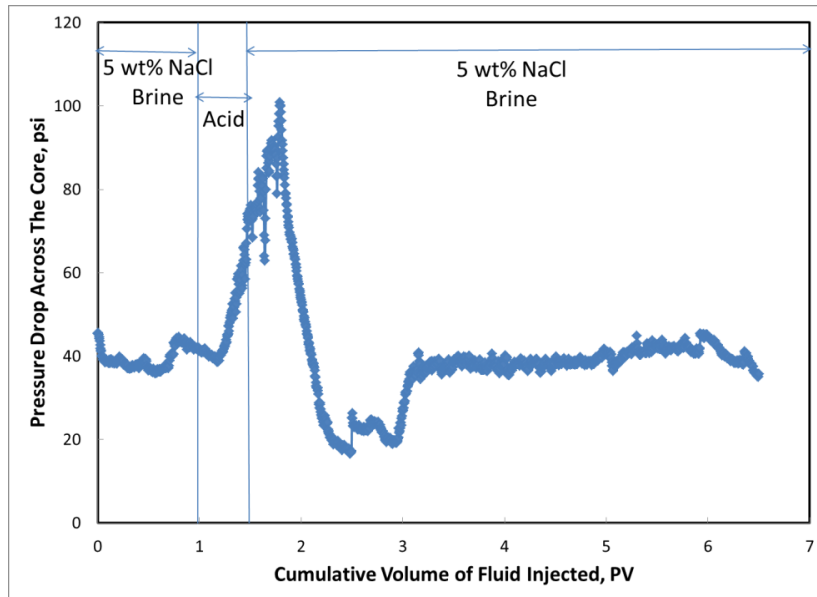
Fig. III.2– Pressure drop across the core for 12.5 wt% HCl solution with no Fe^{3+} at 200°F and a relatively high permeability.
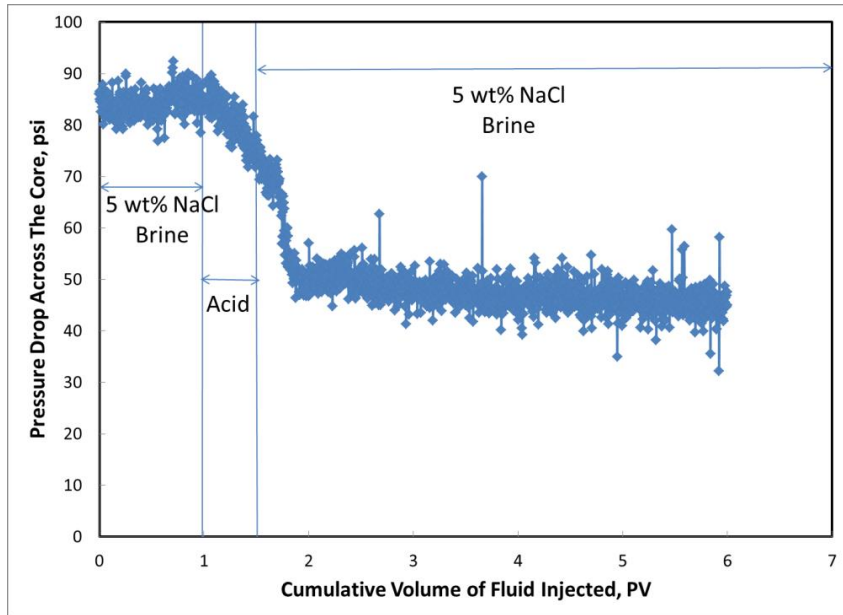
Fig. III.3– Pressure drop across the core for 7.5 wt% live HCl solution with no Fe^{3+} at 200°F.
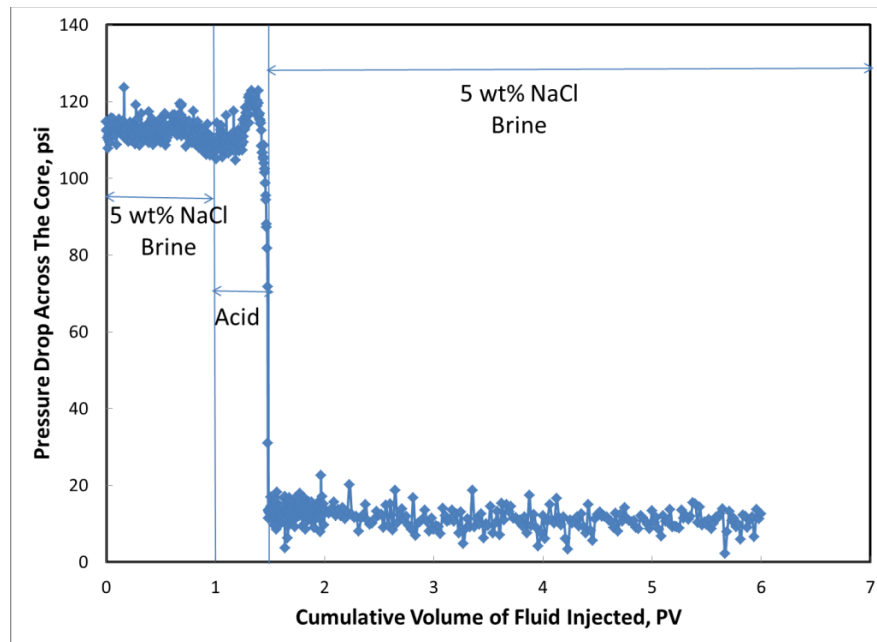
Fig. III.4– Pressure drop across the core for 12.5 wt% live HCl solution with no Fe^{3+} at 200°F.

Figs. III.5 through III.8 show photos of the inlet and outlet of the cores tested with live HCl. Wormholes started on the inlet face of all the cores. In the case of the 12.5 wt% HCl with the low permeability cores, breakthrough occurred. It is clear that the wormholes reached the core outlet.
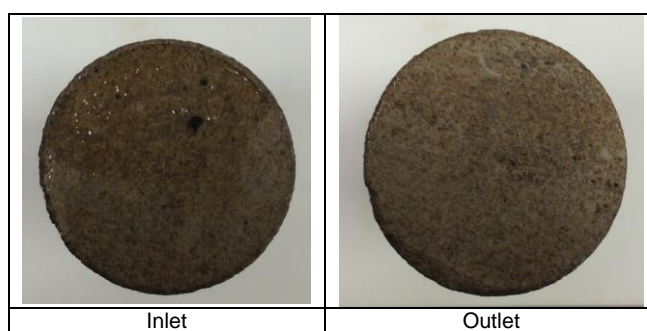
| Inlet | Outlet |

Fig. III.5– Inlet and outlet photos of the core tested with 7.5 wt% HCl solution, no Fe^{3+} and relatively higher permeability.
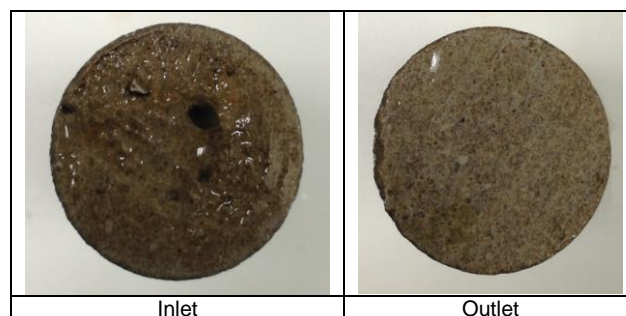
| Inlet | Outlet |

Fig. III.6– Inlet and outlet photos of the core tested with 12.5 wt% HCl solution, no Fe^{3+} and relatively higher permeability.
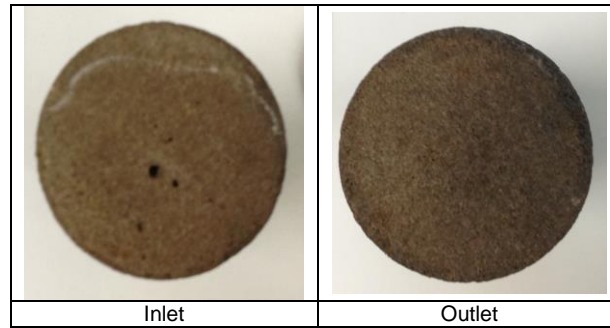
| Inlet | Outlet |

Fig. III.7– Inlet and outlet photos of the core tested with 7.5 wt% HCl solution, no Fe^{3+}.
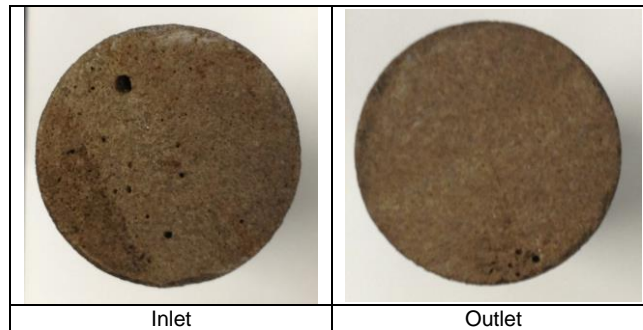
| Inlet | Outlet |

Fig. III.8– Inlet and outlet photos of the core tested with 12.5 wt% HCl solution, no Fe^{3+}.

Effect of iron concentration

Different solutions of HCl (5 – 10 wt%) containing (5,000 - 10,000 ppm) Fe^{3+} were injected through 6 in. low-permeability Indiana Limestone cores (1 – 5 md) to determine the damage due to the iron precipitation. **Table III.3** gives the details of the tested cores.

Table III.3– Data for coreflood experiments with Fe^{3+}.

Run #	Acid Conc., wt%	T, °F	Iron Amount, ppm	Core Length, in.	Core Porosity, Fraction	Initial K, md	Injection Rate, cm³/min	Final K, md	K Enhancement	Iron Recovered, Fraction
1	5	200	10,000	6	0.13	1.05	1.0	1.05	1.00	0.16
2	5	200	5,000	6	0.11	2.31	1.0	2.58	1.12	0.20
3	10	200	10,000	6	0.14	1.01	1.0	1.00	0.99	0.33
4	10	200	5,000	6	0.14	1.62	1.0	2.33	1.44	0.15
5	5	300	10,000	6	0.13	1.10	1.0	0.95	0.86	0.32
6	10	300	10,000	6	0.15	1.86	1.0	2.2	1.18	0.29
7	5	200	10,000	6	0.13	1.12	2.0	Breakthrough*	-	0.65
8	10	200	10,000	20	0.14	1.53	1.0	1.77	1.15	0.58
9	10	200	10,000	6	0.17	159	1	148	0.92	0.34

* At breakthrough, the pressure drop decreased to values around 10 psi. The permeability enhancement was greater than 500 fold in all cases.

In the first set of experiments, (5 – 10 wt%) HCl acid solutions containing 10,000 ppm Fe^{3+} were injected. **Figs. III.9** and **III.10** show the pressure drop profile across the core during HCl solution injection. The pressure drop across the cores was initially constant during the injection of 5 wt% NaCl brine. At the instant when the acid injection started, the pressure drop increased due to the higher viscosity of acid, the CO_2 released during the acid reaction with the rock, and/or the iron precipitation. Then, the pressure drop decreased due to the HCl acid reaction with the rock and wormholes creation. After 0.5 PV of the treatment, the flow was switched back to the 5 wt% NaCl brine. Finally, pressure drop stabilized again. The final pressure drop was almost the same as the initial pressure drop before acid injection, indicating that the acidizing job failed.

Fig. III.9– Pressure drop across the core for the 5 wt% HCl solution with 10,000 ppm Fe^{3+} at 200°F.
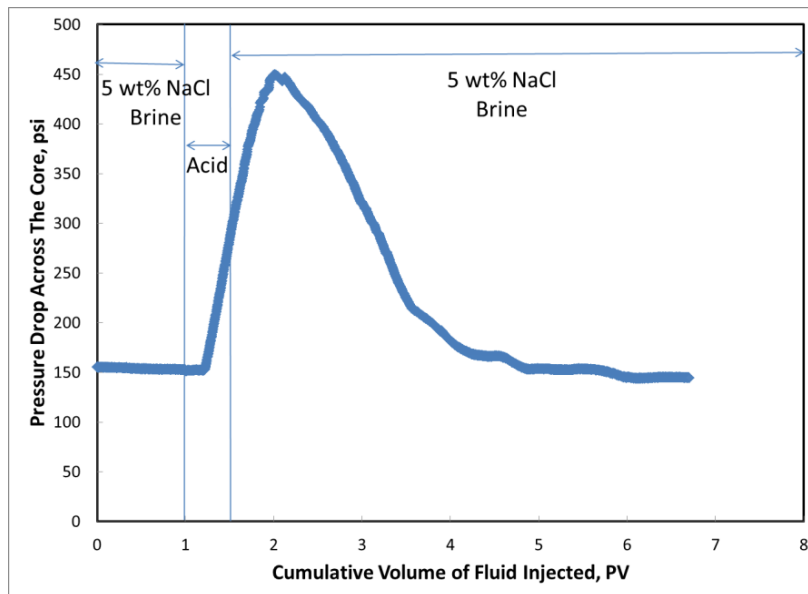
Fig. III.10– Pressure drop across the core for the 10 wt% HCl solution with 10,000 ppm Fe^{3+} at 200°F.

37

In the second set of experiments, (5 – 10 wt%) HCl acid solutions containing 5,000 ppm Fe^{3+} were injected. **Figs. III.11** and **III.12** show the pressure drop profile across the core during the HCl solution injection. The pressure drop across the core was initially constant during the injection of 5 wt% NaCl brine. At the instant when acid injection started, the pressure drop decreased due to the HCl acid reaction with rock and wormholes creation. After 0.5 PV of the treatment, the flow was switched back to 5 wt% NaCl brine. Finally, the pressure drop stabilized again. The final pressure drop was lower than the initial pressure drop before the acid injection, indicating that the final permeability was enhanced although some of the iron had precipitated. The permeability enhancement increased with initial acid concentration.
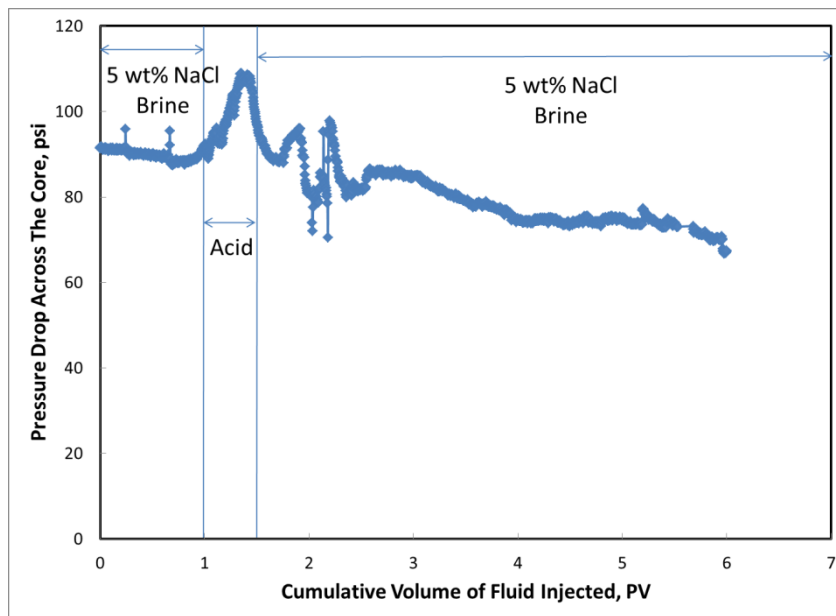
Fig. III.11– Pressure drop across the core for the 5 wt% HCl solution with 5,000 ppm Fe^{3+} at 200°F.
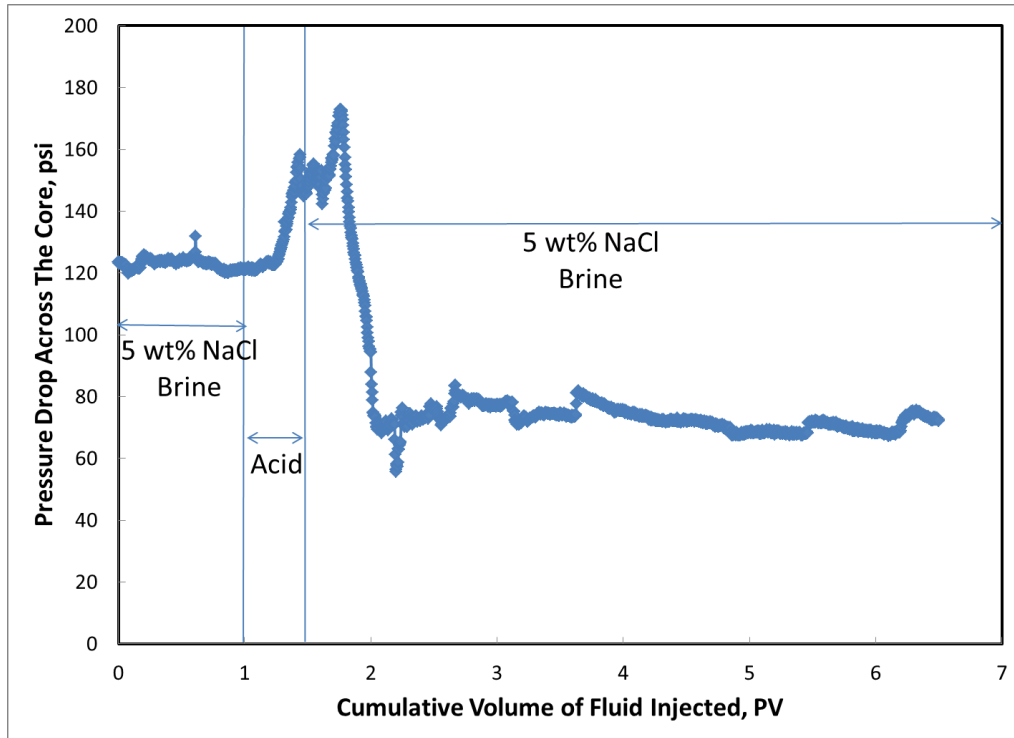
Fig. III.12– Pressure drop across the core for the 10 wt% HCl solution with 5,000 ppm Fe^{3+} at 200°F.

Figs. III.13 through III.16 show photos of the inlet and outlet of some of the cores tested. Iron precipitation occurred on the inlet face and at the walls of wormholes. In these test, no breakthrough occurred. It is clear that wormholes did not reach the core outlet.

39

| Inlet | Outlet |

Fig. III.13– Inlet and outlet photos of the core tested with 5 wt% HCl solution of 10,000 ppm Fe^{3+}.
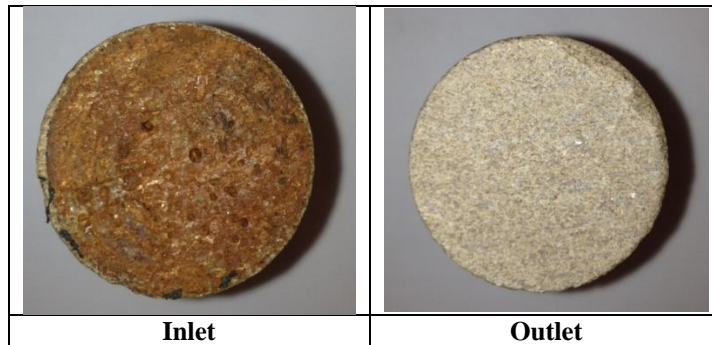
| **Inlet** | **Outlet** |

Fig. III.14– Inlet and outlet photos of the core tested with 10 wt% HCl solution of 10,000 ppm Fe^{3+}.
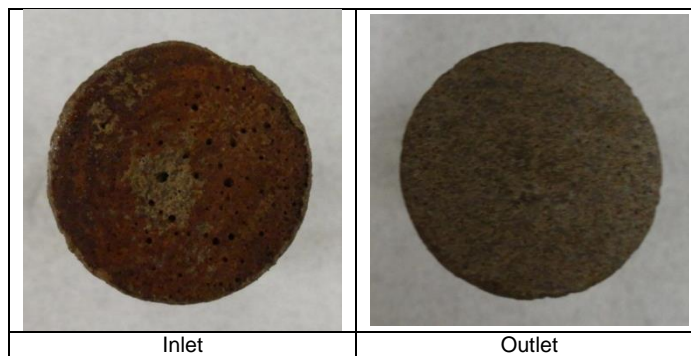
| Inlet | Outlet |

Fig. III.15– Inlet and outlet photos of the core tested with 5 wt% HCl solution of 5,000 ppm Fe^{3+}.

<table>
<tr><td>Inlet</td><td>Outlet</td></tr>
</table>
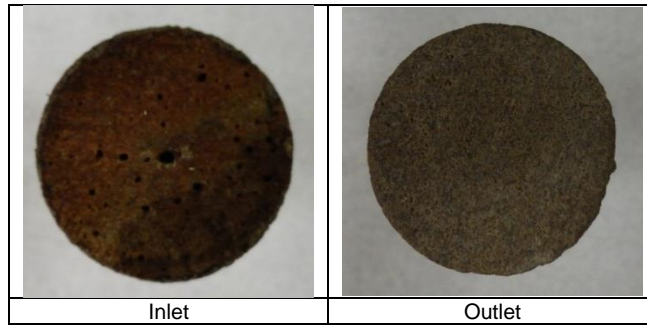
Fig. III.16– Inlet and outlet photos of the core tested with 10 wt% HCl solution of 5,000 ppm Fe^{3+}.

Effect of temperature

Different solutions of HCl (5 – 10 wt%) containing 10,000 ppm Fe^{3+} were injected through 6 in. low-permeability Indiana Limestone cores (1 – 5 md) to determine the effect of temperature on the damage caused by the iron precipitation. **Table III.3** gives the details of the tested cores.

Figs. III.17 and III.18 show the pressure drop profile across the core during the (5 – 10 wt%) HCl solutions injection. The pressure drop across the cores was initially constant during the injection of the 5 wt% NaCl brine. At the instant when acid injection started, the pressure drop increased due to the higher viscosity of the acid, the CO_2 released during the acid reaction with the rock, and/or iron precipitation. Then the pressure drop decreased due to the HCl acid reaction with the rock and wormholes creation. After 0.5 PV of the treatment, the flow was switched back to the 5 wt% NaCl brine. Finally, the pressure drop stabilized again.

At higher temperatures, the degree of damage depends on the initial acid concentration. The core was damaged when 5 wt% HCl solution was used, while 10 wt% HCl solution showed an enhancement in the permeability.
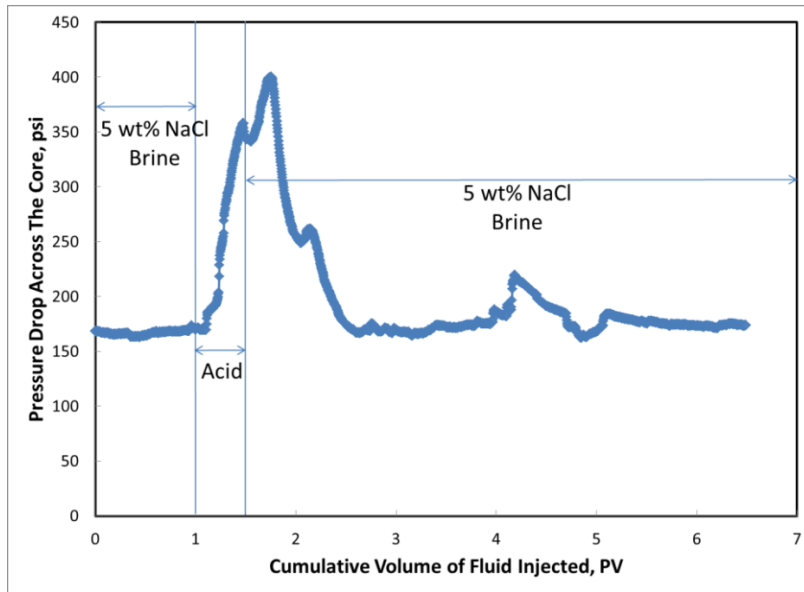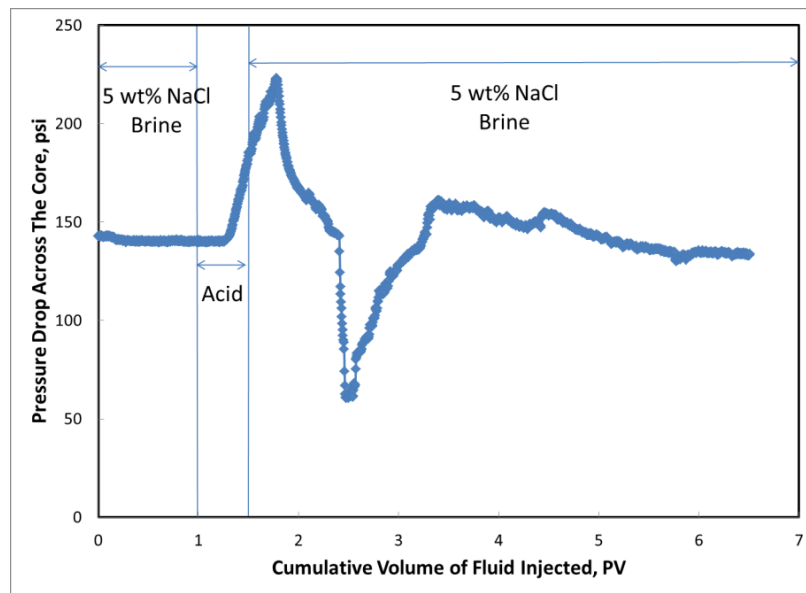

Fig. III.17– Pressure drop across the core for 5 wt% HCl solution with 10,000 ppm Fe^{3+} at 300°F.
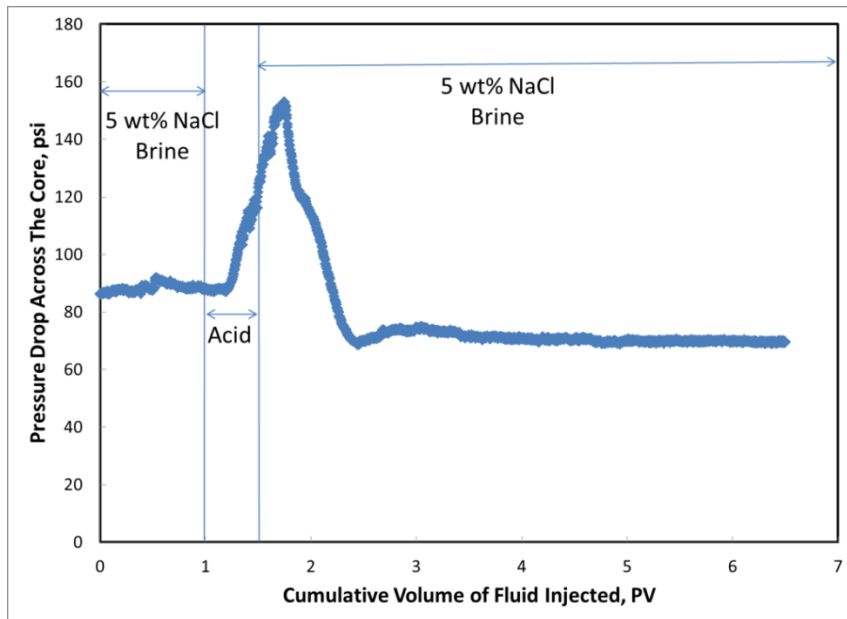
Fig. III.18– Pressure drop across the core for 10 wt% HCl solution with 10,000 ppm Fe^{3+} at 300°F.

Figs. III.19 and III.20 show photos of the inlet and outlet of the cores tested. Iron precipitation occurred on the inlet face and at the walls of wormholes. In these test, no breakthrough occurred. It is clear that wormholes did not reach the core outlet.

Fig. III.19– Inlet and outlet photos of the core tested with 5 wt% HCl solution of 10,000 ppm Fe^{3+} at 300°F.
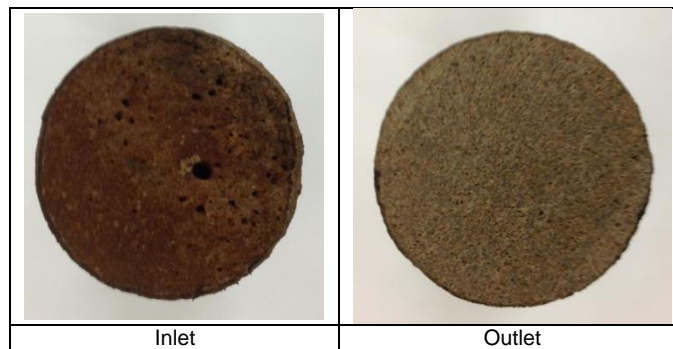
Fig. III.20– Inlet and outlet photos of the core tested with 10 wt% HCl solution of 10,000 ppm Fe^{3+} at 300°F.

Effect of flow rate

A solution of 10 wt% HCl containing 10,000 ppm Fe^{3+} was injected through a 6 in. low-permeability Indiana Limestone core (1.05 md) to determine the effect of flow rate on the damage caused by the iron precipitation. **Table III.3** gives the details of the tested core.

Fig. III.21 shows the pressure drop profile across the core during the acid injection. In this case, breakthrough occurred. It is obvious that the degree of stimulation depends on two factors the acid concentration and the injection rate.

At a higher flow rate, the damage due to iron precipitation was minimized. The final permeability increased and breakthrough occurred, which indicated an overall stimulation in spite of the iron precipitation. The damage due to the iron precipitation is affected by the optimum flow rate.
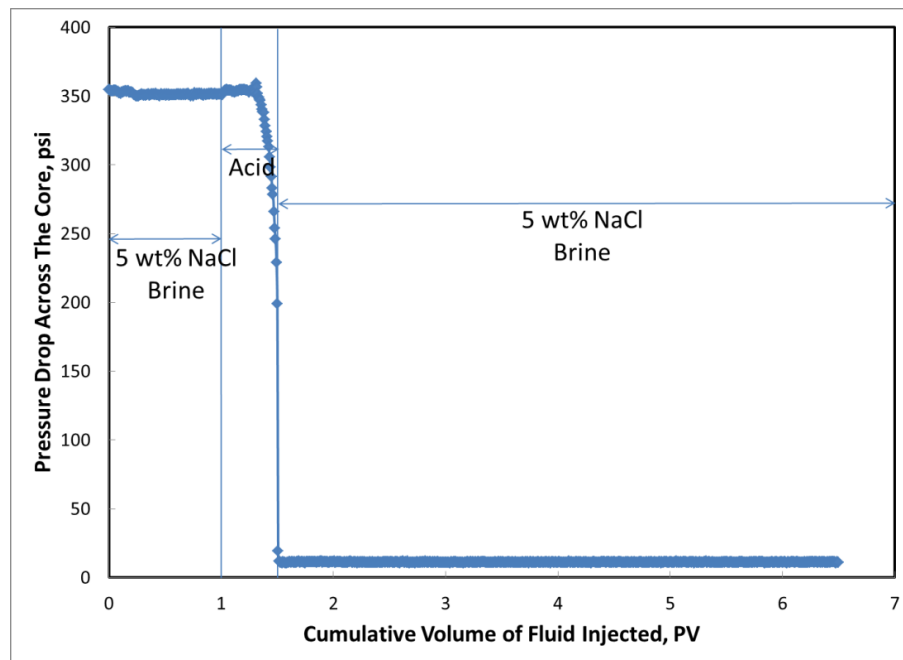
Fig. III.21– Pressure drop across the core for the 10 wt% HCl solution with 10,000 ppm Fe^{3+} at 2 cm^3/min.

Fig. III.22 shows photos of the inlet and outlet of the core tested. Iron precipitation occurred on the inlet face and at the walls of wormholes. In this test, breakthrough occurred. It is clear that the wormholes reached the core outlet.
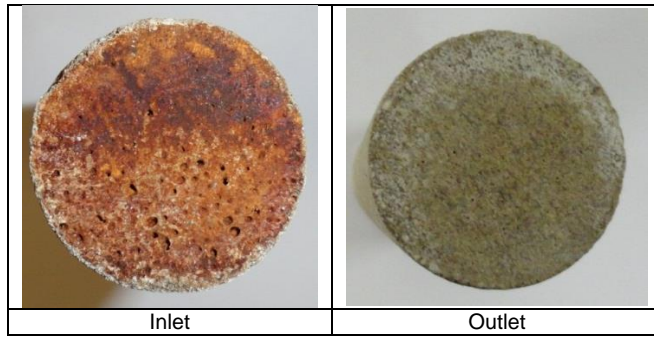

| Inlet | Outlet |

Figure III.22– Inlet and outlet photos of the core tested with 5 wt% HCl solution of 10,000 ppm Fe^{3+} at 2 cm^3/min.

Effect of core length

A solution of 10 wt% HCl containing 10,000 ppm Fe^{3+} was injected through a 20 in. low-permeability Indiana Limestone core (1.53 md) to determine the effect of core length on the damage caused by the iron precipitation. **Table III.3** gives the details of the tested core.

Fig. III.23 shows the pressure drop profile across the core during the 5 wt% HCl solution injection. The pressure drop across the core was initially constant during the injection of the 5 wt% NaCl brine at 170 psi. At the instant when acid injection started,

the pressure drop increased due to the higher viscosity of the acid, the CO_2 released during the acid reaction with the rock, and/or the iron precipitation. Then, the pressure drop decreased due to the HCl acid reaction with the rock and wormholes creation. After 0.5 PV of the treatment, the flow was switched back to 5 wt% NaCl brine. Finally, pressure drop stabilized again at 175 psi. The final pressure drop was almost the same as the initial pressure drop before the acid injection, indicating that the acidizing job failed.

Using longer cores did not affect acid stimulation. Wormholes extended only one tenth of the core length, the same as with the shorter cores. The final permeability remained almost the same indicating a poor acidizing job.
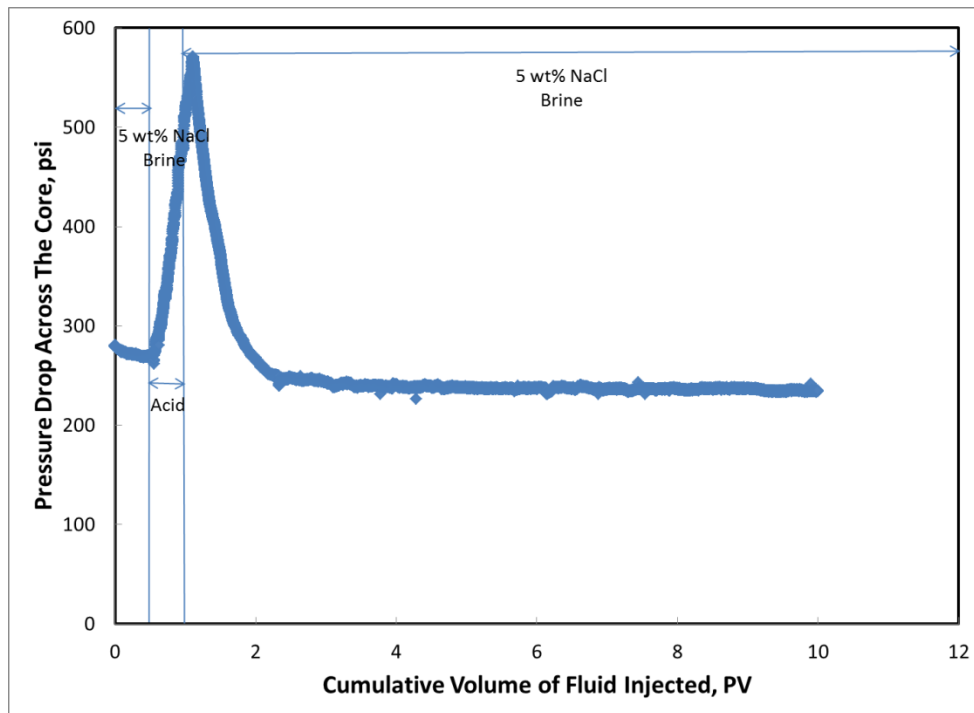
Fig. III.23– Pressure drop across a 20 in. core for 10 wt% HCl solution with 10,000 ppm Fe^3.

Fig. III.24 shows photos of the inlet and outlet of the core tested. Iron precipitation occurred on the inlet face and at the walls of wormholes. In this test, breakthrough occurred. It is clear that the wormholes reached the core outlet.
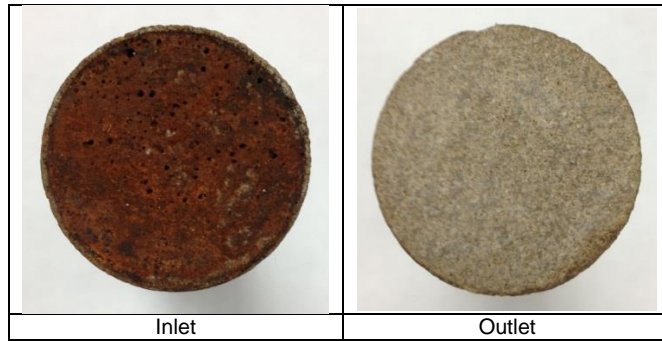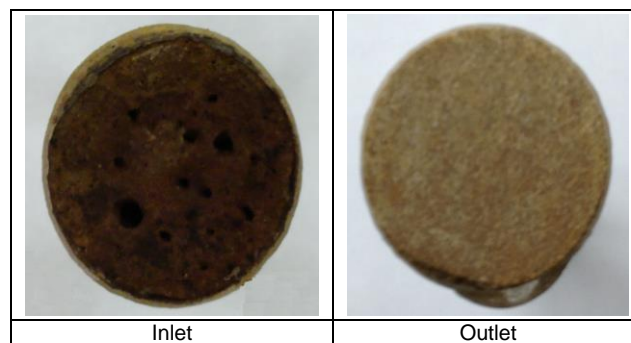

| Inlet | Outlet |

Fig. III.24– Inlet and outlet photos of 20 in. core tested with 10 wt% HCl solution of 10,000 ppm Fe^{3+}.

Effect of initial permeability

A solution of 10 wt% HCl containing 10,000 ppm Fe^{3+} was injected through a high permeability Indiana Limestone core (159 md) at 200°F to determine the effect of the initial core permeability on the damage caused by the iron precipitation. **Table III.3** gives the details of the tested core.

Fig. III.25 shows the pressure drop profile across the core during the 5 wt% HCl solution injection. The pressure drop across the core was initially constant during the injection of the 5 wt% NaCl brine around 4.5 psi. At the instant when acid injection

started, the pressure drop increased due to the higher viscosity of the acid, CO_2 released during the acid reaction with the rock, and/or iron precipitation. Then the pressure drop decreased due to the HCl acid reaction with the rock and wormhole creation. After 0.5 PV of the treatment, the flow was switched back to the 5 wt% NaCl brine. Finally, pressure drop stabilized again around 4 psi. The final pressure drop was almost the same as the initial pressure drop before the acid injection, indicating that the acidizing job failed.

Using high permeability cores did not affect the degree of acid stimulation. The final permeability decreased, indicating damage.
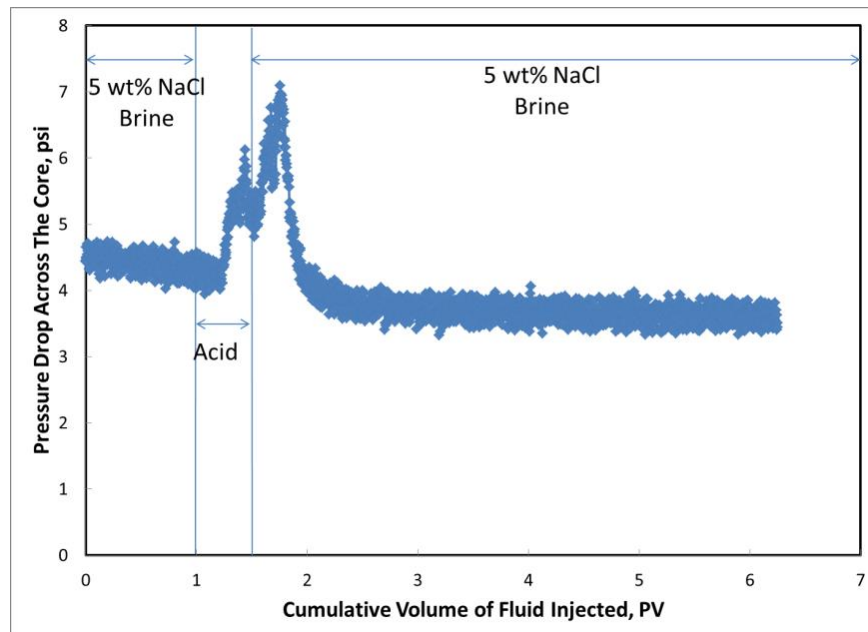
Fig. III.25– Pressure drop across a high permeability core for 10 wt% HCl solution with 10,000 ppm Fe^{3+}.

Fig. III.26 shows photos of the inlet and outlet of the core tested. Iron precipitation occurred on the inlet face and at the walls of wormholes. In this test, no breakthrough occurred. It is clear that wormholes did not reach the core outlet.
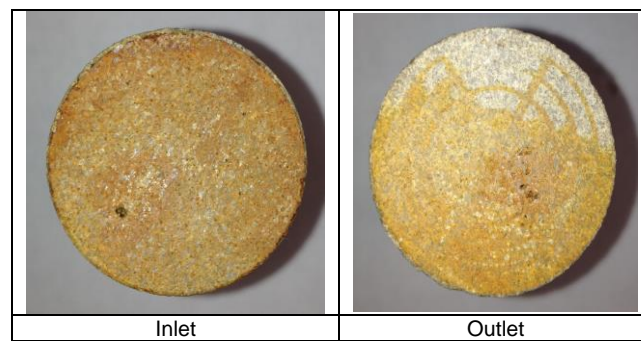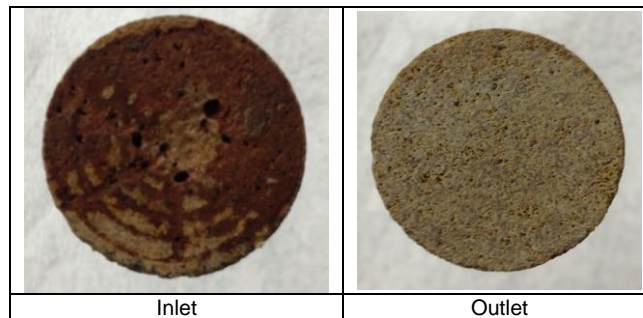

| Inlet | Outlet |

Fig. III.26– Inlet and outlet photos of the high permeability core tested with 10 wt% HCl solution of 10,000 ppm Fe^{3+}.

CT Scan

Cores were scanned using a CT scanner for better understanding of the wormhole propagation. **Figs. III.27** through **III.34** show 2D scan images for the 6 and 20 in. long, low-permeability (1 - 5 md) cores treated by different acid solutions at flow rates of (1-2) cm^3/min, and at a temperature of (200 - 300)ºF. No face dissolution was noticed in the cores inlet face for any of the acid concentrations studied. Upon injection inside the core, acid started to react with the rock and created wormholes. This can be detected through inspection of the dark spots, indicating a low CT number and, so a low density. The 2D images show that, sometimes, there is more than one wormhole created in the core.

Figs. III.27 and III.28 show that the propagation of wormholes does not depend on the initial HCl acid concentration when both high iron concentrations are present and no chelating agent is used.

Fig. III.27– CT scanned image for the 6 in. long low-permeability Indiana limestone cores tested with 5 wt% HCl solution, 10,000 ppm Fe^{3+}.
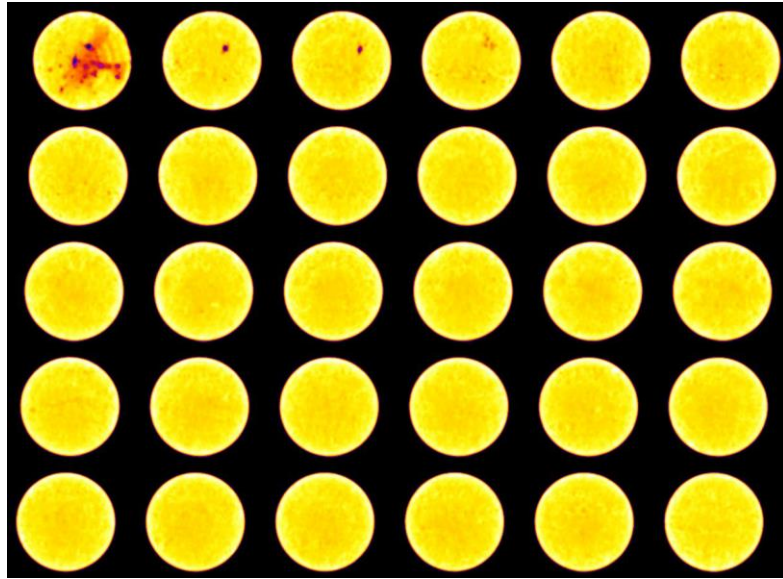
Fig. III.28– CT scanned image for the 6 in. long low-permeability Indiana limestone cores tested with 10 wt% HCl solution, 10,000 ppm Fe^{3+}.

Figs. III.29 and III.30 show that the wormholes propagation increases with both the initial HCl acid concentration when low iron concentrations are present and and no chelating agent is used.

.
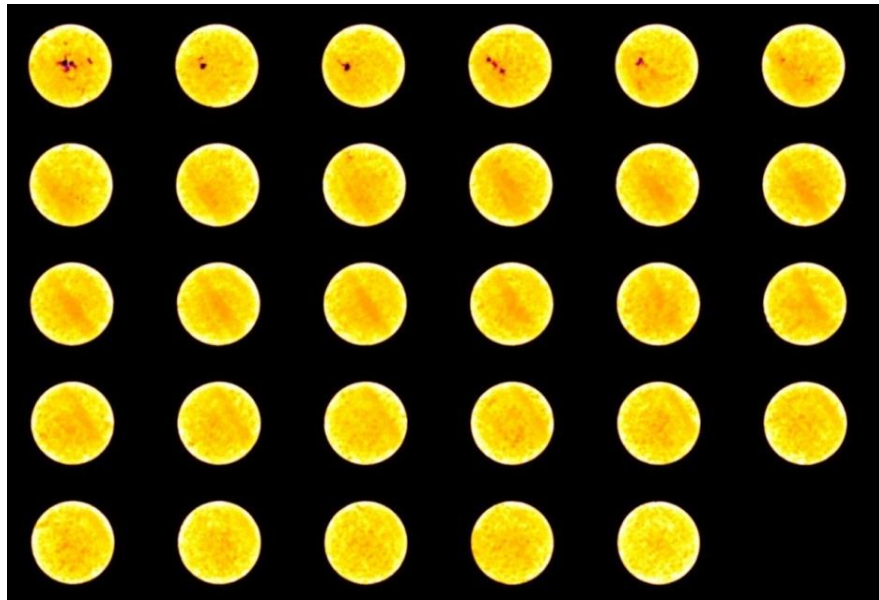
Fig. III.29– CT scanned image for the 6 in. long low-permeability Indiana limestone cores tested with 5 wt% HCl solution, 5,000 ppm Fe^{3+}.
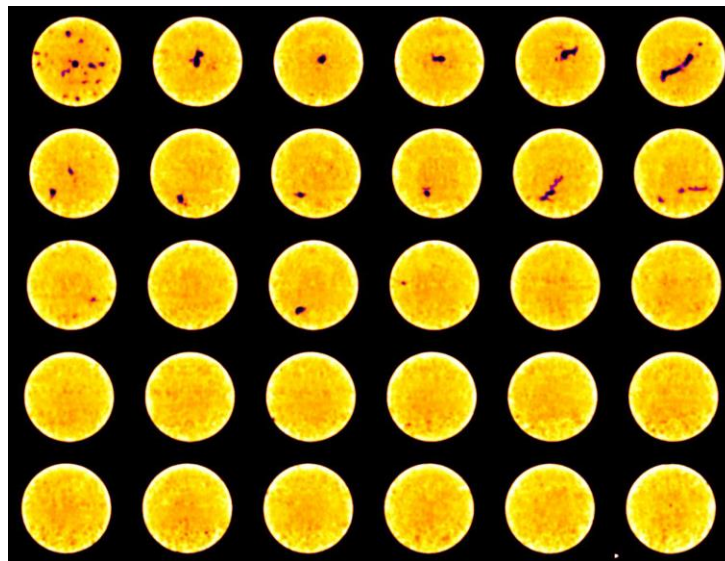
Fig. III.30– CT scanned image for the 6 in. long low-permeability Indiana limestone cores tested with 10 wt% HCl solution, 5,000 ppm Fe^{3+}.

Figs. **III.31 and III.32** show that, at high temperatures when no chelating agent is used, the wormhole extended further with the initial acid concentration. The wormholes get wider with higher acid concentrations.
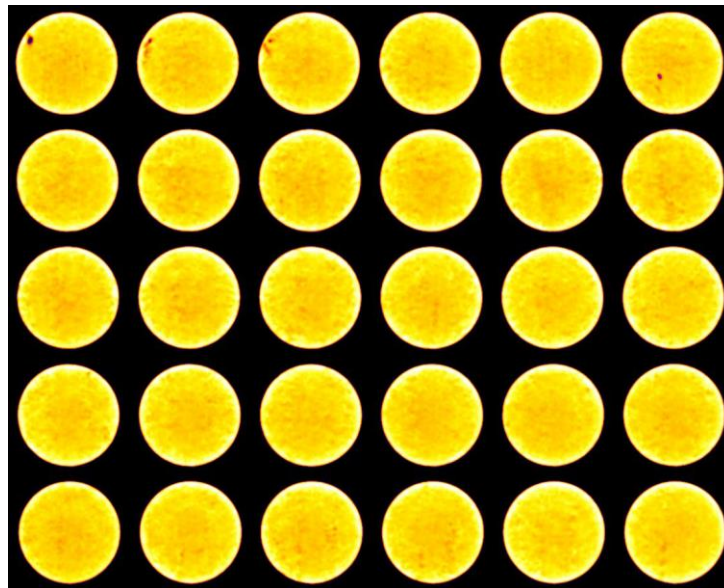
Fig. III.31– CT scanned image for the low-permeability Indiana limestone cores tested with 5 wt% HCl solution, 10,000 ppm Fe^{3+} at 300°F.
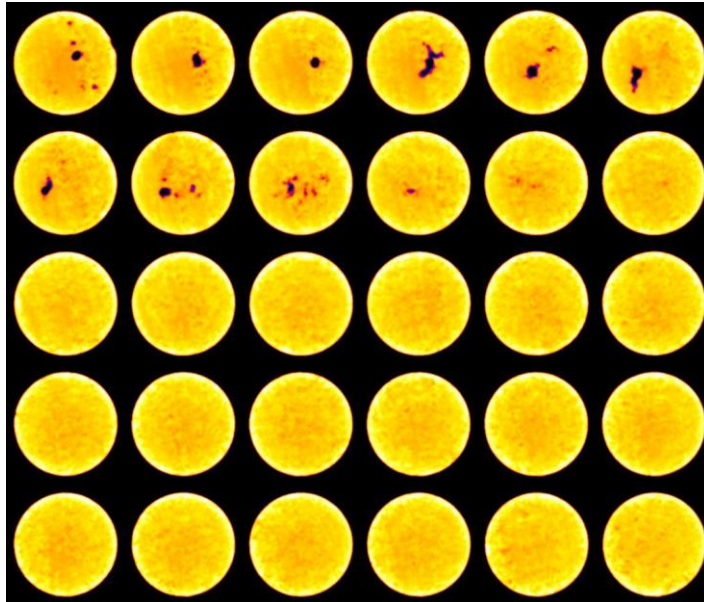
Fig. III.32– CT scanned image for the low-permeability Indiana limestone cores tested with 10 wt% HCl solution, 10,000 ppm Fe^{3+} at 300°F.

Fig. III.33 shows that there is a breakthrough at an injection rate of 2 cm^3/min regardless of the iron precipitation; this can be attributed to optimum HCl acid injection rate. When comparing **Figs. III.34 and Fig III.24,** it is clear that, for the same injection conditions when no chelating agent is used, the wormhole did not extend further in the core regardless of the core length. The pressure drop across the cores was recorded during the acid injection, the initial permeability, the final permeability, and the permeability ratio were calculated. These results are shown in **Tables III.3,** and reveal that, in the absence of iron control agents for low-permeability Indiana limestone cores (1 - 5 md), there was no overall enhancement in the final permeability in most cases

except in the case of higher flow rates, or the combination of a higher acid concentration

and temperature.
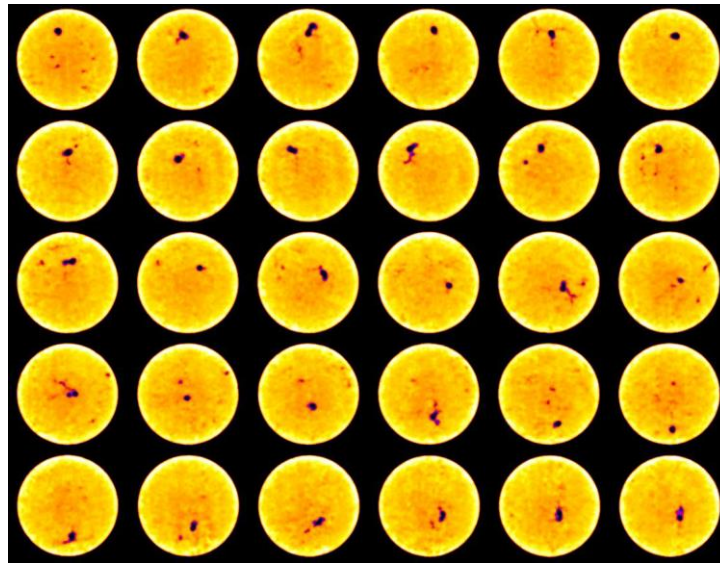
Fig. III.33– CT scanned image for the low-permeability Indiana limestone cores tested with 5 wt% HCl solution, 10,000 ppm Fe^{3+} at 2 cm^3/min.
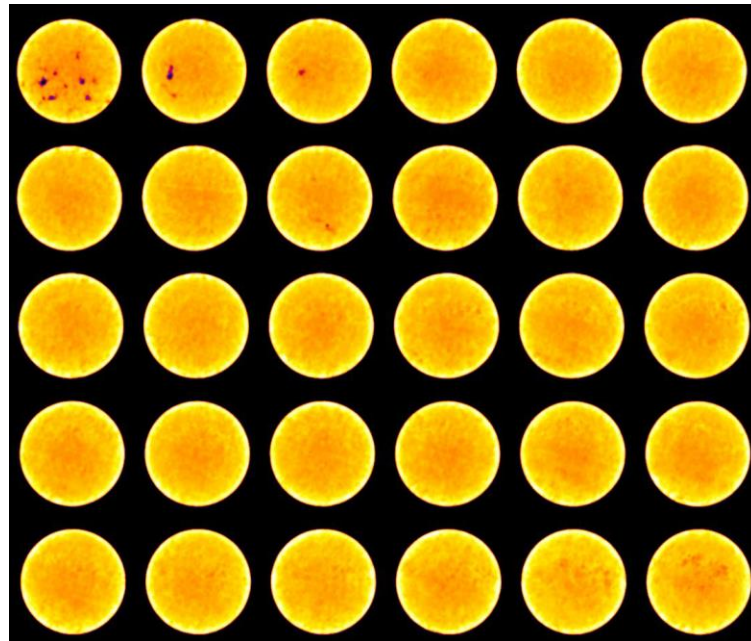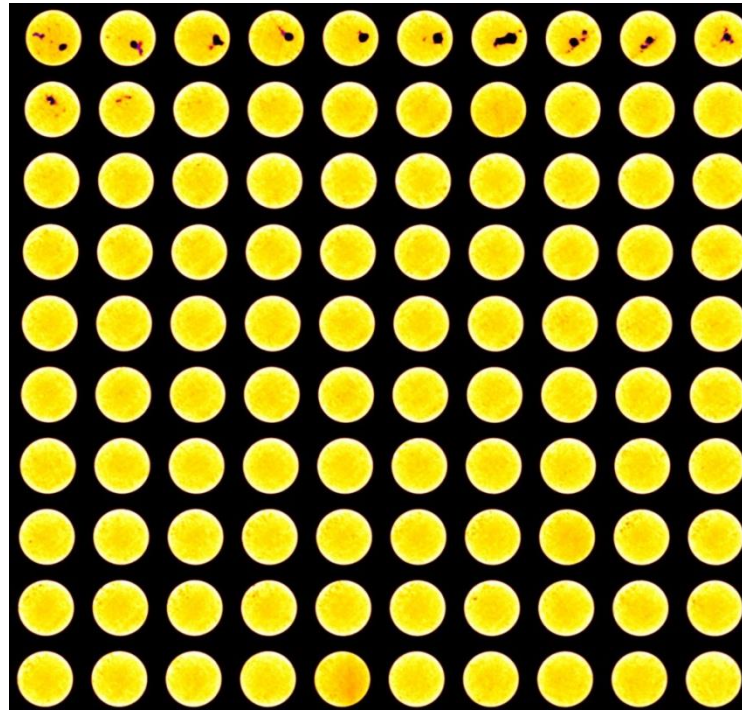
Fig. III.34– CT scanned image for the 20 in. long low-permeability Indiana limestone cores tested with 10 wt% HCl solution, 10,000 ppm Fe^{3+}.

Analysis of Core Effluent Samples

Figs. III.35 through III.37 show the total iron and calcium concentrations in the core effluent samples for some of the experiments performed without at different conditions. Knowing the initial amount of iron injected, the volume and the iron concentration recovered from each sample, the percent of iron recovered can be calculated from the following equation:

$$\% \text{ iron recovered} = \frac{\sum sample\ volume \times iron\ concentration}{Total\ iron\ injected} \times 100\ \% \tag{3.2}$$
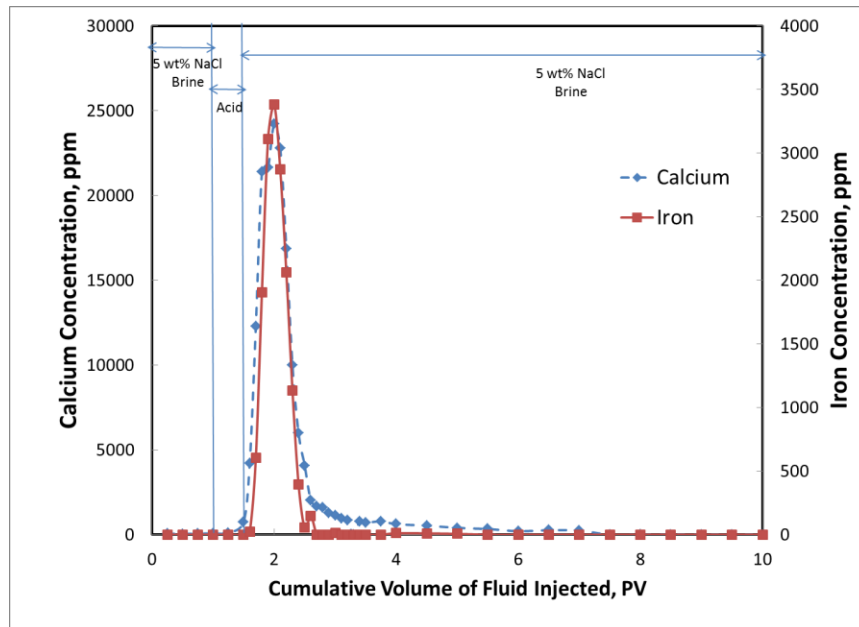
Fig. III.35– Total calcium and iron concentration for 10 wt% HCl, 10,000 ppm Fe^{3+} at 200°F for 20 in. core.
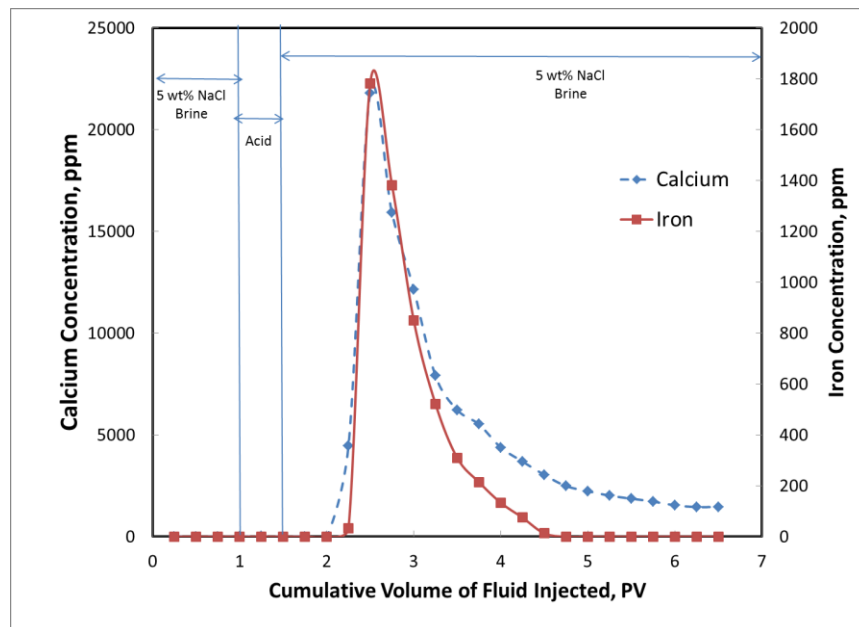
Fig. III.36– Total iron concentration for 10 wt% HCl, 10,000 ppm Fe^{3+} at 300°F.
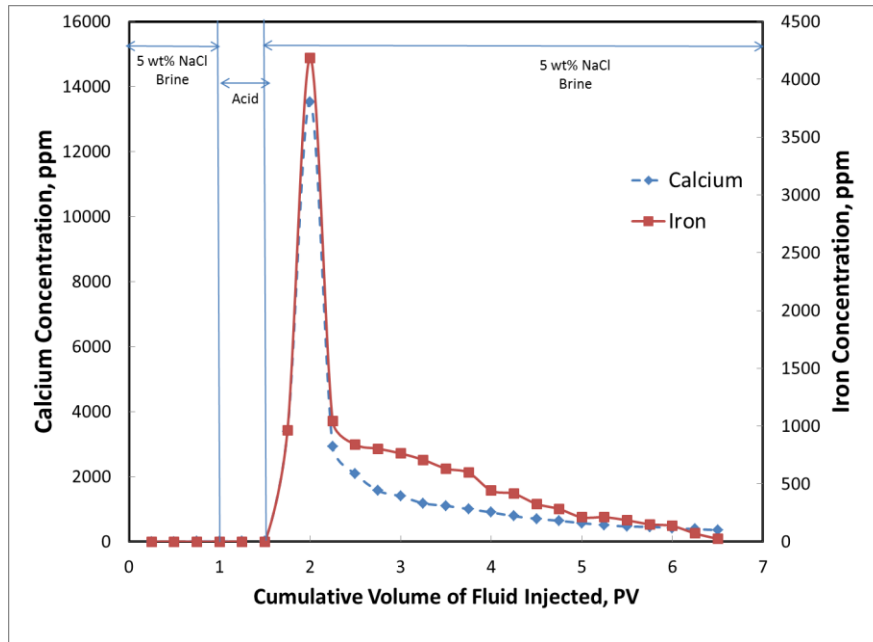
Fig. III.37– Total calcium and iron concentration for 10 wt% HCl, 10,000 ppm Fe^{3+} at 2 cm^3/min.

Some of the samples showed iron precipitation. HCl acid was used to dissolve these precipitates and was taken into account while measuring the iron concentrations in the core effluent samples. **Fig III.38** shows an example of these samples before and after adding live HCl to the core effluent samples. After acid is introduced to the samples, the iron precipitates dissolve and the samples become clear.
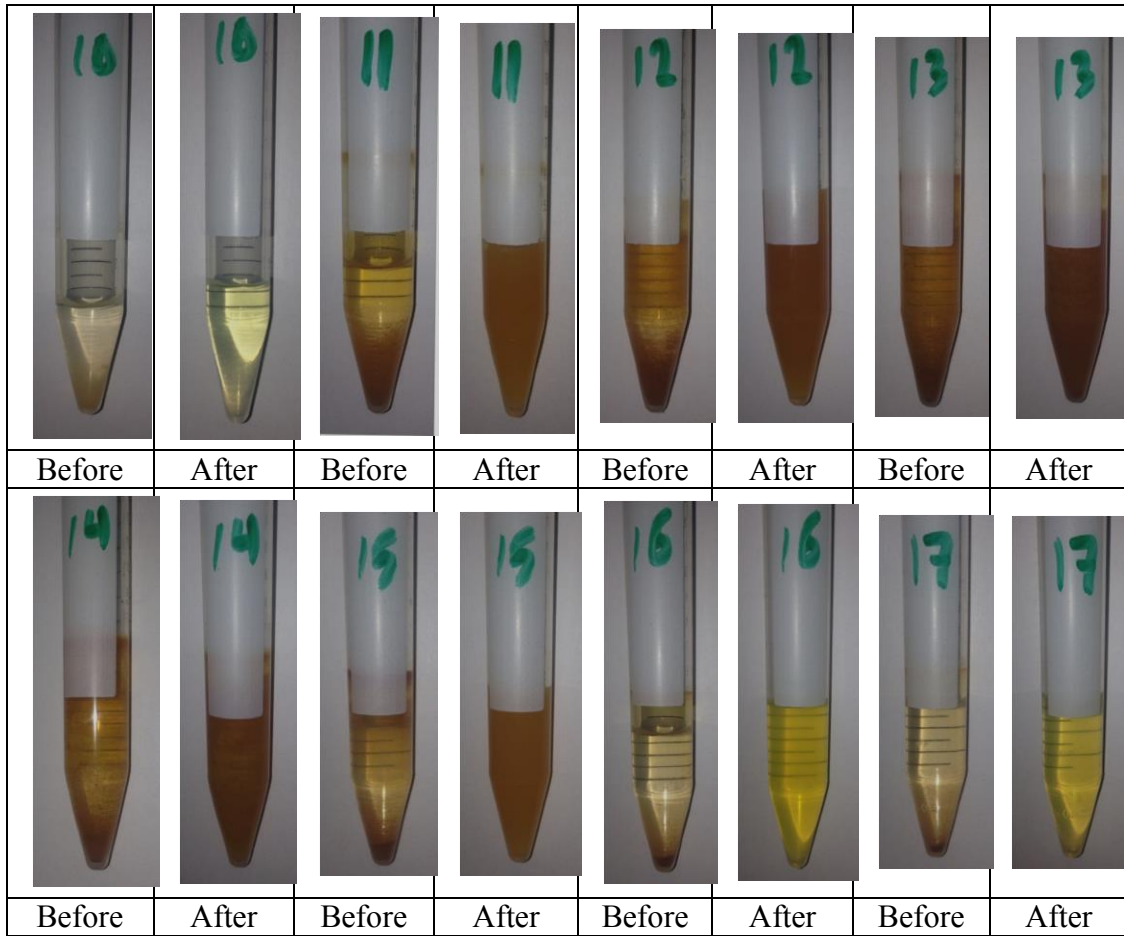
Fig. III.38– Core effluent samples before and after adding live HCl.

In general, the amounts of iron recovered without iron control are low except for some cases where acid breakthrough occurred. Also, the final permeability in most of the experiments did not change much from initial permeability, which means poor acidizing jobs. The data is given in **Table III.3**.

CHAPTER IV

USING CHELATING AGENTS TO MINIMIZE FORMATION

DAMAGE

Introduction

During matrix acidizing, successful iron control can be critical to the success of the treatment. Iron (III) precipitation occurs when acids are spent and the pH rises above 1, which can cause severe formation damage. Chelating agents are used during these treatments to minimize iron precipitation.

In this chapter, the effect of iron precipitation in acidizing operations is studied. HCl solutions (5 - 20 wt%) containing 5,000 to 10,000 ppm of Fe^{3+} were used in these experiments. Two chelating agents, widely used HEDTA and biodegradable GLDA (glutamic-N, N-diacetic acid), were studied in these experiments. The effect of varying acid concentration and chelate-to-iron mole ratio was examined. Coreflood experiments were conducted on low permeability Indiana limestone (1 - 5 md) at 200°F. The cores were scanned after treatments using a CT scanner. The core effluent samples were analyzed for the total iron and calcium concentrations using ICP-OES. A calcium ion-selective electrode was used to determine the concentration of free calcium ions, i.e. calcium ions not complexed by the chelate, in the core effluent samples.

Results showed that the amount of iron recovered depended on both the chelate-to-iron mole ratio and the initial permeability of the cores. Calcium is chelated along with iron, which limits the effectiveness of chelating agents to control iron (III)

precipitation. Chelating agents are supposed to control iron now that calcium is also chelated, this amount should be accounted for. Acid solutions should be designed considering this important finding for more successful treatments. This paper will discuss the results obtained and give recommendations to enhance the effectiveness of these chemicals in the field.

Experimental Studies

Equipment

The coreflood setup, described in **Fig. II.1**, was constructed to simulate matrix stimulation treatment. The total iron and calcium concentrations of the core effluent samples were measured using the Optima 7000 ICP-OES Spectrometer. Finally, density, pH, and retained HCl concentration were measured for core effluent samples.

Results and Discussion

Coreflood Experiments

Coreflood experiments were run using the coreflood setup shown in **Fig. II.1**. Two sets of coreflood experiments were performed using low-permeability Indiana limestone .The first set of experiments was performed with different concentrations of HCl acid solutions containing $5,000 - 1,000$ ppm Fe^{3+} with GLDA. In the second set of HEDTA was used instead.

Before the acid treatment, the core was saturated using 5 wt% NaCl brine, the initial permeability was measured when pressure stabilized. During coreflood runs, 5 wt% NaCl brine was injected while the core was heated to the desired temperature. After

that 0.5 PV of the acid solution was injected then the cores were flushed again with 5 wt% NaCl brine. Finally, the cores were left to cool down and 5 wt% NaCl brine was injected at a constant rate until the pressure drop restabilized and the final permeability was measured.

These runs were performed to test the effect of amount of iron, acid concentration, and chelate-to-iron mole ratio on the iron precipitation. For each coreflood experiment, the pressure drop across the core was plotted using Lab-View software. Samples of the core effluent were analyzed for both iron and calcium concentrations. The pH values of the effluent samples were measured.

Limestone Cores with GLDA

Two sets of coreflood experiments were performed using low-permeability Indiana limestone. The first set of experiments was performed with 10,000 ppm Fe^{3+} and the data is given in **Table IV.1**. Five coreflood runs were performed using low-permeability Indiana limestone cores that were saturated with 5 wt% NaCl brine. The coreflood experiments were performed at a constant injection rate of 1 cm^3/min. These runs were performed to test the effect of chelate-to-iron mole ratio and acid concentration on iron recovery. All coreflood runs were performed at a temperature of 200ºF. The pressure drop across the core was recorded during acid injection at different acid concentrations 5 wt% HCl (with both chelate-to-iron mole ratios 1:1 and 2:1), 10 wt% HCl, 15 wt% HCl, and 20 wt% HCl. Samples of the core effluent were analyzed for both iron and calcium concentrations. The pH values of the effluent samples were measured.

Table IV.1– Data for coreflood experiments with GLDA, 10,000 ppm Fe^{3+}.

Run #	Acid Conc., wt%	Chelate-to-Iron Mole Ratio	Core Porosity, Fraction	Initial K, md	Injection Rate, cm³/min	Final K, md	K Enhancement	Iron Recovered, Fraction
1	5	1:1	0.14	1.34	1.0	1.87	1.40	0.16
2	5	2:1	0.14	1.75	1.0	7.94	4.55	0.37
3	10	1:1	0.12	0.95	1.0	1.94	2.03	0.20
4	15	1:1	0.13	2.91	1.0	Breakthrough*	-	0.62
5	20	1:1	0.14	1.42	1.0	5.01	3.54	0.18

* At breakthrough, the pressure drop decreased to values around 10 psi. The permeability enhancement was greater than 500 fold in all cases.

Figs. IV.1 through **IV.5** show the pressure drop profile across the cores. **Fig. IV.2** shows a typical pressure drop profile across the core during acid treatments. The pressure drop across the core was initially constant during the injection of 5 wt% NaCl brine at 170 psi. At the instant when acid injection started, the pressure drop increased due to the higher viscosity of acid, CO_2 released during the acid reaction with the rock, and/or iron precipitation. Then the pressure drop decreased due to HCl acid reaction with rock and wormholes creation. After 0.5 PV of the treatment, the flow was switched back to 5 wt% NaCl brine. Finally, pressure drop stabilized again at 95 psi. The final pressure drop was lower than the initial pressure drop before acid injection, indicating that the final permeability was enhanced although some of the iron precipitated as shown later in ICP. **Fig. IV.4** shows another typical pressure drop profile across the core acid treatments. The pressure drop across the core was initially constant during the injection of 5 wt% NaCl brine at 85 psi. When acid injection started, the pressure drop decreased due to HCl acid reaction with rock and creating wormholes. After 0.5 PV of the

treatment, the flow was switched back to 5 wt% NaCl brine. Finally, breakthrough occurred.
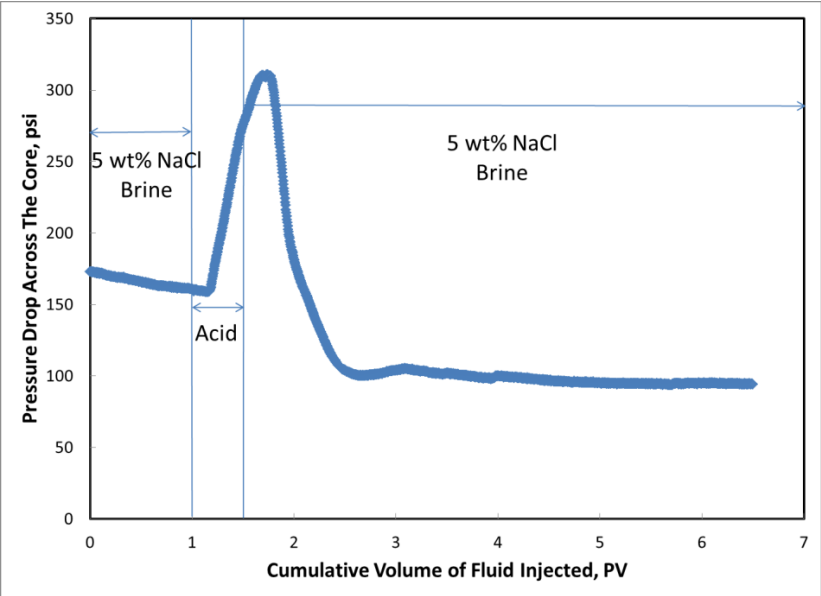
Fig. IV.1– Pressure drop across the core for 5 wt% HCl, 10,000 ppm Fe^{3+}, GLDA:Fe = 1:1.
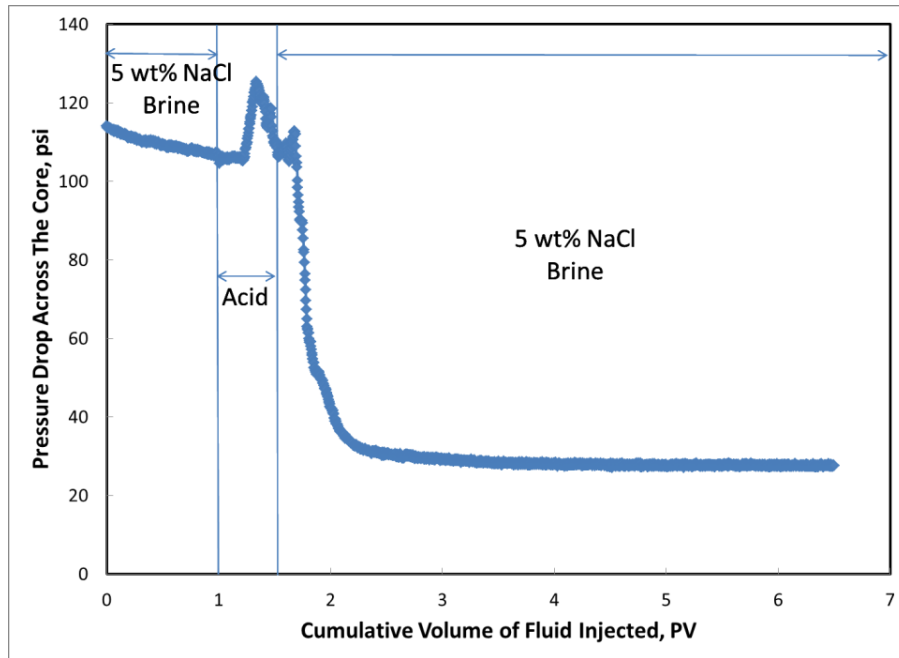
Fig. IV.2– Pressure drop across the core for 5 wt% HCl, 10,000 ppm Fe^{3+}, GLDA:Fe = 2:1.
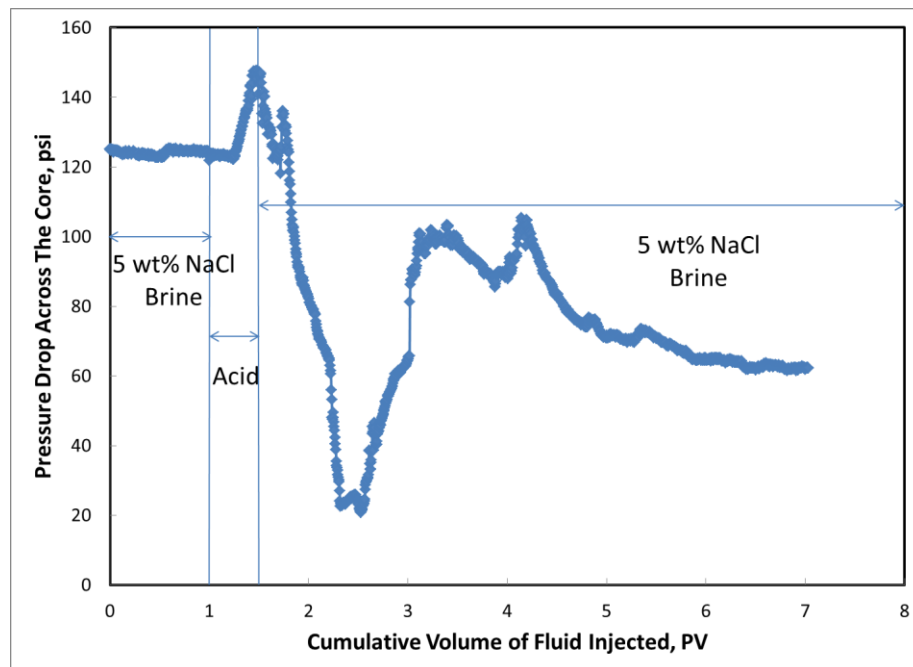
Fig. IV.3– Pressure drop across the core for 10 wt% HCl, 10,000 ppm Fe^{3+}, GLDA:Fe = 1:1.
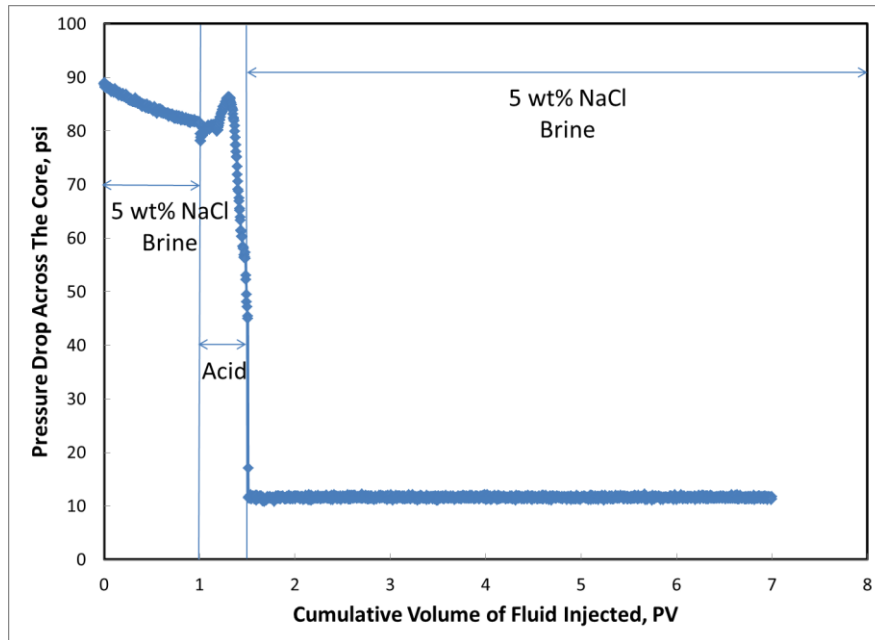
Fig. IV.4– Pressure drop across the core for 15 wt% HCl, 10,000 ppm Fe^{3+}, GLDA:Fe = 1:1.
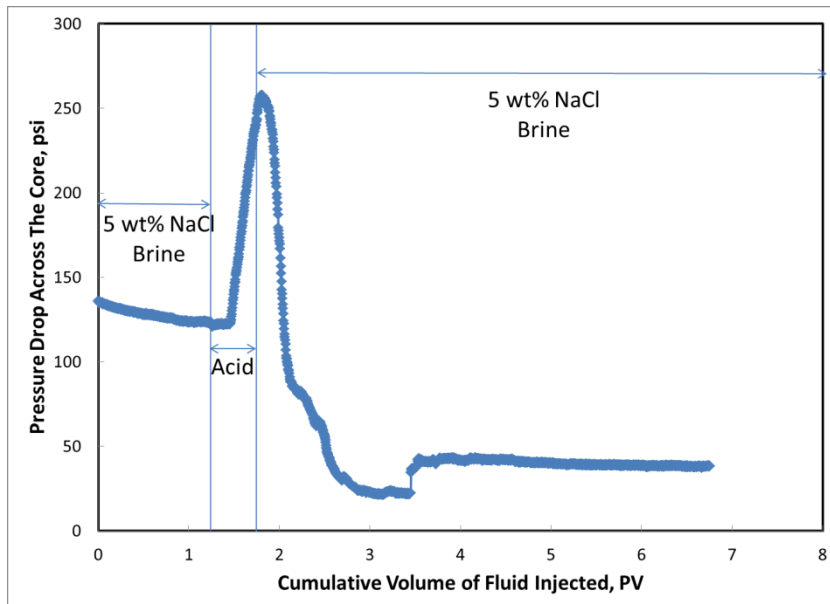
Fig. IV.5– Pressure drop across the core for 20 wt% HCl, 10,000 ppm Fe^{3+}, GLDA:Fe = 1:1.

Figs. IV.6 through IV.10 show photos of the inlet and outlet of the core tested with (5 - 20 wt%) HCl solutions of 10,000 ppm Fe^{3+} with GLDA. Significantly less iron precipitation occurred on the inlet face and at the walls of wormholes. At 15 wt% HCl, breakthrough occurred. It is clear that the wormholes reached the core outlet.

| Inlet | Outlet |

Fig. IV.6– Inlet and outlet for a core tested with 5 wt% HCl, 10,000 ppm Fe^{3+}, GLDA:Fe = 1:1.

| Inlet | Outlet |

Fig. IV.7– Inlet and outlet for a core tested with 5 wt% HCl, 10,000 ppm Fe^{3+}, GLDA:Fe = 2:1.
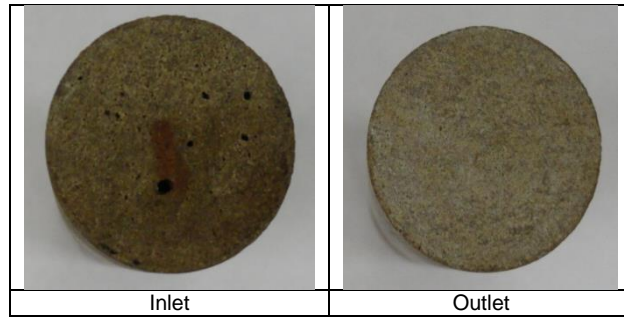
| Inlet | Outlet |

Fig. IV.8– Inlet and outlet for a core tested with 10 wt% HCl, 10,000 ppm Fe^{3+}, GLDA:Fe = 1:1.
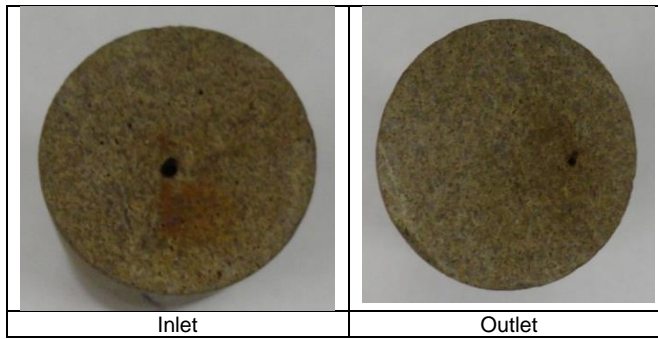
| Inlet | Outlet |

Fig. IV.9– Inlet and outlet for a core tested with 15 wt% HCl, 10,000 ppm Fe^{3+}, GLDA:Fe = 1:1.
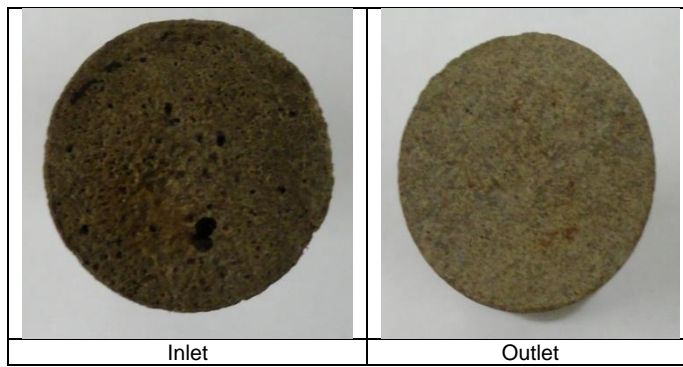
| Inlet | Outlet |

Fig. IV.10– Inlet and outlet for a core tested with 20 wt% HCl, 10,000 ppm Fe^{3+}, GLDA:Fe = 1:1.

The second set of experiments was performed with 5,000 ppm Fe^{3+} and the data is given in **Table IV.2**. Three coreflood runs were performed using low-permeability Indiana limestone cores that were saturated with 5 wt% NaCl brine. The coreflood experiments were performed at a constant injection rate of 1 cm^3/min. These runs were performed to test the effect of chelate-to-iron mole ratio and acid concentration on iron recovery. All the coreflood runs were performed at a temperature of 200ºF. The pressure drop across the core was recorded during acid injection at different acid concentrations 5 wt% HCl (with both chelate-to-iron mole ratios 1:1 and 2:1), and 10 wt% HCl. Samples of the core effluent were analyzed for both iron and calcium concentrations. The pH values of the effluent samples were measured.

Table IV.2– Data for coreflood experiments with GLDA, 5,000 ppm Fe^{3+}.

Run #	Acid Conc., wt%	Chelate-to-Iron Mole Ratio	Core Porosity, Fraction	Initial K, md	Injection Rate, cm³/min	Final K, md	K Enhancement	Iron Recovered, Fraction
1	5	1:1	0.14	1.08	1.0	2.29	2.12	0.26
2	5	2:1	0.13	0.97	1.0	2.69	2.78	0.21
3	10	1:1	0.13	1.32	1.0	1.76	1.34	0.11

* At breakthrough, the pressure drop decreased to 10 psi. The permeability enhancement was greater than 500 folds in all cases.

Figs. IV.11 through **IV.13** show the pressure drop profile across the cores. **Fig. IV.12** shows the pressure drop profile across the core tested with 5 wt% HCl and 5,000

ppm Fe^{3+}. The pressure drop across the core was initially constant during the injection of 5 wt% NaCl brine at 160 psi. When acid injection started, the pressure drop decreased. After 0.5 PV of the treatment, the flow was switched back to 5 wt% NaCl brine. Finally, pressure drop stabilized again at 70 psi. The final pressure drop was lower than the initial pressure drop before acid injection, indicating that the final permeability was enhanced, although some of the iron precipitated as shown later in ICP.
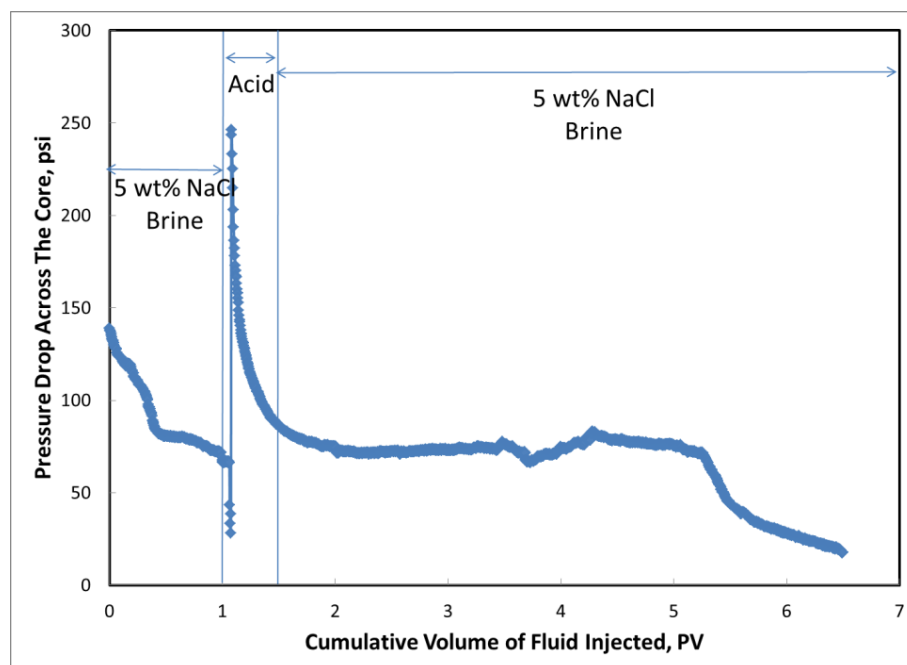
Fig. IV.11– Pressure drop across the core for 5 wt% HCl, 5,000 ppm Fe^{3+}, GLDA:Fe = 1:1.
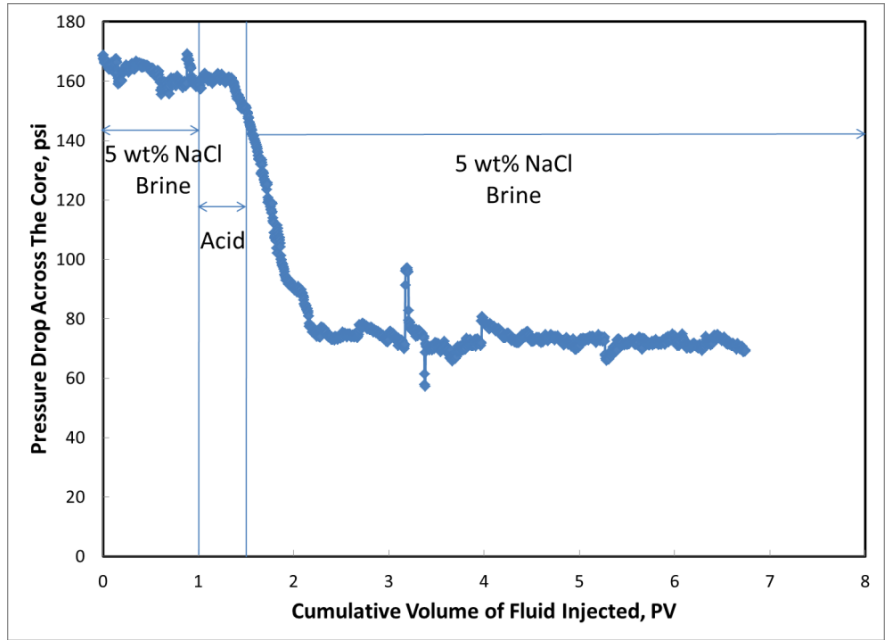
Fig. IV.12– Pressure drop across the core for 5 wt% HCl, 5,000 ppm Fe^{3+}, GLDA:Fe = 2:1.
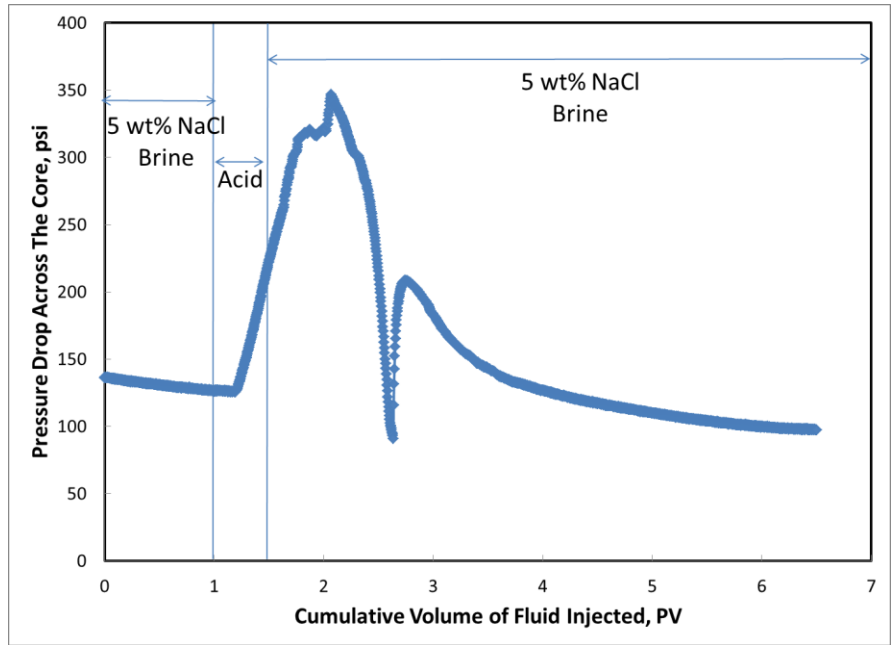
Fig. IV.13– Pressure drop across the core for 10 wt% HCl, 5,000 ppm Fe^{3+}, GLDA:Fe = 1:1.

Figs. IV.14 through IV.16 show photos of the inlet and outlet of the core tested with (5 - 10 wt%) HCl solutions of 5,000 ppm Fe^{3+} with GLDA. Fig. IV.14 shows images of the inlet and outlet of the core tested with 5 wt% HCl solution of 5,000 ppm Fe^{3+} and GLDA at a chelate-to-iron ratio of 1:1. A small amount of iron precipitation occurred on the inlet face and at the walls of wormholes. In this test, no breakthrough occurred. It is clear that the wormholes did not reach the core outlet.
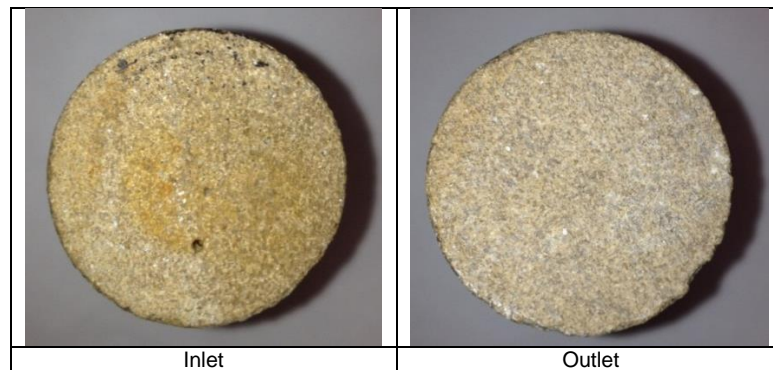
| Inlet | Outlet |

Fig. IV.14– Inlet and outlet for a core tested with 5 wt% HCl, 5,000 ppm Fe^{3+}, GLDA:Fe = 1:1.
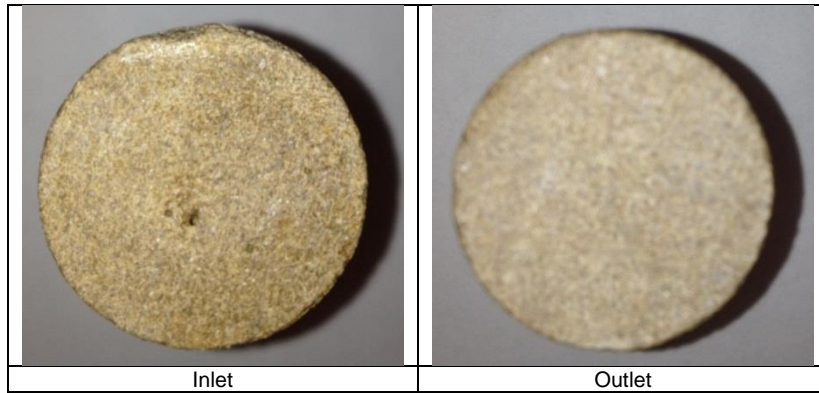
| Inlet | Outlet |

Fig. IV.15– Inlet and outlet for a core tested with 5 wt% HCl, 5,000 ppm Fe^{3+}, GLDA:Fe = 2:1.
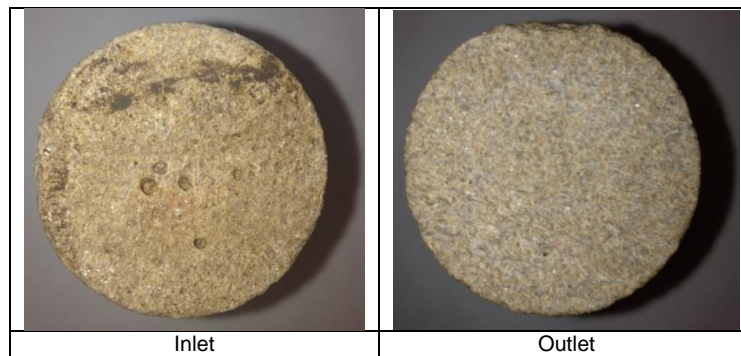
| Inlet | Outlet |

Fig. IV.16– Inlet and outlet for a core tested with 10 wt% HCl, 5,000 ppm Fe^{3+}, GLDA:Fe = 1:1.

Limestone Cores with HEDTA

Two sets of coreflood experiments were performed using low-permeability Indiana limestone. The first set of experiments was performed with 10,000 ppm Fe^{3+} and the data is given in **Table IV.3**. Five coreflood runs were performed using low-permeability Indiana limestone cores that were saturated with 5 wt% NaCl brine. The coreflood experiments were performed at a constant injection rate of 1 cm^3/min. These runs were

performed to test the effect of chelate-to-iron mole ratio and acid concentration on iron recovery. All coreflood runs were performed at a temperature of 200ºF. The pressure drop across the core was recorded during acid injection at different acid concentrations 5 wt% HCl (with both chelate-to-iron mole ratios 1:1 and 2:1), 10 wt% HCl, 15 wt% HCl, and 20 wt% HCl. Samples of the core effluent were analyzed for both iron and calcium concentrations. The pH values of the effluent samples were measured.

Table IV.3– Data for coreflood experiments with HEDTA, 10,000 ppm Fe^{3+}.

Run #	Acid Conc., wt%	Chelate-to-Iron Mole Ratio	Core Porosity, Fraction	Initial K, md	Injection Rate, cm³/min	Final K, md	K Enhancement	Iron Recovered, Fraction
1	5	1:1	0.14	1.22	1.0	2.16	1.76	0.27
2	5	2:1	0.12	1.21	1.0	8.88	7.35	0.43
3	10	1:1	0.13	1.39	1.0	18.09	13.04	0.20
4	15	1:1	0.14	2.29	1.0	Breakthrough*	-	0.24
5	20	1:1	0.14	1.90	1.0	9.30	4.90	0.25

* At breakthrough, the pressure drop decreased to 10 psi. The permeability enhancement was greater than 500 folds in all cases.

Figs. IV.17 through **IV.21** show the pressure drop profile across the cores tested with HEDTA. They have similar trends like the ones tested with GLDA.
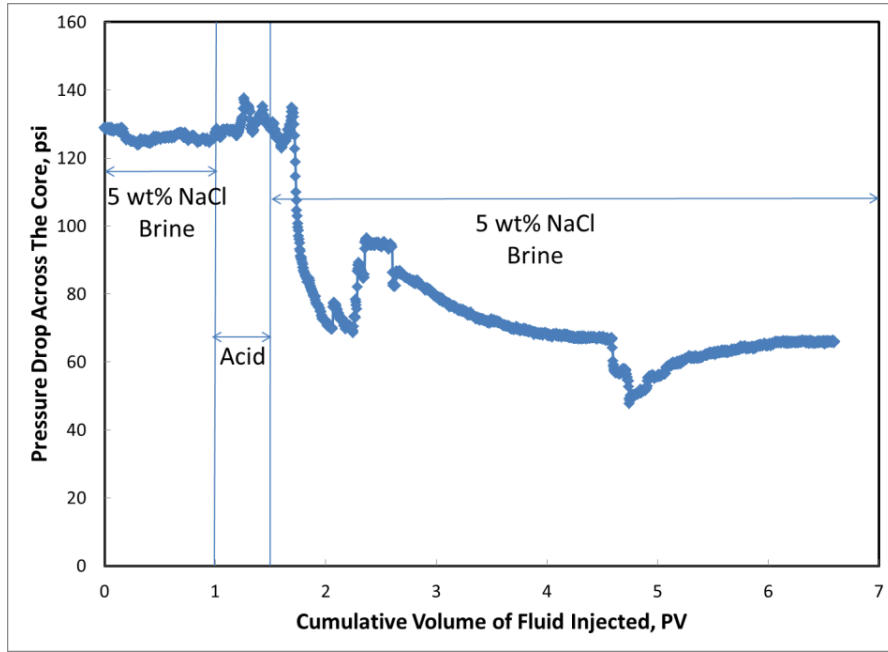
Fig. IV.17– Pressure drop across the core for 5 wt% HCl, 10,000 ppm Fe^{3+}, HEDTA:Fe = 1:1.
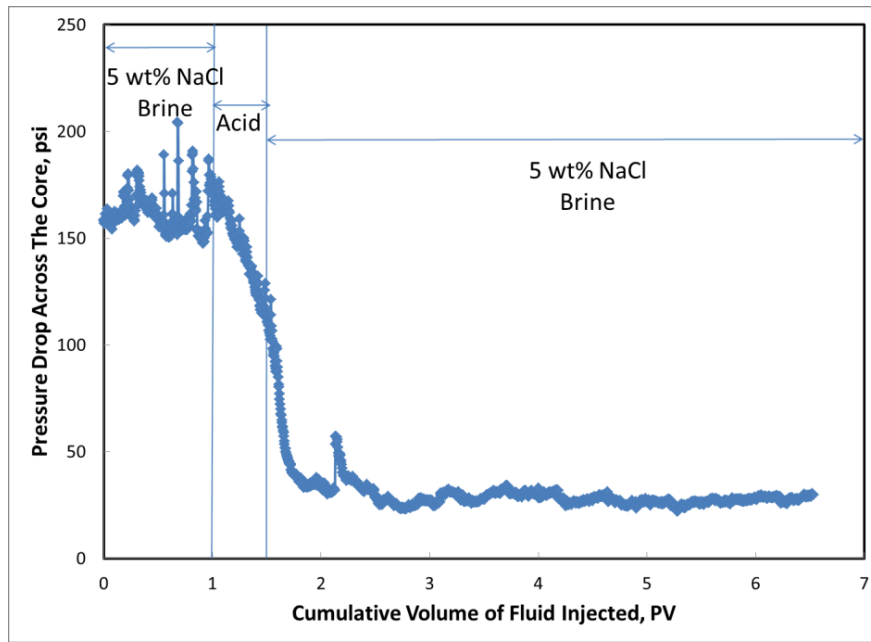
Fig. IV.18– Pressure drop across the core for 5 wt% HCl, 10,000 ppm Fe^{3+}, HEDTA:Fe = 2:1.
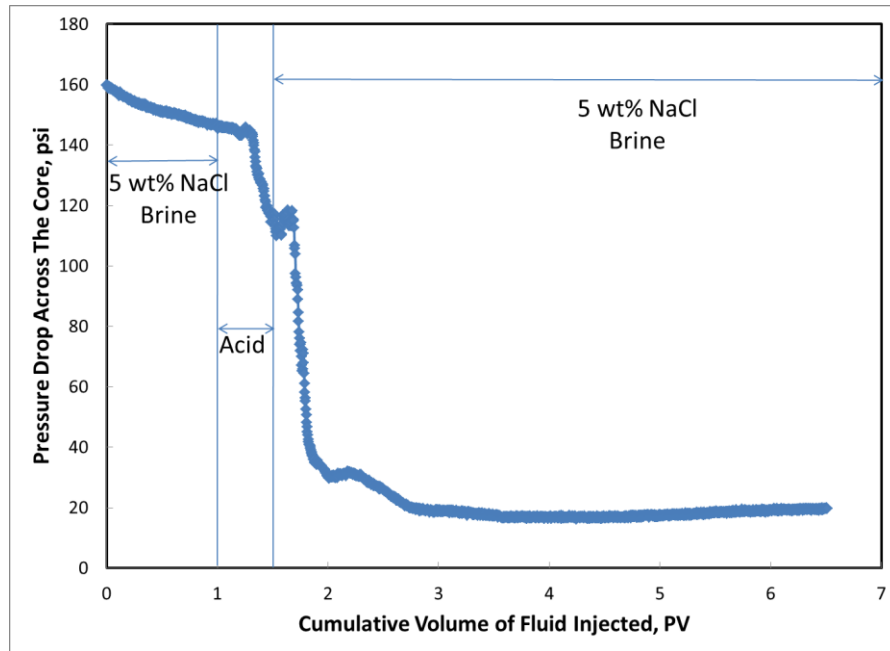
Fig. IV.19– Pressure drop across the core for 10 wt% HCl, 10,000 ppm Fe^{3+}, HEDTA:Fe = 1:1.
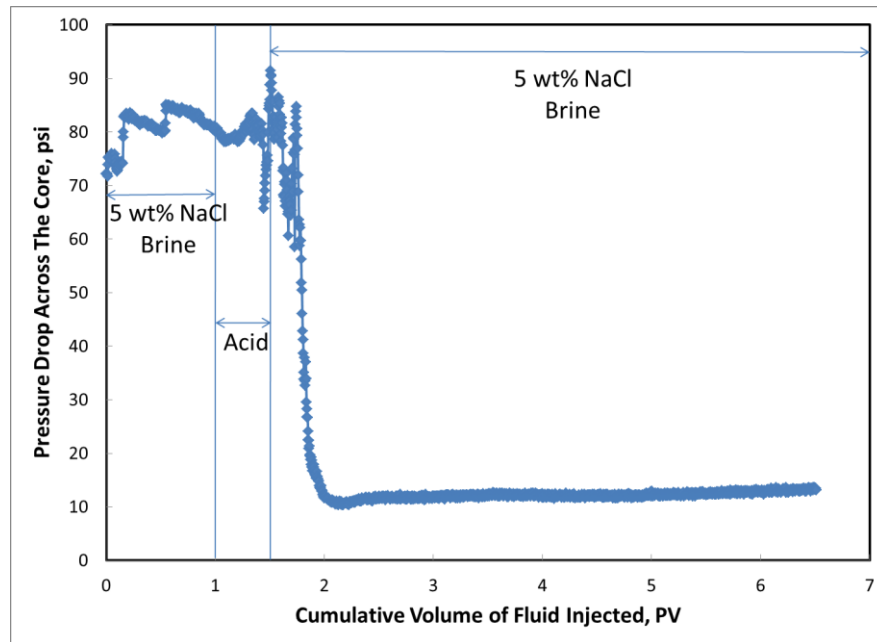
Fig. IV.20– Pressure drop across the core for 15 wt% HCl, 10,000 ppm Fe^{3+}, HEDTA:Fe = 1:1.
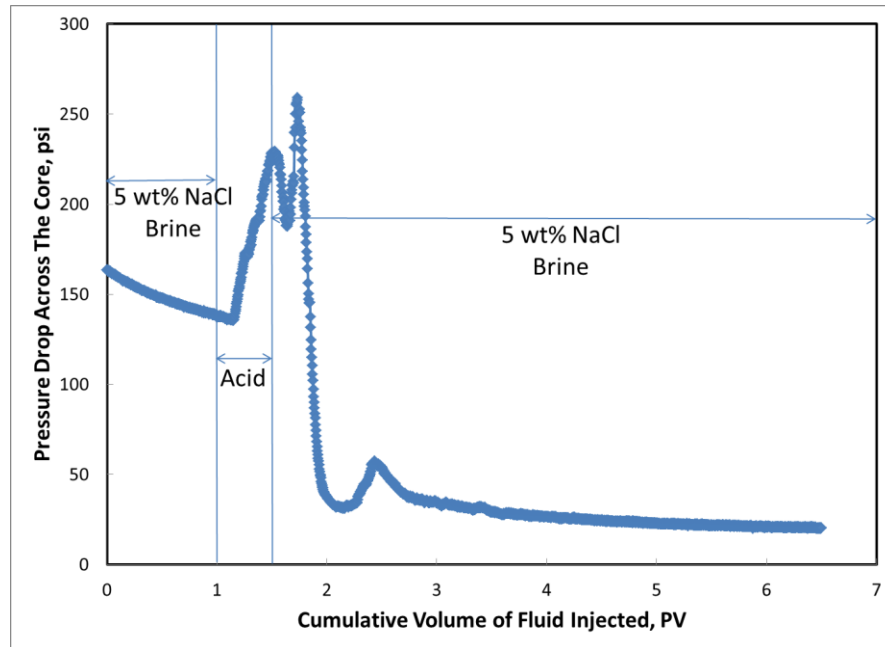
Fig. IV.21– Pressure drop across the core for 20 wt% HCl, 10,000 ppm Fe³⁺, HEDTA:Fe = 1:1.

      Figs. IV.22 through IV.26 show photos of the inlet and outlet of the core tested with (5 - 20 wt%) HCl solutions of 10,000 ppm Fe^{3+} with HEDTA. Significantly less iron precipitation occurred on the inlet face and at the walls of wormholes.
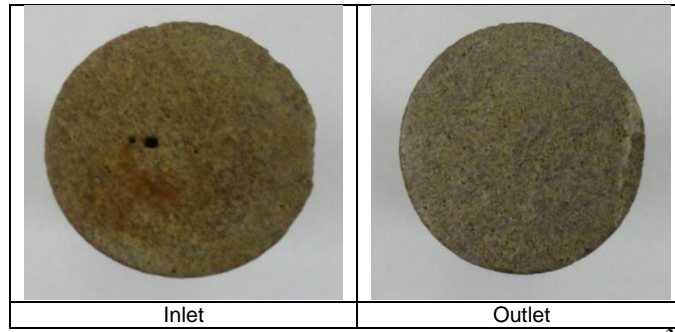
Fig. IV.22– Inlet and outlet for a core tested with 5 wt% HCl, 10,000 ppm Fe^{3+}, HEDTA:Fe = 1:1.
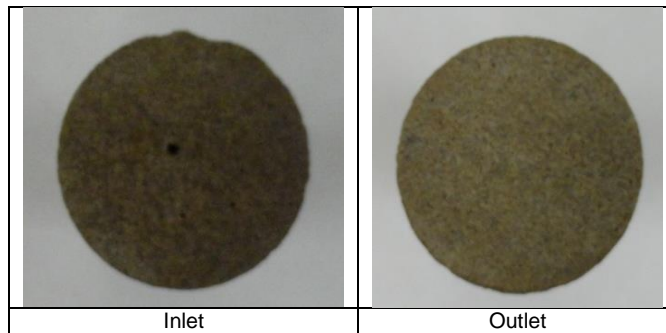
Fig. IV.23– Inlet and outlet for a core tested with 5 wt% HCl, 10,000 ppm Fe^{3+}, HEDTA:Fe = 2:1.
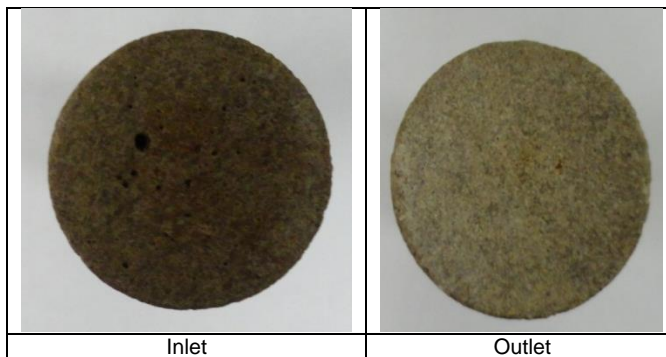
Fig. IV.24– Inlet and outlet for a core tested with 10 wt% HCl, 10,000 ppm Fe^{3+}, HEDTA:Fe = 1:1.

Fig. IV.25– Inlet and outlet for a core tested with 15 wt% HCl, 10,000 ppm Fe^{3+}, HEDTA:Fe = 1:1.
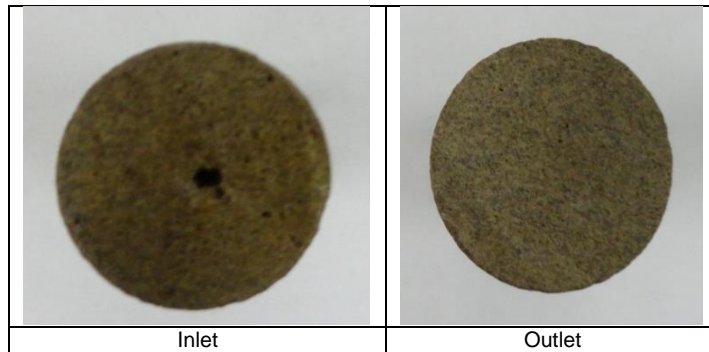
Fig. IV.26– Inlet and outlet for a core tested with 20 wt% HCl, 10,000 ppm Fe^{3+}, HEDTA:Fe = 1:1.

The second set of experiments was performed with 5,000 ppm Fe^{3+} and the data is given in **Table IV.4**. Three coreflood runs were performed using low-permeability Indiana limestone cores that were saturated with 5 wt% NaCl brine. The coreflood experiments were performed at a constant injection rate of 1 cm^3/min. These runs were performed to test the effect of chelate-to-iron mole ratio and acid concentration on iron recovery. All the coreflood runs were performed at a temperature of 200ºF. The pressure

drop across the core was recorded during acid injection at different acid concentrations 5

wt% HCl (with both chelate-to-iron mole ratios 1:1 and 2:1), and 10 wt% HCl. Samples

of the core effluent were analyzed for both iron and calcium concentrations. The pH

values of the effluent samples were measured.

Table IV.4– Data for coreflood experiments with HEDTA, 5,000 ppm Fe^{3+}.

Run #	Acid Conc., wt%	Chelate-to-Iron Mole Ratio	Core Porosity, Fraction	Initial K, md	Injection Rate, cm^3/min	Final K, md	K Enhancement	Iron Recovered, Fraction
1	5	1:1	0.13	1.01	1.0	3.30	3.27	0.41
2	5	2:1	0.14	1.05	1.0	2.76	2.64	0.46
3	10	1:1	0.13	1.33	1.0	Breakthrough*	-	0.42

* At breakthrough, the pressure drop decreased to 10 psi. The permeability enhancement was greater than 500 folds in all cases.

Figs. IV.27 through **IV.29** show the pressure drop profile across the cores tested

with HEDTA. They have similar trends like the ones tested with GLDA.
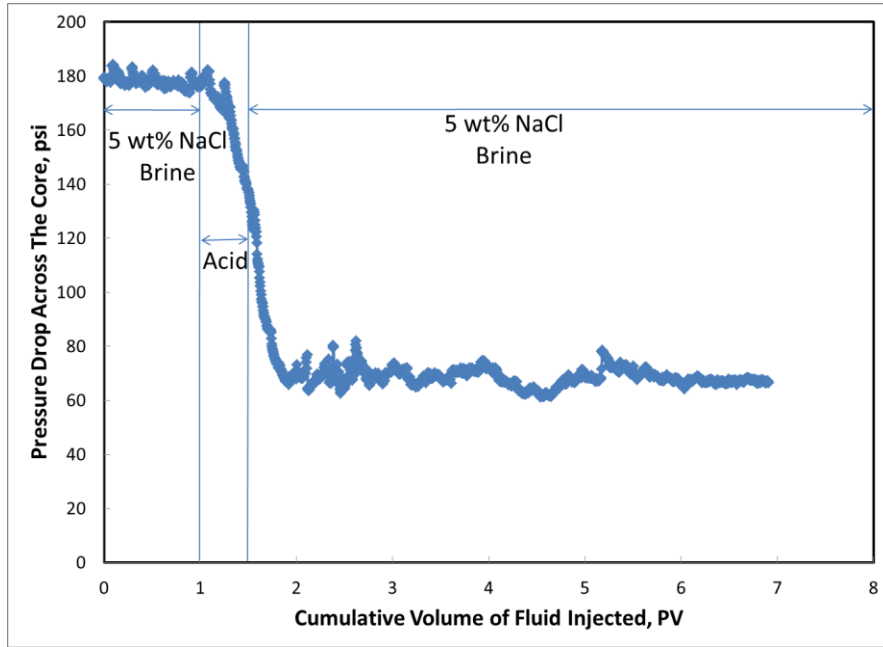
Fig. IV.27– Pressure drop across the core for 5 wt% HCl, 5,000 ppm Fe^{3+}, HEDTA:Fe = 1:1.
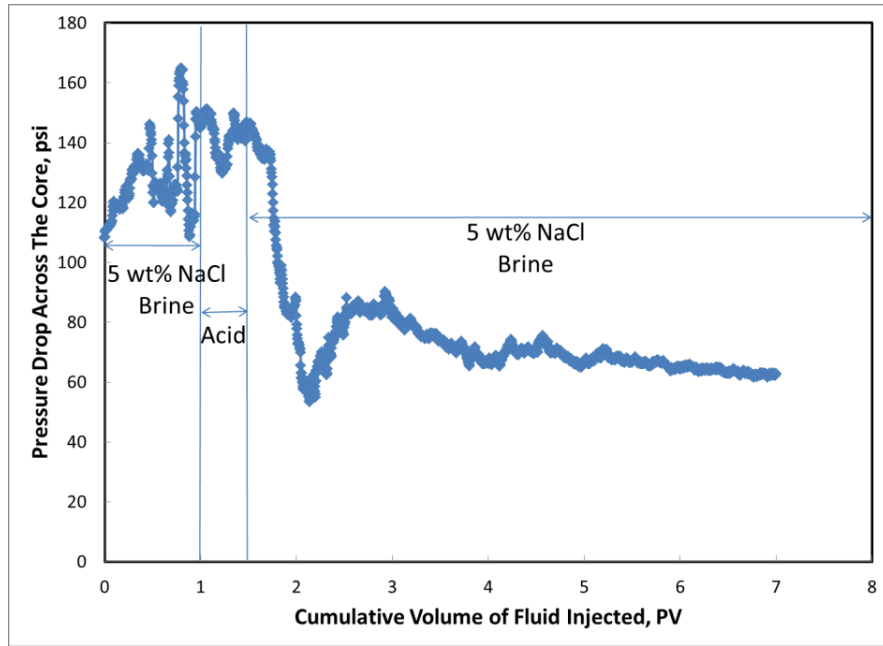
Fig. IV.28– Pressure drop across the core for 5 wt% HCl, 5,000 ppm Fe^{3+}, HEDTA:Fe = 2:1.
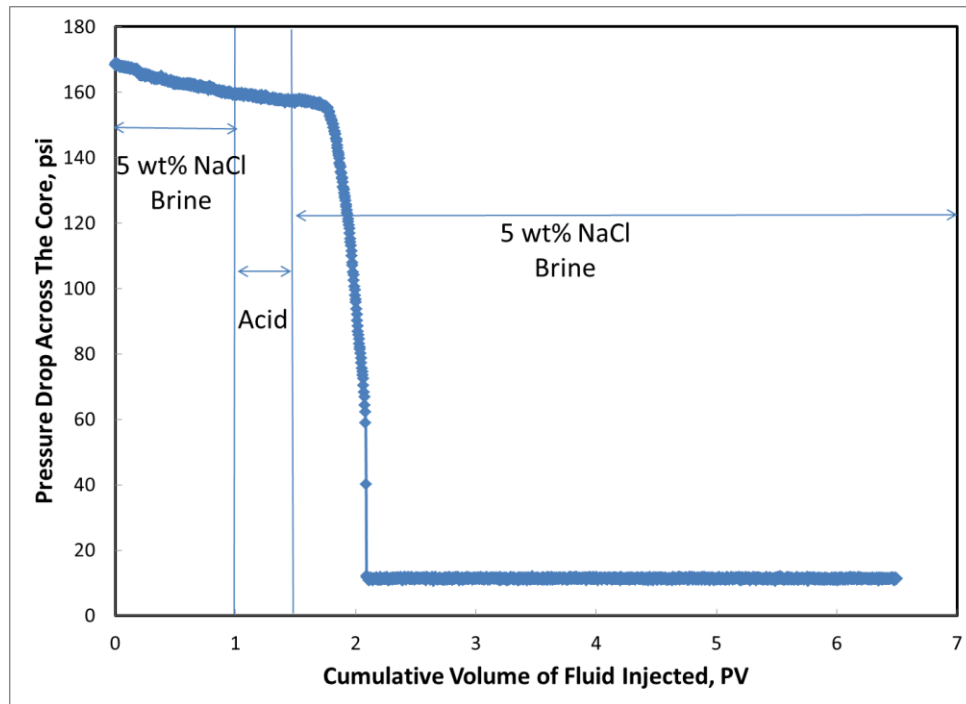
Fig. IV.29– Pressure drop across the core for 10 wt% HCl, 5,000 ppm Fe^{3+}, HEDTA:Fe = 1:1.

Figs. IV.30 through IV.32 show photos of the inlet and outlet of the core tested with (5 - 10 wt%) HCl solutions of 5,000 ppm Fe^{3+} with HEDTA. **Fig. IV.32** shows images of the inlet and outlet of the core tested with 10 wt% HCl solution of 5,000 ppm Fe^{3+} and GLDA at a chelate-to-iron ratio of 1:1. A small amount of iron precipitation occurred on the inlet face and at the walls of wormholes. In this test, no breakthrough occurred. It is clear that the wormholes did not reach the core outlet.
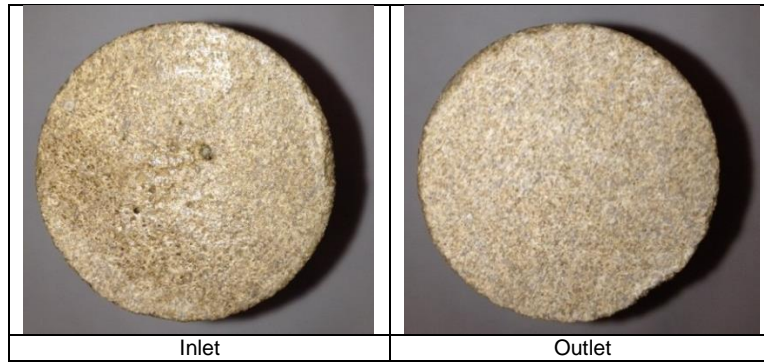
Fig. IV.30– Inlet and outlet for a core tested with 5 wt% HCl, 5,000 ppm Fe^{3+}, HEDTA:Fe = 1:1.

Fig. IV.31– Inlet and outlet for a core tested with 5 wt% HCl, 5,000 ppm Fe^{3+}, HEDTA:Fe = 2:1.
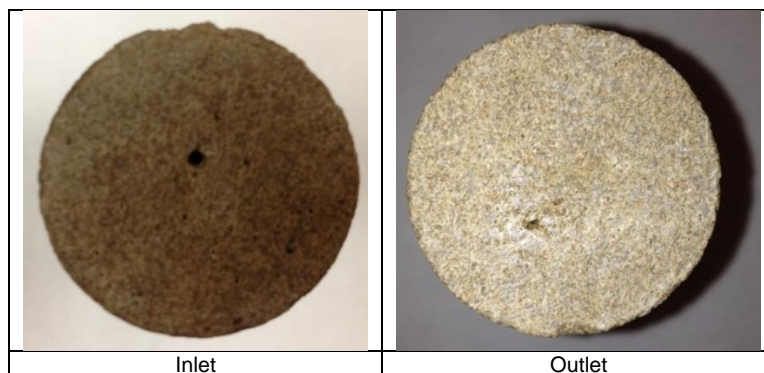
Fig. IV.32– Inlet and outlet for a core tested with 10 wt% HCl, 5,000 ppm Fe^{3+}, HEDTA:Fe = 1:1.

CT Scan

Cores were scanned using a CT scanner for better understanding of the wormhole propagation. **Figs. IV.33 through IV.48** show 2D scanned images for the 6 in. long, low-permeability (1 - 5 md) cores treated by different acid solutions at flow rat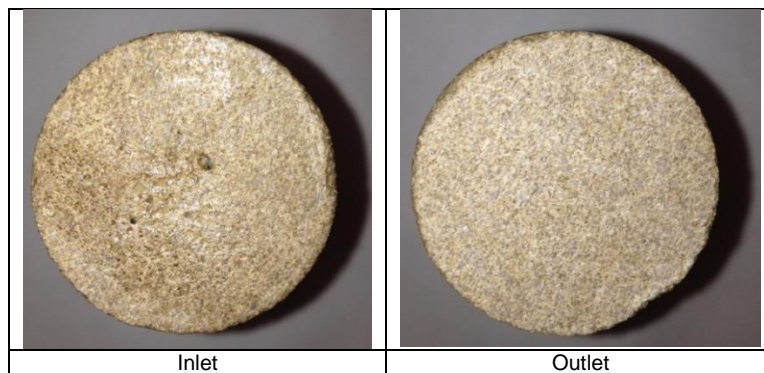e of 1 cm^3/min, and at a temperature of 200ºF. No face dissolution was noticed in the cores inlet face for any of the acid concentrations studied. Upon injection inside the core, acid started to react with the rock and created wormholes. This can be detected through inspection of the dark spots indicating a low CT number and, so a low density. The 2D images show that, sometimes, there is more than one wormhole created in the core. **Fig. IV.36** shows that there is a breakthrough at 10,000 ppm Fe^{3+} and 15 wt% HCl. It is noticed that **Figs. IV.38** and **IV.39** have a large dark area in the middle of the core. This is not dissolution; the cores were broken while measuring the final permeability. From the pressure drop recorded during acid injection, the initial and final permeability, and the permeability ratio were calculated. These results are shown in **Tables IV.1** through **IV.4,** and reveal that for low-permeability (1 - 5 md) limestone cores; there was an overall enhancement in the final permeability in all cases.

Fig. IV.33– CT scanned image for the 6 in. long low-permeability Indiana limestone cores tested with 5 wt% HCl, 10,000 ppm Fe^{3+}, GLDA:Fe = 1:1.

Fig. IV.34– CT scanned image for the 6 in. long low-permeability Indiana limestone cores tested with 5 wt% HCl, 10,000 ppm Fe^{3+}, GLDA:Fe = 2:1.

Fig. IV.35– CT scanned image for the 6 in. long low-permeability Indiana limestone cores tested with 10 wt% HCl, 10,000 ppm Fe^{3+}, GLDA:Fe = 1:1

Fig. IV.36– CT scanned image for the 6 in. long low-permeability Indiana limestone cores tested with 15 wt% HCl, 10,000 ppm Fe^{3+}, GLDA:Fe = 1:1.

Fig. IV.37– CT scanned image for the 6 in. long low-permeability Indiana limestone cores tested with 20 wt% HCl, 10,000 ppm Fe^{3+}, GLDA:Fe = 1:1.

Fig. IV.38– CT scanned image for the 6 in. long low-permeability Indiana limestone cores tested with 5 wt% HCl, 10,000 ppm Fe^{3+}, HEDTA:Fe=1:1.

Fig. IV.39– CT scanned image for the 6 in. long low-permeability Indiana limestone cores tested with 5 wt% HCl, 10,000 ppm Fe^{3+}, HEDTA:Fe=2:1.

Fig. IV.40– CT scanned image for the 6 in. long low-permeability Indiana limestone cores tested with 10 wt% HCl, 10,000 ppm Fe^{3+}, HEDTA:Fe=1:1.
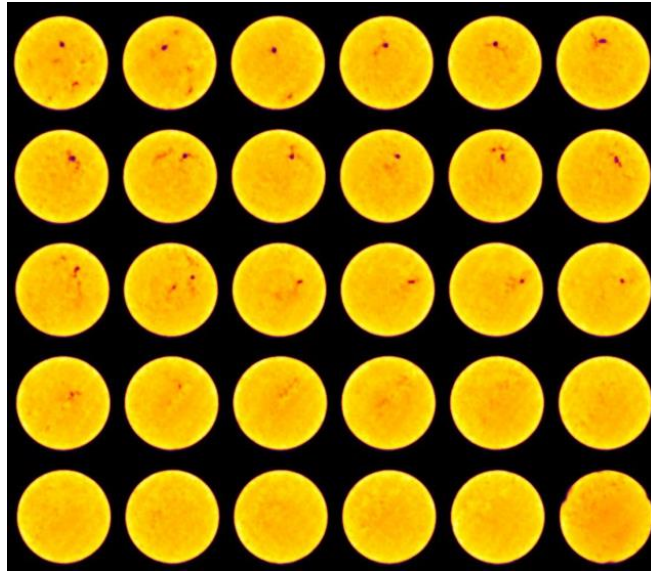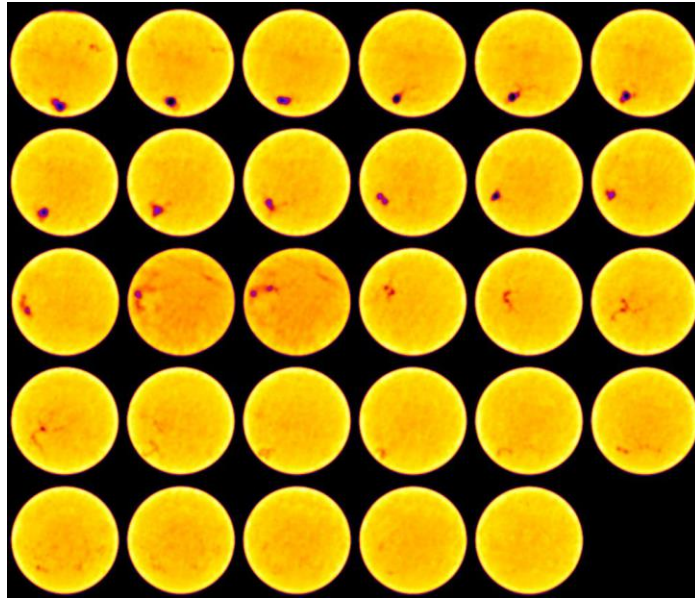
Fig. IV.41– CT scanned image for the 6 in. long low-permeability Indiana limestone cores tested with 15 wt% HCl, 10,000 ppm Fe^{3+}, HEDTA:Fe=1:1.
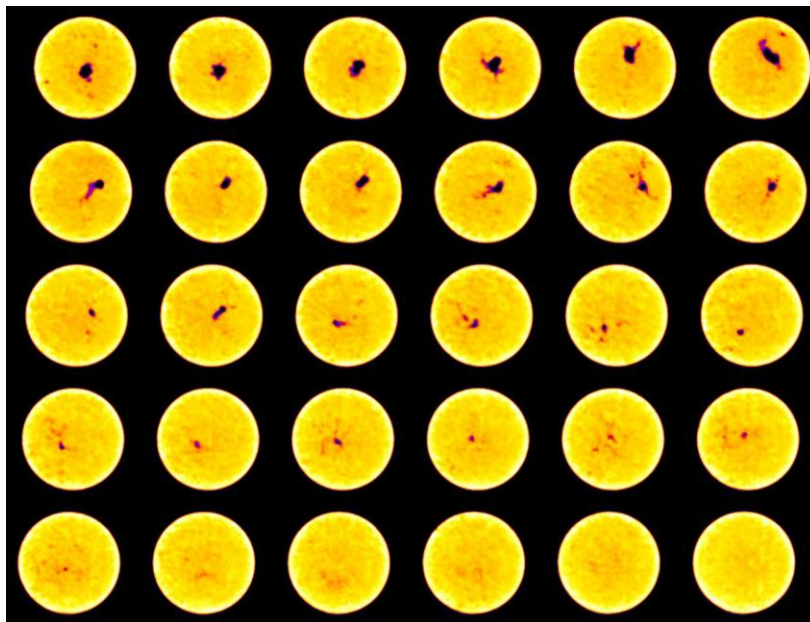
Fig. IV.42– CT scanned image for the 6 in. long low-permeability Indiana limestone cores tested with 20 wt% HCl, 10,000 ppm Fe^{3+}, HEDTA:Fe=1:1.
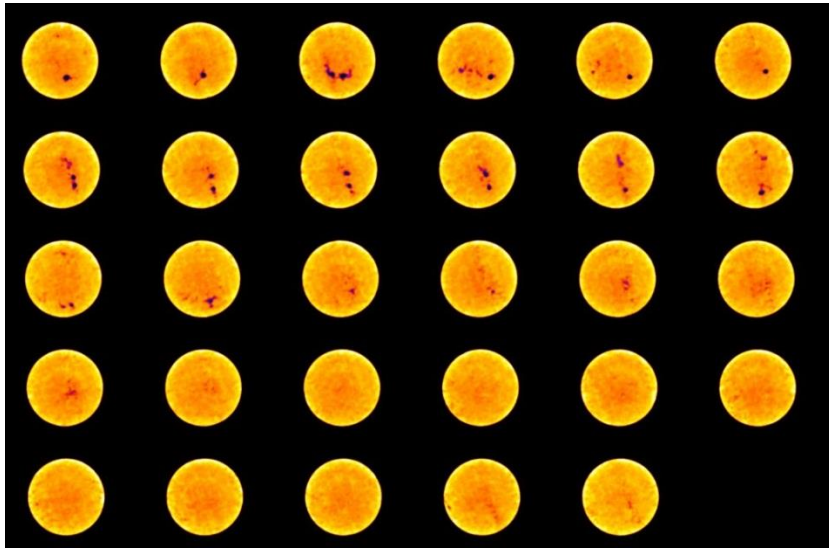
Fig. IV.43– CT scanned image for the 6 in. long low-permeability Indiana limestone cores tested with 5 wt% HCl, 5,000 ppm Fe^{3+}, GLDA:Fe = 1:1.
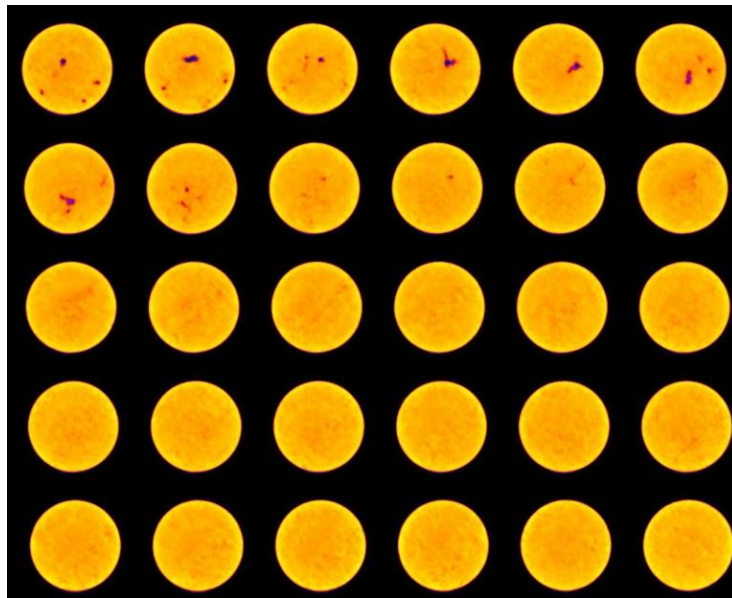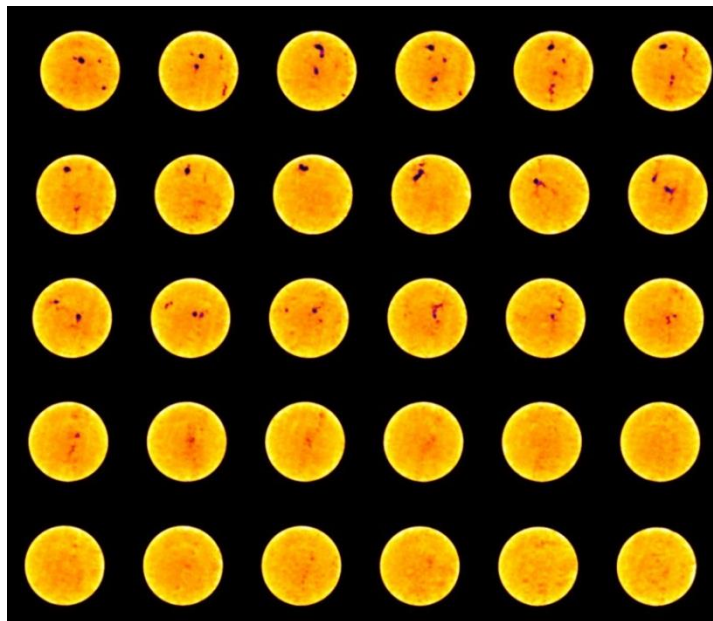

Fig. IV.44– CT scanned image for the 6 in. long low-permeability Indiana limestone cores with 5 wt% HCl, 5,000 ppm Fe^{3+}, GLDA:Fe = 2:1.
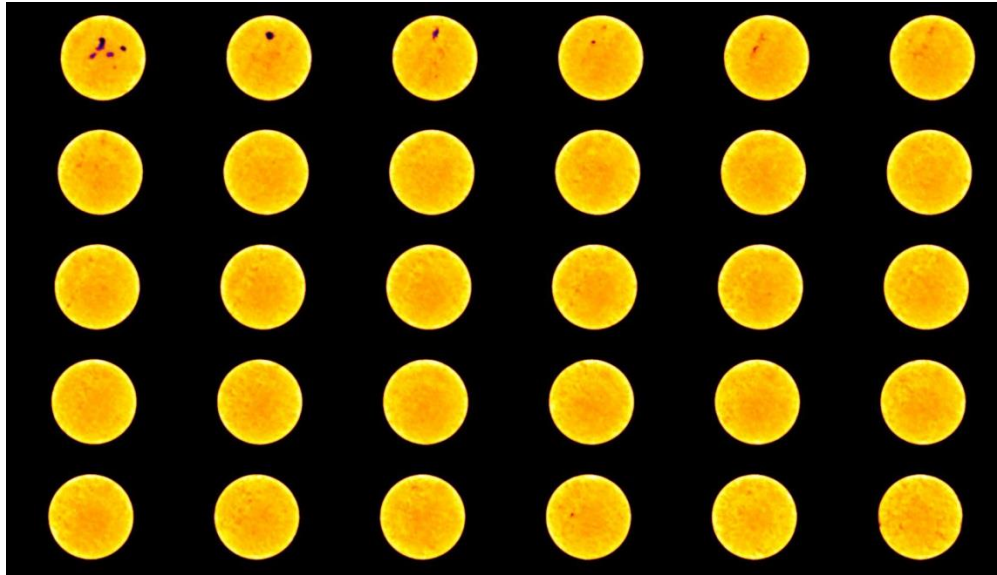
Fig. IV.45– CT scanned image for the 6 in. long low-permeability Indiana limestone cores tested with 10 wt% HCl, 5,000 ppm Fe^{3+}, GLDA:Fe = 1:1.
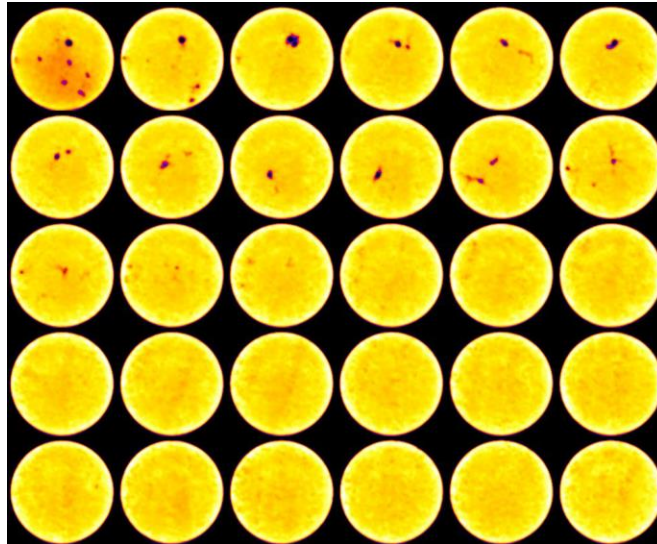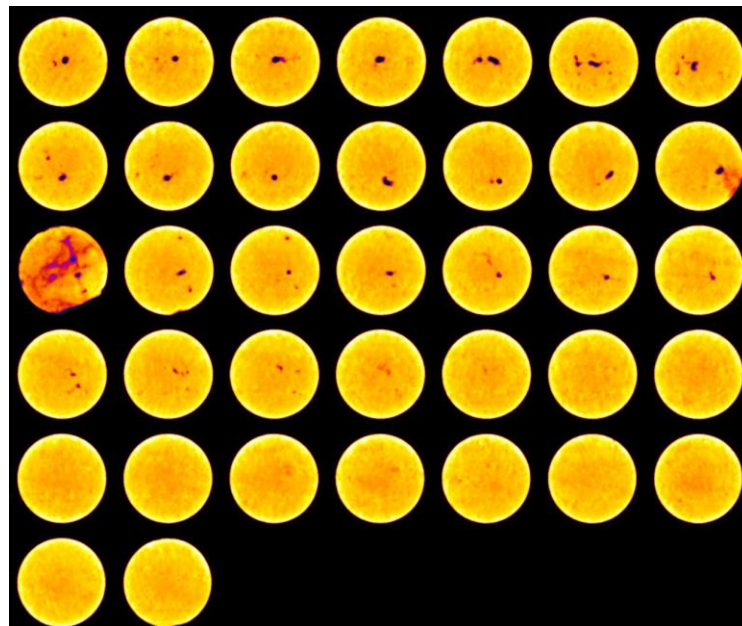

Fig. IV.46– CT scanned image for the 6 in. long low-permeability Indiana limestone cores tested with 5 wt% HCl, 5,000 ppm Fe^{3+}, HEDTA:Fe=1:1.
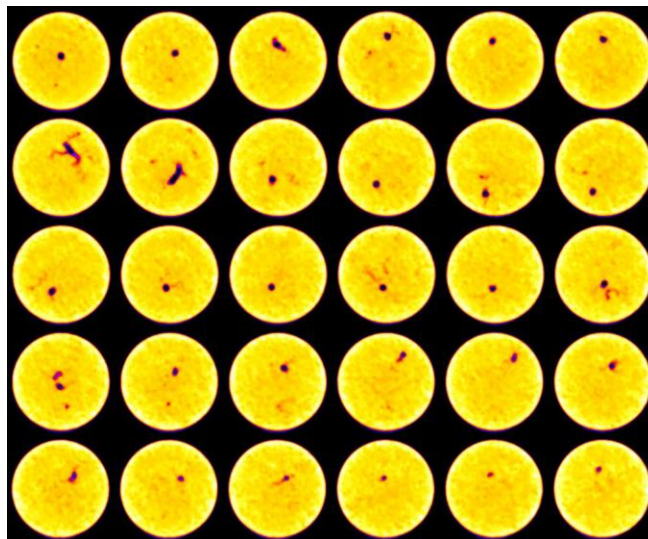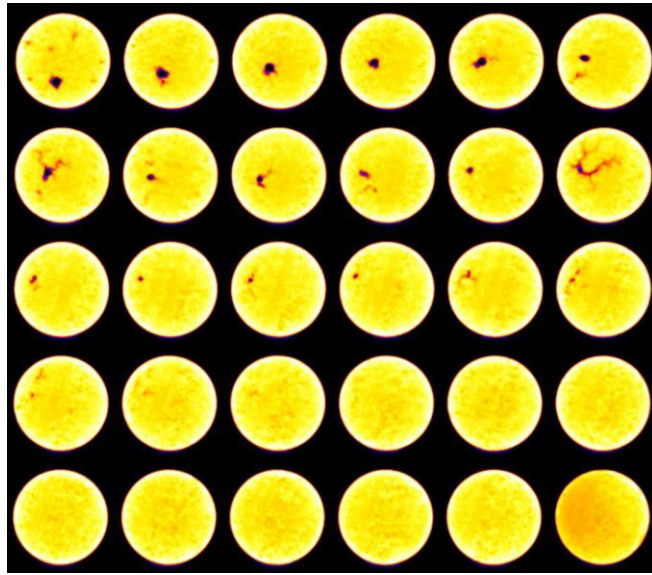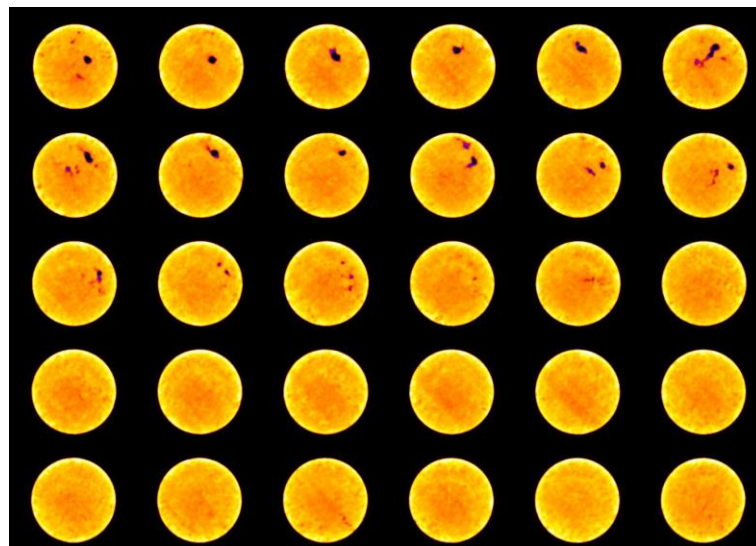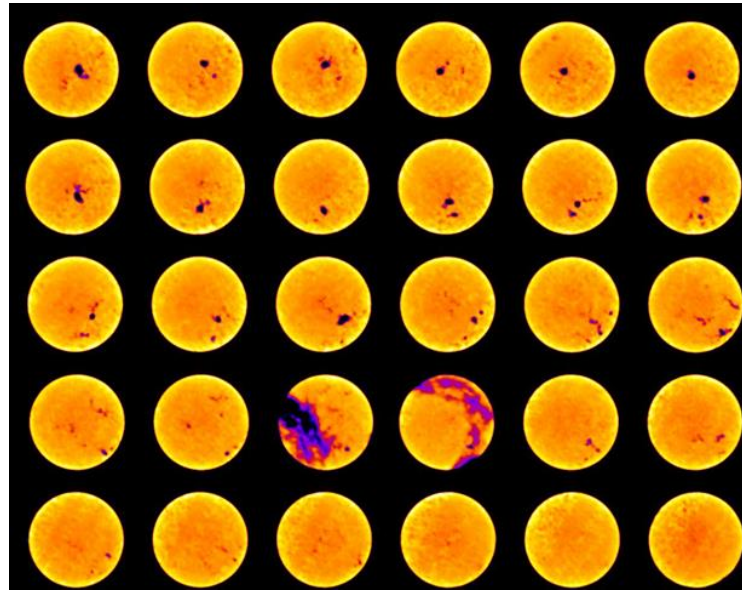
Fig. IV.47– CT scanned image for the 6 in. long low-permeability Indiana limestone cores tested with 5 wt% HCl, 5,000 ppm Fe3+, HEDTA:Fe=2:1
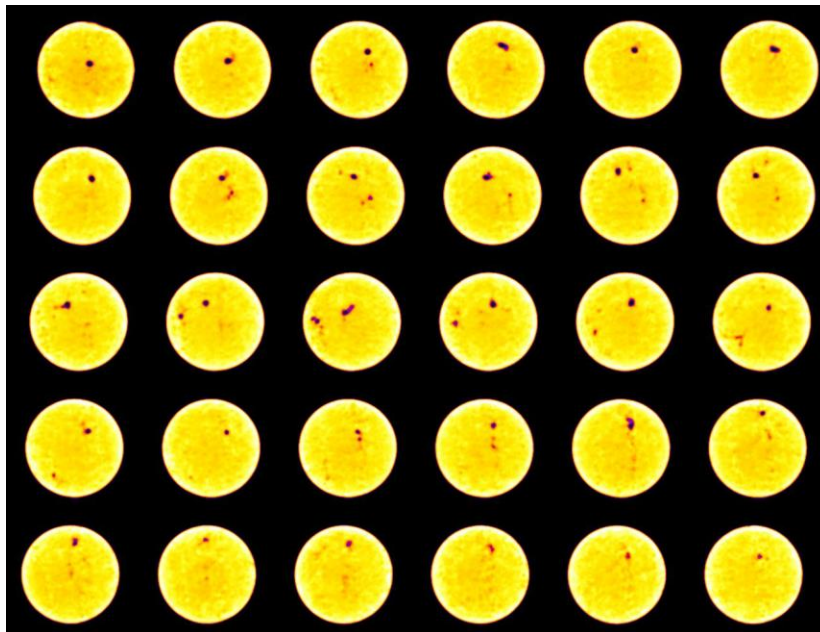
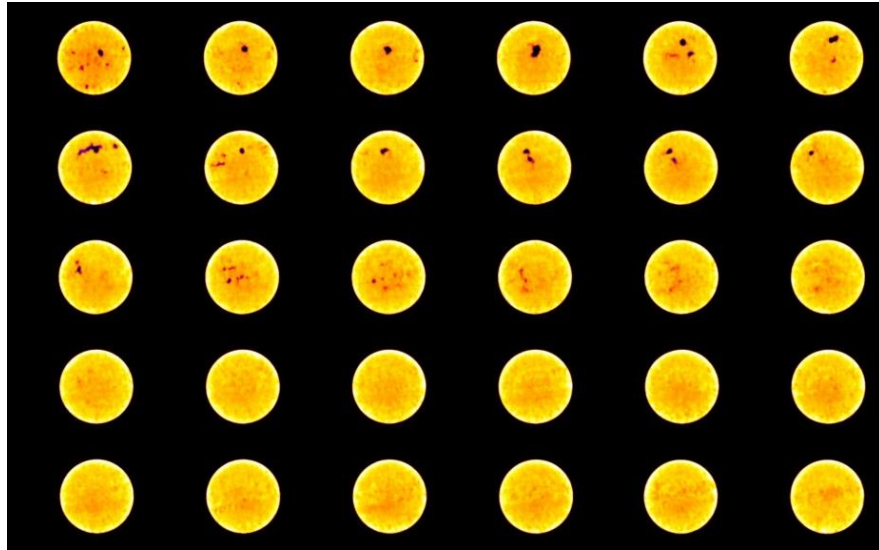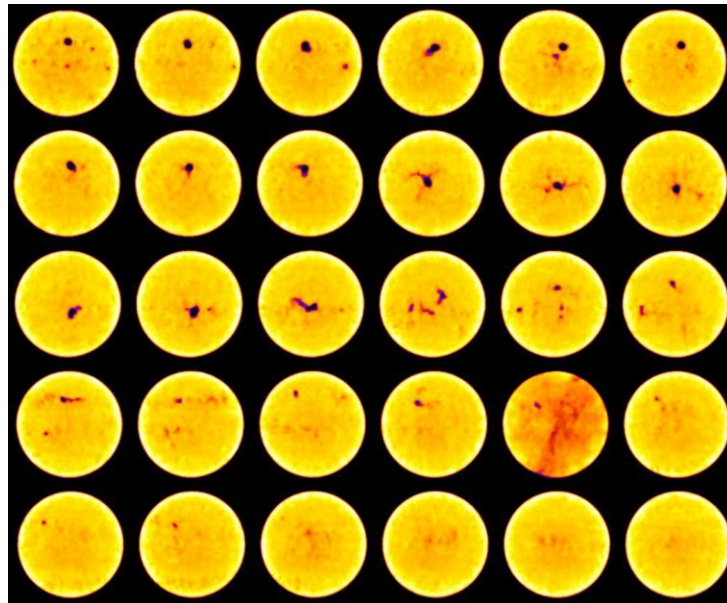**Figure IV.48– CT scanned image for the 6 in. long low-permeability Indiana limestone cores tested with 10 wt% HCl, 5,000 ppm Fe^{3+}, HEDTA:Fe=1:1.**

*Analysis of Core Effluent Samples*

ICP Analysis

Iron and calcium concentrations in the core effluent samples were measured. Core effluent samples showed that the total iron recovered increased with the initial core permeability and acid concentration. Iron precipitated at the core inlet face and inside the cores along wormholes. Concentrations of the total iron and calcium versus the pore volume injected are shown in **Figs. IV.49 through IV.56**. Knowing the volume and iron concentration of each sample, iron recovery as a percent of the total iron injected can be measured from the following equation:

$$\text{\% iron recovered} = \frac{\sum sample\ volume \times iron\ concentration}{Total\ iron\ injected} \times 100\ \% \tag{IV.1}$$

Results are given in **Tables IV.1 through IV.4**.

      Figs. IV.49 and IV.50 show that the amount of iron recovered and the total calcium concentrations increased with the increase of chelate-to-iron mole ratio at 5 wt% HCl with GLDA.
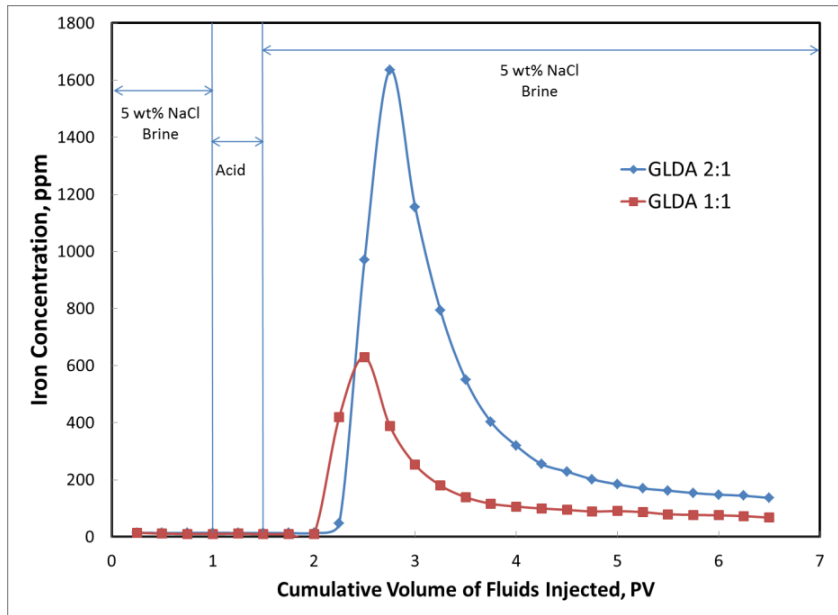
Fig. IV.49– Iron concentration for 5 wt% HCl, 10,000 ppm Fe^{3+} with GLDA at chelate-to-iron mole ratios of 1:1 and 2:1.
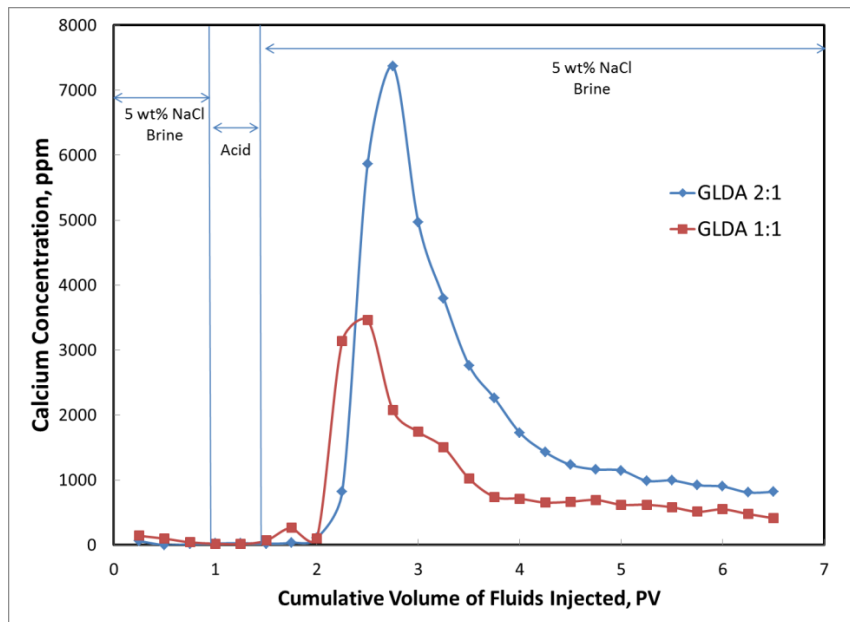
Fig. IV.50– Total calcium concentration for 5 wt% HCl, 10,000 ppm Fe^{3+} with GLDA at chelate-to-iron mole ratios of 1:1 and 2:1.
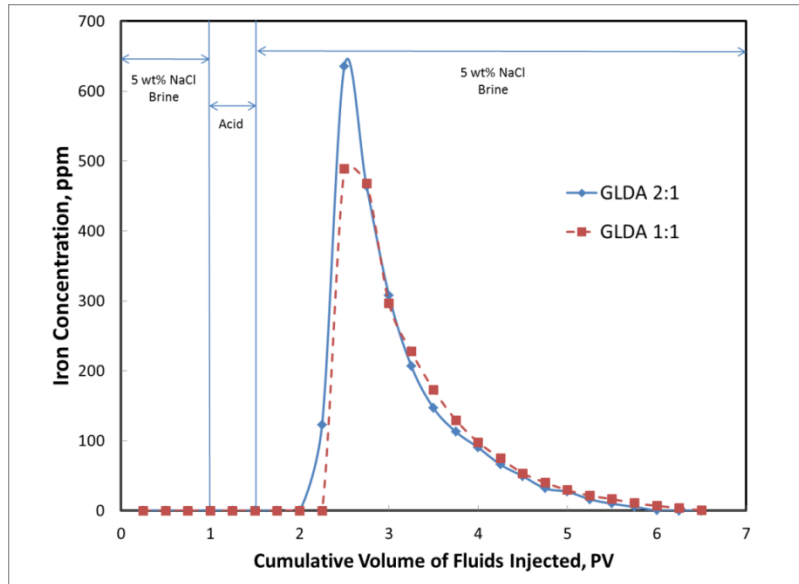
Fig. IV.51– Iron concentration for 5 wt% HCl, 5,000 ppm Fe^{3+} with GLDA at chelate-to-iron mole ratios of 1:1 and 2:1.
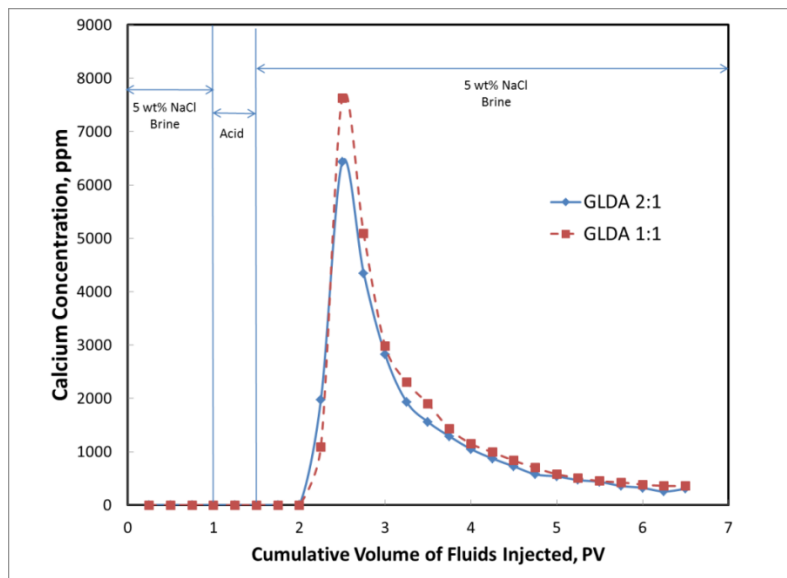
Fig. IV.52– Total calcium concentration for 5 wt% HCl, 5,000 ppm Fe^{3+} with GLDA at chelate-to-iron mole ratios of 1:1 and 2:1.

Figs. IV.53 and IV.54 show that the amount of iron recovered and the total calcium concentrations increased with the increase of chelate-to-iron mole ratio at 5 wt% HCl with HEDTA.
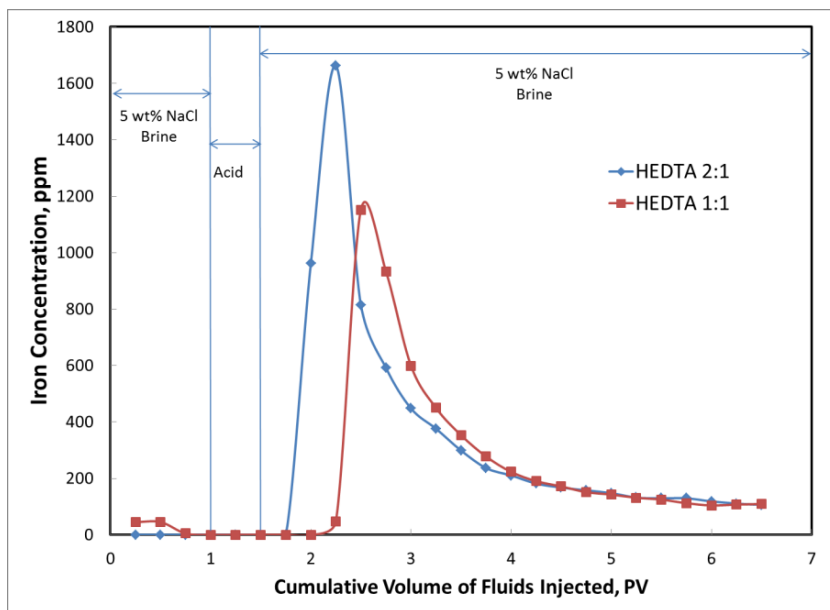
Fig. IV.53– Iron concentration for 5 wt% HCl, 10,000 ppm Fe^{3+} with HEDTA at chelate-to-iron mole ratios of 1:1 and 2:1.
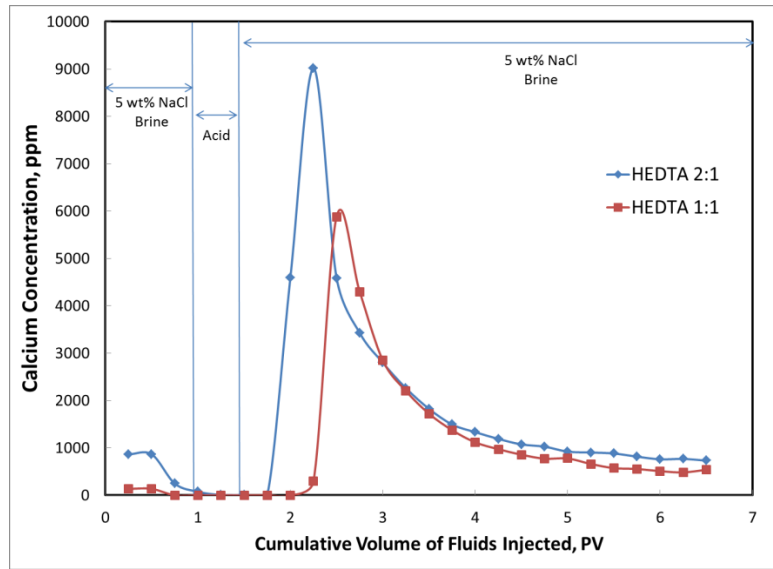
Fig. IV.54– Total calcium concentration for 5 wt% HCl, 10,000 ppm Fe³⁺ with HEDTA at chelate-to-iron mole ratios of 1:1 and 2:1.
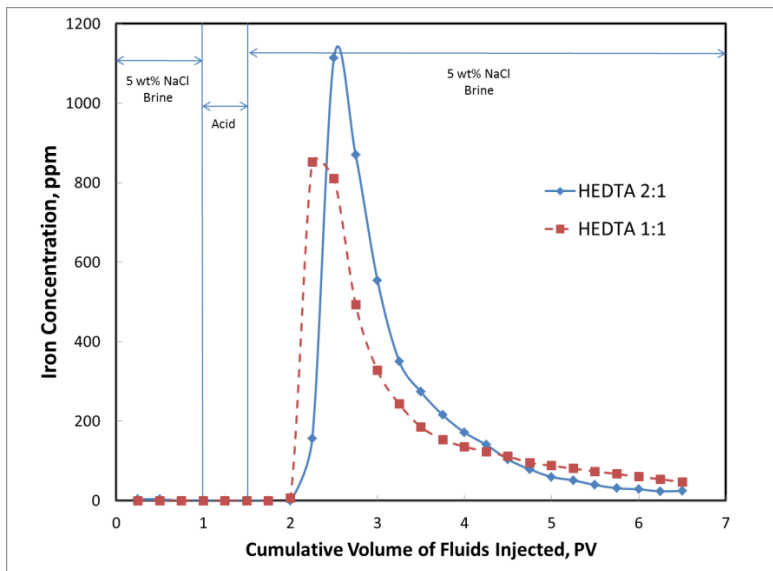
Fig. IV.55– Iron concentration for 5 wt% HCl, 5,000 ppm Fe³⁺ with HEDTA at chelate-to-iron mole ratios of 1:1 and 2:1.

98
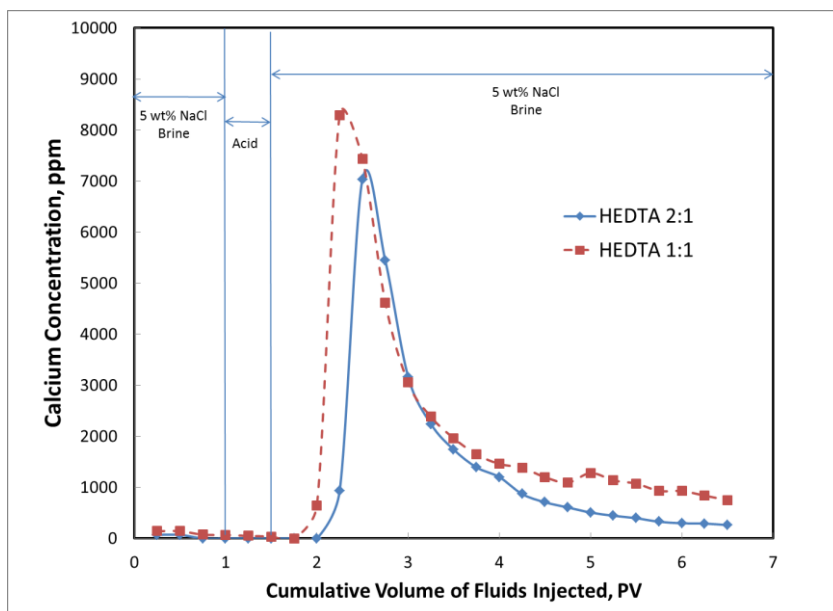
Fig. IV.56– Total calcium concentration for 5 wt% HCl, 5,000 ppm Fe^{3+} with HEDTA at chelate-to-iron mole ratios of 1:1 and 2:1.

Calcium Ion-Selective Electrode Analysis

When optimizing the chelating agent concentration for sufficient iron control, it is important to understand the chelate-iron-calcium system. The pH, precipitation reactions, chelating agent, the concentration of the metal ions, and type of metal ions all affect the amount of chelating agent required for better iron control, especially when dealing with carbonate formations. In these formations, iron can be exchanged for calcium, so the amount of chelating agent available for iron control is reduced depending on the affinity of the chelate for either iron or calcium under the specific conditions.

The affinity of a chelating agent for a metal is often expressed in the stability constant (K_s):

$$M + L \leftrightarrow ML \qquad\qquad (IV.2)$$

$$k_s = \frac{[ML]}{[M] \times [L]} \qquad\qquad (IV.3)$$

Where L is the ligand and M is the divalent or trivalent cation.

For example, when a similar chelating agent, like EDTA is used as an iron control agent in a calcite reservoir the affinity of the chelate for both Fe and Ca need to be taken into account. The effect can be illustrated with simulations in diluted systems. Based on the conditional stability constant curves for Fe-EDTA and Ca-EDTA shown in **Fig. IV.57,** it can be concluded that above pH 9.9 the Ca complex of EDTA is more stable than the Fe complex. Assuming that no precipitate is formed, the speciation diagram for a system containing equal concentrations of Ca, Fe and EDTA (1 mM each) is shown in **Fig. IV.58**. It is clear that the crossing point of the conditional stability constant curves corresponds to the point in the speciation graph where half of each metal is chelated by EDTA and the other half is not chelated.
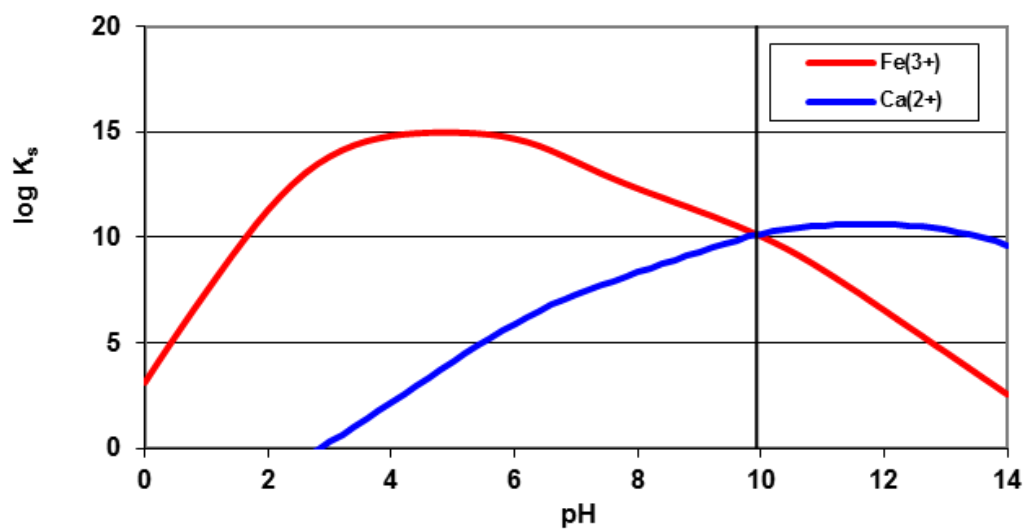
Fig. IV.57– Effect of pH on the stability constant between EDTA with Fe³⁺ and Ca²⁺ where ions are equal in concentration (1 mM each).
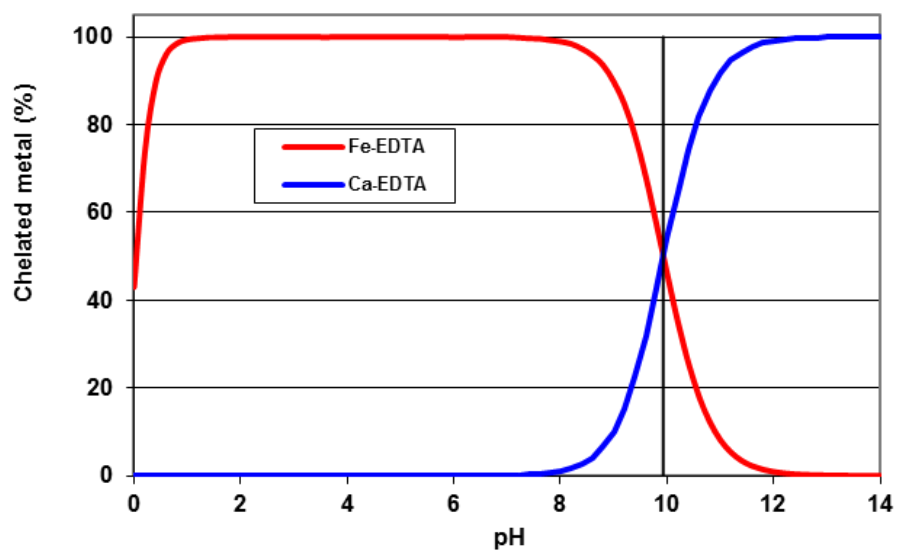
Fig. IV.58– Effect of pH on the percent of chelated Fe³⁺ and Ca²⁺ with EDTA where ions are equal in concentration (1 mM each).

101

However, if the concentrations of metal ions are not equal, as will be the case in a calcite formation, **Fig. IV.59** is obtained. The situation is shown in which the Ca concentration is 10 times higher than the Fe concentration ([Fe] = [EDTA] = 1 mM, [Ca] = 10 mM). It is clear that at pH>7 the affinity of EDTA changes from Fe to Ca.
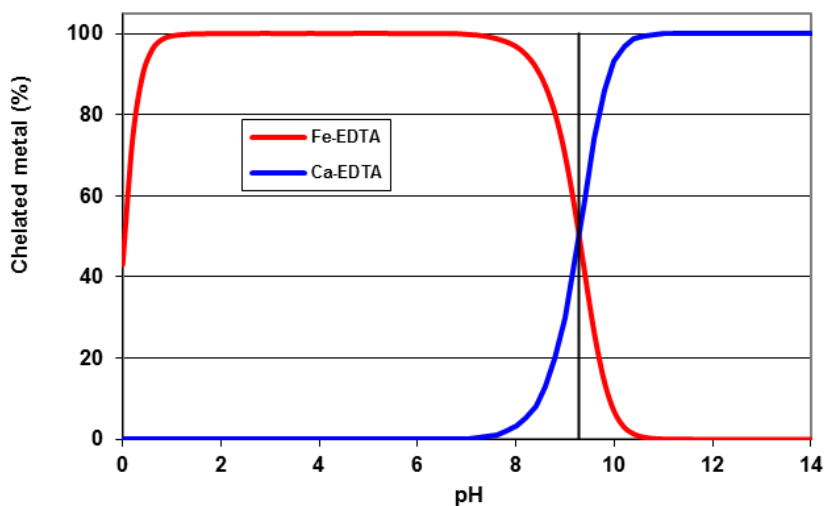
Fig.IV.59– Effect of pH on the percent of chelated Fe^{3+} and Ca^{2+} with EDTA, ([Fe] = [EDTA] = 1 mM) while ([Ca] = 10 mM) assuming no precipitation.

Another complication arises, when the concentration of unchelated metal ions is limited by the precipitation of badly soluble minerals. As metal chelates are often used to prevent the formation of precipitates, this will often be the case in real situations. If the concentration of the free metal ion in solution is limited by the formation of a

precipitate, also the concentration of the chelated metal ion that is possible in solution will be limited. As an example, the speciation diagram for a system containing equal concentrations of Ca, Fe and EDTA (1 mM each) was again obtained. However, this time the formation of poorly soluble amorphous iron hydroxide was allowed in the calculations. The result is shown in **Fig. IV.60**. It is clear that at pH>6 already some of the Fe will be exchanged for Ca, so the amount of EDTA available for iron control is reduced. In real downhole conditions, the concentrations of Fe, Ca and chelating agent will be much higher but the trends will remain the same; part of the iron control agent will be consumed by Ca-complexation, when the acid is spent and the pH increases. In this study we studied the effect of overdosing the iron control agent concentration to compensate for this effect.
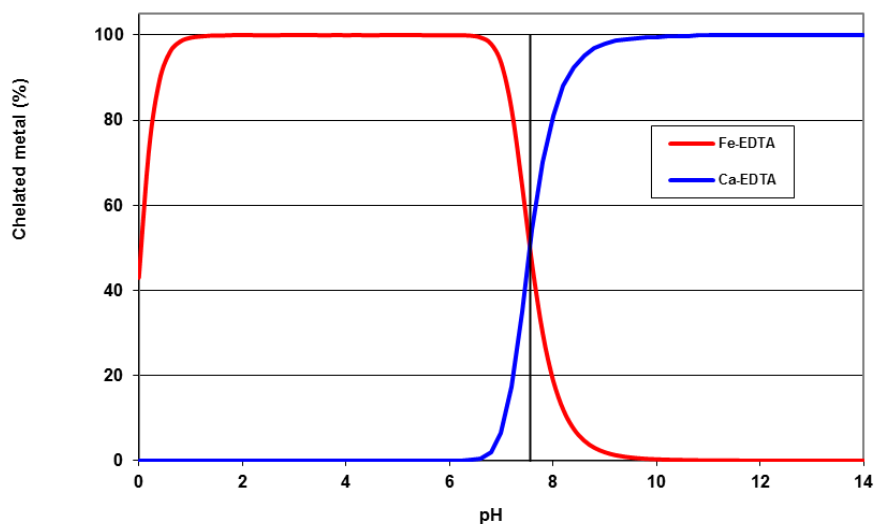
Fig. IV.60– Effect of pH on the percent of chelated Fe^{3+} and Ca^{2+} with EDTA, ([Fe] = [EDTA] = 1 mM) while ([Ca] = 10 mM) in case of precipitation.

Relatively low iron recovery in the cores tested can be attributed to these factors. pH rises when the acid is spent as it goes through the core. The iron starts to precipitate along the walls of the wormholes as the acid reacts to the rock and some of the iron chelated is replaced by calcium.

The calcium ion concentration measured by ICP, is the total calcium concentration. A calcium ion-selective electrode was used to measure the free calcium concentration in the core effluent samples. The difference between the two concentrations indicated the amount of calcium chelated. An ionic strength adjustor was used to minimize the interferences of other ions with the readings. Iron ions interfere with the readings, meaning that the values of free calcium read by the electrode would be greater than the real values. In general, the amount of the calcium chelated will be always less or equal to the real values. **Fig. IV.61** shows the total and chelated calcium concentrations with GLDA at different chelate-to-iron mole ratios. The amount of chelated calcium increased with increasing chelate-to-iron mole ratio.
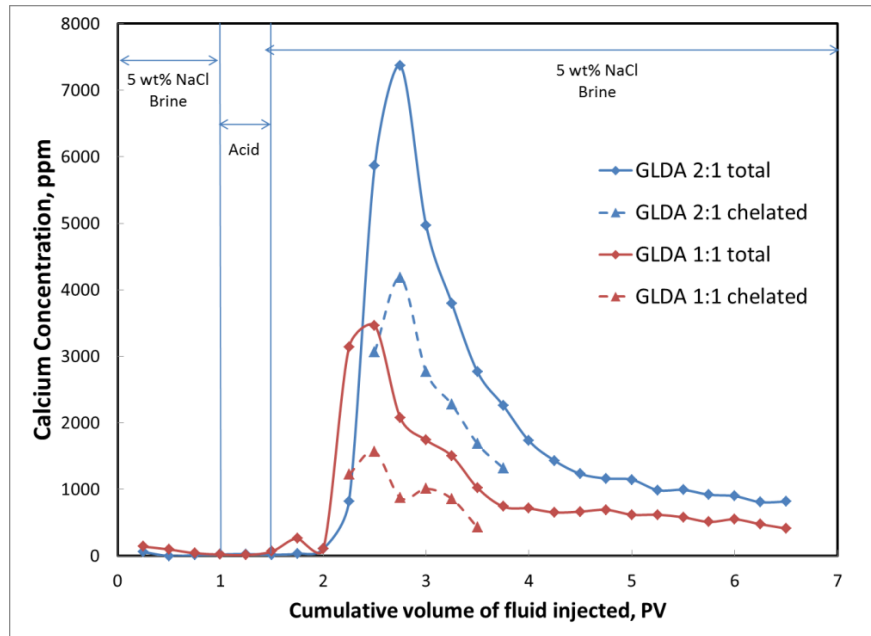
Fig. IV.61– Total and chelated calcium concentration for 5 wt% HCl, 10,000 ppm Fe^{3+} with GLDA at chelate-to-iron mole ratios of 1:1 and 2:1.

CHAPTER V

CONCLUSIONS AND RECOMMENDATIONS

Iron precipitation is one of the most critical problems that are frequently encountered during acid treatments. In the absence of iron control agents, acid treatments will be unsuccessful if iron is present. In this study different variables were changed. Based on the results obtained, the following conclusions can be drawn:

1. As the concentration of ferric iron is increased, the damage increases.

2. At higher temperatures, the damage also exists; but at higher acid concentration there might be a slight enhancement of permeability.

3. At lower flow rates, iron precipitation cause damage to both low and high permeability Indiana limestone cores.

    The damage at high flow rates was not significant.

    GLDA and HEDTA were examined at different amounts of iron, acid concentrations and chelate-to-iron mole ratios. Based on the results obtained, the following conclusions can be drawn:

1. The amount of iron recovered increases with:

    - The increase of the chelate-to-iron mole ratio.

    - The increase in the initial iron concentration.

2. In most cases, HEDTA showed higher iron recovery compared with GLDA.

3. Chelating agents contribute to the calcite dissolution.

    A portion of the chelating agents was consumed in calcium chelation, which limits their main purpose of use. This amount should be identified and taken into

consideration when the treatment is designed. It is recommended to increase the amount of chelating agents while designing field treatments to compensate this effect. An advantage of the calcium dissolving by chelation is that it contributes, with the main acid, to the overall stimulation.

REFERENCES

Al-Mutairi, S.H. and Nasr-El-Din, H.A. 2005. Tube Pickling Procedures: Case Studies. Paper SPE 95004 presented at the SPE European Formation Damage Conference, Sheveningen, The Netherlands, 25-27 May.

Crowe, C.W. 1986. Prevention of Undesirable Precipitates from Acid Treating Fluids. Paper SPE 14090 presented at the International Meeting on Petroleum Engineering, Beijing, China, 17-20 March.

Dill, W.R. and Fredette, G. 1983. Iron Control in the Appalachian Basin. Paper SPE 12319 presented at the SPE Eastern Regional Meeting, Pittsburgh, Pennsylvania, 9-11 November.

Dill, W. and Smolarchuk, P. 1988. Iron Control in Fracturing and Acidizing Operations. *Journal of Canadian Petroleum Technology* **27** (3): 75-78.

Ewing, B.C., Pabley, A.S., and Callaway, R.E. 1983. A Synergistic Chelation System for Acidizing in the Presence of High Iron Concentrations. Paper SPE 11795 presented at the SPE Oilfield and Geothermal Chemistry Symposium, Denver, Colorado, 1-3 June.

Ford, W.G.F., Walker, M.L., Halterman, M.P., Parker, D.L., Brawley, D.G., and Fulton, R.G. 1992. Removing a Typical Iron Sulfide Scale: The Scientific Approach. Paper SPE 24327 presented at the SPE Rocky Mountain Regional Meeting, Casper, Wyoming, 18-21 May.

Fredd, C.N. 1998. The Influence of Transport and Reaction on Wormhole Formation in Carbonate Porous Media: A Study of Alternative Stimulation Fluids. Ph.D. Dissertation, University of Michigan, Ann Arbor, MI.

Fredd, C.N. 2000a. Reservoir Stimulation: Appendix: Advances in Understanding and Predicting Wormhole Formation. 3rd edition, Prentice Hall, USA A16-1: A16-18.

Fredd, C.N. 2000b. Dynamic Model for Wormhole Formation Demonstrates Conditions for Effective Skin Reduction During Carbonate Matrix Acidizing. Paper SPE 59537 presented at the SPE Permian Basin Oil and Gas Recovery Conference, Midland, Texas, 21-23 March.

Fredd, C.N. and Fogler, H.S. 1997. Chelating Agents as Effective Matrix Stimulation Fluid for Carbonate Formations. Paper SPE 37212 presented at the SPE International Symposium on Oilfield Chemistry held in Houston, Texas, 18-21 February.

Fredd, C.N., and Fogler, H.S. 1999. Optimum Conditions for Wormhole Formation in Carbonate Porous Media: Influence of Transport and Reaction. *SPE Journal* **4** (3): 196-205.

Frenier, W.W., Brady, M., Al-Harthy, S., Arangath, R., Chan, K.S., Flamant, N., and Samuel, M. 2004. Hot Oil and Gas Wells can be Stimulated without Acids. *SPEPF* **19** (4): 189-199.

Frenier, W.W., Fredd, C.N., and Chang, F. 2001. Hydroxyaminocarboxylic Acids Produce Superior Formulations for Matrix Stimulation of Carbonates at High Temperatures. Paper SPE 71696 presented at the SPE Annual Technical Conference and Exhibition held in New Orleans, Louisiana, 30 September-3 October.

Frenier, W.W., Rainey, M., Wilson, D., Crump, D., and Jones, L. 2003. A Biodegradable Chelating Agent is Developed for Stimulation of Oil and Gas Formations. Paper SPE 80597 presented at the SPE/EPA/DOE Exportation and Production Environmental Conference held in San Antonio, Texas, 10-12 March.

Gougler Jr., P.D., Hendrick, J.E., and Coulter, A.W. 1985. Field Investigation Identifies Source and Magnitude of Iron Problems. Paper SPE 13812 presented at the SPE Production Operations Symposium, Oklahoma City, Oklahoma, 10-12 March.

Hall, B.E. and Dill, W.R. 1988. Iron Control Additives for Limestone and Sandstone Acidizing of Sweet and Sour Wells. Paper SPE 17157 presented at the SPE Formation Damage Control Symposium, Bakersfield, California, 8-9 February.

Haung, T., Hill, A.D., and Schechter, R.S. 1997. Reaction Rate and Fluid Loss: The Keys to Wormhole Initiation and Propagation in Carbonate Acidizing. Paper SPE 37312 presented at the SPE International Symposium on Oilfield Chemistry, Houston, Texas, 18-21 February.

Huang, T., McElfresh, M.P., and Gabrysch, A.D. 2003. Carbonate Acidizing Fluids at High Temperatures: Acetic Acid, Chelating Agents or Long-Chained Carboxylic Acids? Paper SPE 82268 presented at the SPE European Formation Damage Conference held in The Hague, The Netherlands, 13-14 May.

Kolodynska, D. 2010. The Effect of the Novel Complexing Agent in Removal of Heavy Metal Ions from Waters and Waste Waters. *Chemical Engineering Journal* **165** (3): 835-845.

LePage, J., De Wolf, C.A., Bemelaar, J.H., and Nasr-El-Din H.A. 2011. An Environmentally Friendly Stimulation Fluid for High-Temperature Applications. *SPE Journal* **16** (1): 104-110.

Nasr-El-Din, H.A. and Al-Humaidan, A.Y. 2001. Iron Sulfide Scale: Formation, Removal and Prevention. Paper SPE 68315 presented at the International Symposium on Oilfield Scale, Aberdeen, United Kingdom, 30-31 January.

Nasr-El-Din, H.A., Al-Humaidan, A.Y., Fadhel, B.A., Frenier, W.W., Hill, D.G. 2002. Investigation of Sulfide Scavengers in Well-Acidizing Fluids. SPE Production & Operations **17** (4): 229-235.

Nasr-El-Din, H.A., Garzon, F.O., Al-Mutairi, S.H., Al-Driweesh, S., Al-Harith, A.M. 2007. Lessons Learned from Repickling Old/Sour Gas Wells. Paper SPE 105633 presented at the SPE Middle East Oil and Gas Show and Conference, Kingdom of Bahrain, 11-14 March.

Schechter, R.S. 1992. Oil Well Stimulation. Prentice Hall, New York City. Ch. 18, pp:528 – 547, Ch. 14: 403-423.

Smith, C.F., Crowe, C.W., and Nolan III, T.J. 1969. Secondary Deposition of Iron Compounds Following Acidizing Treatments. *SPE Journal of Petroleum Technology* **21** (9): 1121-1129.

Taylor, K.C., Nasr-El-Din, H.A., and Al-Alawi, M.J. 1999a. Field Test Measures Amount and Type of Iron in Spent Acids. Paper SPE 50780 presented at the SPE International Symposium on Oilfield Chemistry, Houston, Texas, 16-19 February.

Taylor, K.C., Nasr-El-Din, H.A., and Al-Alawi, M.J. 1999b. Systematic Study of Iron Control Chemicals Used During Well Stimulation. *SPE Journal* **4** (3): 19-24.

Taylor, K.C., Nasr-El-Din, H.A., and Saleem, J.A. 2001. Laboratory Evaluation of Iron-Control Chemicals for High-Temperature Sour-Gas Wells. Paper SPE 65010 presented at the SPE International Symposium on Oilfield Chemistry, Houston, Texas, 13-16 February.

Walker, M.L., Dill, W.R., and Besler, M.R. 1990. Iron Control Provides Sustained Production Increase in Wells Containing Sour Gas. *Journal of Canadian Petroleum Technology* **29** (6): 46-50.

Walker, M.L., Dill, W.R., Besler, M.R., and McFatridge, D.G. 1991. Iron Control in West Texas Sour-Gas Wells Provides Sustained Production Increases. *SPE Journal of Petroleum Technology* **43** (5): 603-607.

Williams, B.B., Gidley, J.L., and Schechter, R.S. 1979. Acidizing Fundamentals, Monograph Series, SPE, Richardson, TX, Chapter 2, pp: 5-9.